THE DESIGN, VALIDATION, AND PERFORMANCE EVALUATION OF AN UNTETHERED ANKLE EXOSKELETON

By Greg Orekhov

A Dissertation

Submitted in Partial Fulfillment

of the Requirements for the Degree of

Doctor of Philosophy

in Bioengineering

Northern Arizona University

May 2022

Approved:

Zachary F. Lerner, Ph.D., Chair

Constantin Ciocanel, Ph.D.

Robert Severinghaus, Ph.D.

Michael Shafer, Ph.D.

ABSTRACT

THE DESIGN, VALIDATION, AND PERFORMANCE EVALUATION OF AN UNTETHERED ANKLE EXOSKELETON

GREG OREKHOV

Individuals with neuromuscular impairment from conditions like cerebral palsy face reduced quality of life due to diminishing mobility and independence. Lower-limb exoskeletons, particularly ankle exoskeletons, have potential to aid mobility in impaired populations and augment performance in unimpaired populations and have been extensively researched for the past decade. Few untethered ankle exoskeletons exist due to the difficulty of providing enough mechanical power to offset the weight of the exoskeleton on top of improving human biomechanics and metabolic efficiency. Short battery life is also an obstacle to widespread adoption of untethered ankle exoskeletons in the clinic and at home. In this work, we assess the efficacy of our prototype devices during over-ground walking, design new exoskeleton controllers, develop a new ankle exoskeleton device from the ground up, and evaluate the potential for parallel elasticity to improve the performance of our refined exoskeleton platform. In the first study, we observed that our ankle exoskeleton prototype improved metabolic economy, increased walking speed, and lowered plantarflexor muscle activity in a small cohort of individuals with cerebral palsy during over-ground walking – a significant obstacle to the adoption of exoskeletons in free-living settings. In the second study, we presented a framework for developing adaptive, torque sensor-less open-loop controllers that were competitive with our standard closed-loop controllers in mechanical terms while reducing motor energy consumption and noise. The shortcomings of our prototypes in the first and second chapters inspired a third study to develop new lightweight

and modular ankle exoskeleton design with a significantly higher torque and power output and joint-level sensing that improved metabolic economy in both unimpaired and impaired cohorts – our device is the second ever to improve metabolic economy in unimpaired adults. We also presented the first-ever lower-limb exoskeleton usability study. In the final study, we use our new hardware platform to design, validate, and demonstrate that a simple parallel elastic element can significantly improve the performance and battery life of our device. Together, these studies establish our untethered ankle exoskeletons as effective and versatile tools for rehabilitation and human augmentation and support the continued research of exoskeletons in clinical and at-home settings.

ACKNOWLEDGEMENTS

I'd like to acknowledge Dr. Zachary F. Lerner for his constant support, encouragement, and advice throughout my time at Northern Arizona University. Thank you for your efforts to mold me into a competent researcher and confident engineer. Thank you also for the occasional swift kick in the ass that pushed me to be a better person and scientist. You challenged me in ways I've never been challenged before, helped me make strides towards unlocking my potential, and provided incredible opportunities to meet people and travel to places I hadn't even dreamt of. With the tools we developed together, the world moves a step closer towards being a better and more inclusive place.

Thank you to my committee members and to other professors at Northern Arizona University for your advice and suggestions in elevating this work into something that represents and improves upon the university standard.

I would also like to thank past and present members of the Biomechatronics Lab for the much-needed assistance, willingness to be test subjects, laughs, chats, many drinks, and for introducing me to new activities in Flagstaff. Though my name happens to be on the front of this document, none of this work would have been possible without your support. I hope I was even a fraction of a pleasure to work with for you all as you all have been for me.

My family and friends back home, thank you for your patience in waiting for me these last three-odd years that I've been away. I miss you all dearly and without the regular communication and unique love from each of you in good times and in hard times, I would've fallen apart many times over. All this is for you. Thank you for believing in me.

TABLE OF CONTENTS

LIST OF TABLES

LIST OF FIGURES

Chapter 1: Introduction

Preface

The main body of this dissertation comprises chapters organized for publication in scientific peer-reviewed journals. Each chapter besides the first and last chapter is an individual journal article that has been published or currently under review. Some content will be redundant to adhere to Northern Arizona University's formatting requirements. Chapter 2, titled "Ankle Exoskeleton Assistance Can Improve Over-Ground Walking Economy in Individuals with Cerebral Palsy", was published in the IEEE Transactions on Neural Systems and Rehabilitation Engineering on January 8th, 2020. Chapter 3, titled "Closing the Loop on Exoskeleton Motor Controllers: Benefits of Regression-Based Open-Loop Control", was published in the IEEE Robotics and Automation Letters on July 22nd, 2020. Chapter 4, titled "Usability and Performance Validation of an Ultra-Lightweight and Versatile Untethered Robotic Ankle Exoskeleton", was published in the Journal of NeuroEngineering and Rehabilitation on November 10th, 2021. Chapter 5, titled "Design and Electromechanical Performance Evaluation of a Powered Parallel-Elastic Ankle Exoskeleton", was submitted for initial review in IEEE Robotics and Automation Letters on March 7th, 2022. Supplemental material is included at the end of each chapter and includes additional analysis not part of the respective publications. A short conclusion section summarizes the impact of each chapter. Figures, tables, and references are numbered sequentially throughout this document for clarity. A single list of figures, list of tables, and bibliography are included.

Background

Motivation

Cerebral palsy (CP) is the most common of motor disability among children [1] and impacts the lives of about 500,000 individuals in the US [2] and millions more around the world [3]. Individuals with CP have inefficient motor control during gait [4] that progressively worsens with age leading to limited or lost mobility and independence [5]. Similarly, millions of people are affected by stroke [6] and face similar limitations due to inefficient gait patterns [7]. Some specific symptoms of both CP and impairment due to stroke are similar and include slow walking speeds [8–10], muscle weakness and spasticity [11,12], and limited ankle dorsiflexion strength resulting in foot drop and increased risk of tripping [13,14]. Rehabilitation and treatments for these symptoms are also similar and include prescription of walkers or passive orthoses as the standard of care [15,16], though success is often limited and these aids do not restore natural gait function [15,17]. Functional electrical stimulation has been effective at improving kinematics in both populations [14,18] but so far has limited applicability outside of a lab setting and has limited long-term benefits versus orthotics [13]. Functional gait training, however, has proven to be an effective method for improving gait mechanics for children and adults with CP [19,20] and complications due to stroke [21].

Powered exoskeletons have the potential to maximize and hasten the effects of functional gait training and have been researched extensively in recent years for the specific purpose of improving gait mechanics and energetics in impaired and unimpaired populations [16,21–29]. Ankle exoskeletons, specifically, hold potential to augment walking performance in both unimpaired individuals and in individuals with neurological conditions [16,30–32]. The ankle joint is a

frequent target for powered assistance due to its critical role in efficient bipedal locomotion [33–35] and because it is a commonly affected joint in individuals with neurological deficits [36,37]. Individuals with CP, for example, typically have ankle plantarflexor weakness and limited push-off power that contributes to slow, inefficient walking, particularly on graded terrain, like stairs [38–40].

In this work, I will focus on lightweight exoskeletons that supplement the wearer's ankle function only [22,29,41], which includes our own devices. Our group's specific focus is improving gait mechanics and energetics in children and adults with CP using untethered, lightweight ankle exoskeletons to provide bidirectional assistance for mobility [25,26] or resistance for rehabilitation [42,43] with the ultimate goal of solidifying our device as an effective rehabilitation tool in the clinic and at home.

Prior Work

Unburdened by the need to carry motors and a power supply, users walking with tethered ankle plantarflexor assistance have consistently demonstrated improved walking economy for nearly a decade [28,35,44,45]. However, achieving improvements in walking economy with untethered ankle exoskeletons has apparently been more challenging, with only a small number of studies reporting activity performance benefits compared to walking without the device [16,22,25,26,31]. Untethered ankle exoskeletons capable of mobility augmentation outside of the laboratory follow two general design approaches: placing motors on the shank close to the joint or placing motors at the waist. Opting to minimize mass and the physical profile added to the lower-limb, Awad et al. [16,22] developed a unilateral soft exosuit with waist-mounted motors that improved paretic limb function, walking speed and walking economy in stroke survivors. Mooney et al. [31] took a shank

mounted motor approach instead, and addressed the metabolic detriment of adding mass distally on the leg by incorporating a clever mechanical design achieving high torque and power output, and demonstrated improvements in loaded and unloaded walking in healthy adults; this appears to be the only published work demonstrating a group-level improvement in energy efficiency in unimpaired individuals when walking with a bilateral, untethered, battery-powered ankle exoskeleton compared to no device. Few other untethered ankle exoskeletons exist and none have demonstrated any sufficient impact on human performance to be considered successful. The exoskeleton field has a clear need for a lightweight, untethered device that provides bidirectional ankle assistance for children and adults with CP.

Our group developed such a device in 2018 [46] and subsequently demonstrated its effectiveness at reducing metabolic cost [47], improving gait mechanics and muscle activation patterns, and increasing walking speeds in small cohorts of people with CP [25,27]. However, early prototypes had poor reliability and durability, and proved ineffective for individuals of body mass greater than approximately 45 kg because of limited torque production and significant motion of the ankle assembly relative to the shank and foot [25,47]. Certain aspects of the mechanical design including the torque transfer interfaces (i.e., footplates and shank cuffs) were refined as part of another student's graduate work [48]. Still, there remained significant room to improve the mechanical design, widen the effective mass range of the device, and explore the exoskeleton's effectiveness in other populations besides children and small adults with CP and other terrains besides level treadmill walking.

Scope of Present Work

General Overview

The specific focus of this dissertation was to identify and address the shortcomings of our previous prototypes to develop and refine a novel untethered ankle exoskeleton design, validate the performance of new exoskeleton hardware and control under appropriate use cases, and investigate the effects of exoskeleton assistance on human performance in small impaired and unimpaired cohorts on variable terrain. The knowledge gained from this research will help improve the reliability, effectiveness, and safety of our ankle exoskeletons as we continue to refine the mechanical and controller designs and provide a thorough reference for other groups interested in entering the exoskeleton field.

Aims

The ultimate goal of my research was to improve energy efficiency and walking ability in impaired and unimpaired participants during variable walking tasks using a novel ankle exoskeleton hardware platform. The specific aims below meet the need for a functional device capable of producing adaptive ankle assistance to improve energy efficiency during variable-terrain walking and daily living for children and adults with and without neuromuscular impairments.

Aim 1: To design and validate an ankle exoskeleton hardware platform with custom torque and angle sensing capability. Approach: Develop calibration curves for custom torque sensors instrumented with strain gages. Analyze the torque sensor's strength, stiffness, sensitivity to out-of-plane loads, and overall measurement uncertainty using simulations and functional tests. Perform motion capture experiments to validate on-board measurements of exoskeleton ankle joint

angular position and velocity. Hypotheses: 1) The torque sensor sufficiently withstands variable terrain assisted walking up to 30 Nm and is sufficiently insensitive to out-of-plane loads. 2) On-board measurements of joint angular position and velocity are similar to the motion capture standard.

Aim 2: To assess and improve the performance and electrical-to-mechanical efficiency of the ankle exoskeleton. Approach: Using validated exoskeleton hardware, collect on-board measurements during exoskeleton-assisted walking tasks to assess overall exoskeleton performance and electrical-to-mechanical efficiency. Assess the effectiveness of open-loop control strategies and parallel elasticity as methods for improving exoskeleton performance and efficiency. Hypotheses: 1) Open-loop motor current controllers perform just as well or better than our standard closed-loop torque controller in mechanical terms (energy consumption, torque production, responsiveness, etc.). 2) Parallel elasticity has a significant effect of lowering motor energy consumption and improving overall exoskeleton power efficiency.

Aim 3: To improve mobility outcomes in individuals with and without neuromuscular impairments during variable walking conditions with exoskeleton assistance. Approach: Perform moderate and high intensity stair-stepping, level and inclined treadmill, and overground walking experiments with exoskeleton assistance to study the effects on mobility and energetics in unimpaired adults and both children and adults with CP. Hypothesis: Exoskeleton assistance significantly improves walking speed, reduces energy expenditure, and improves other mobility outcomes during all walking tasks.

The central hypothesis of this research is that our lightweight, untethered ankle exoskeleton can improve walking ability and energy efficiency in impaired and unimpaired cohorts during variable

walking tasks. To this end, the following chapters address one or multiple aims. Specifically, Chapter 2 addresses Aim 3 and provides a baseline for the exoskeleton design refinement in Aim 1. Chapters 3 and 5 address Aim 2. Chapter 4 addresses Aim 1, Aim 2, and Aim 3.

Contributions to the Field

Here, the specific contributions to the field that are a direct result of the research presented in the following chapters are summarized:

1. The first demonstration that ankle exoskeleton assistance can improve overground walking economy, walking speed, and plantarflexor muscle activity in children and adults with CP.

2. An effective framework for developing open-loop exoskeleton motor current controllers that led to improvements in battery energy consumption, efficiency, and audible exoskeleton noise without sacrificing exoskeleton torque production.

3. A bilateral, lightweight, and untethered ankle exoskeleton with the greatest peak torque to mass ratio of any untethered ankle exoskeleton currently available. This system was the second device ever to demonstrate an improvement in metabolic efficiency in unimpaired adults. This exoskeleton platform also featured joint-level sensing that provided real-time insight into exoskeleton performance and created avenues for future research to refine exoskeleton mechanical and controller performance.

4. A practical usability assessment of a lower-limb exoskeleton for impaired and unimpaired users.

5. A refined model of exoskeleton augmentation factor [49] that accounts for battery life to estimate potential metabolic impact during exoskeleton-assisted walking.

6. Design and demonstration of the effectiveness of parallel elasticity to improve ankle exoskeleton mechanical performance and reduce motor energy consumption.

7. Several invention disclosures submitted including:

- US Patent Application No. 17/343,628: Cable-Actuated, Kinetically-Balanced, Parallel Torque Transfer Exoskeleton Joint Actuator with or without Strain Sensing
- US Patent Application No. 62/992,636: Open-Loop Control for Motor Controller
- US Patent Application No. 17/515,300: Differential and Variable Stiffness Orthosis Design with Adjustment Methods, Monitoring and Intelligence

Chapter 2: Ankle Exoskeleton Assistance Can Improve Over-Ground Walking Economy in Individuals with Cerebral Palsy

Authors: Greg Orekhov, Ying Fang, Jason Luque, and Zachary F. Lerner

Abstract

Individuals with neuromuscular impairment from conditions like cerebral palsy face reduced quality of life due to diminishing mobility and independence. Lower-limb exoskeletons have potential to aid mobility, yet few studies have investigated their use during over-ground walking – an exercise that may contribute to our understanding of potential benefit in free-living settings. The goal of this study was to determine the potential for adaptive plantar-flexor assistance from an untethered ankle exoskeleton to improve over-ground walking economy and speed. Six individuals with cerebral palsy completed three consecutive daily over-ground training sessions to acclimate to, and tune, assistance. During a final assessment visit, metabolic cost, walking speed, and soleus electromyography were collected for baseline, unpowered, low, training-tuned, and high assistance conditions. Compared to each participant's baseline condition, we observed a 3.9 ± 1.9% ($p=0.050$) increase in walking speed and a 22.0 ± 4.5% ($p=0.002$) reduction in soleus activity with training-tuned assistance; metabolic cost of transport was unchanged ($p=0.130$). High assistance resulted in an 8.5 ± 4.0% ($p=0.042$) reduction in metabolic cost of transport, a 6.3 ± 2.6% ($p=0.029$) increase in walking speed, and a 25.0 ± 4.0% ($p<0.001$) reduction in soleus activity. Improvement in exoskeleton-assisted walking economy was related to pre-training baseline walking speed ($R^2=0.94$, $p=0.001$); the slower and more impaired participants improved the most. Energy cost and preferred walking speed remained generally unchanged for the faster

and less impaired participants. These findings demonstrate that powered ankle exoskeletons have the potential to improve mobility-related outcomes for some people with cerebral palsy.

Index Terms—Adaptive control, ankle assistance, cerebral palsy, exoskeleton, metabolic cost of transport, over-ground walking, plantarflexion, walking speed, soleus muscle activity.

Introduction

Cerebral palsy (CP) is a set of child-onset neuromuscular disorders and is the most common motor disability in childhood [1]. Individuals with CP have abnormal and inefficient walking patterns [4] that can worsen with age until ambulatory ability is lost [5]. Surgical intervention for pathological walking patterns in CP, such as tendon lengthening, have proven to be only moderately effective in improving long-term mobility [50,51]. Ankle-foot-orthoses (AFOs), commonly prescribed for ambulatory children with CP, also only have limited long-term benefits on gait and mobility [15,17].

Pathological gait patterns associated with CP are characterized by significantly reduced positive ankle joint power during push-off [52], increased hip and knee joint flexion, and reduced ankle plantarflexion and plantar-flexor power [53]. These inefficient gait mechanics drastically decrease walking speed [10], increase the energy cost of walking [54], and reduce levels of physical activity [55]. There is clear need for effective interventions that can improve free-living mobility, walking speed, and efficiency.

Powered ankle exoskeletons have demonstrated potential to reduce metabolic cost of transport during controlled treadmill walking. Several studies utilizing different exoskeleton designs during

Table 1: Participant Information

Subject	Age [Years]	Sex	Height [m]	Mass [kg]	Baseline Condition	GMFCS[b] Level	Walking Preference
P1	9	M	1.37	30.7	Shoe Inserts	I	Exoskeleton
P2	31	M	1.70	53.8	Shod	II	None
P3	23	F	1.47	46.0	AFOs[a] & Walker	III	Exoskeleton
P4	10	M	1.39	38.8	Shod	I	Exoskeleton
P5	9	M	1.26	23.9	Walker	III	Exoskeleton
P6	13	M	1.51	44.0	Shod	I	Exoskeleton

[a]AFOs: Ankle-foot orthoses. [b]GMFCS: Gross Motor Function Classification System (ranges from I-V, from least to most impairment, with level III unable to walk without the use of a walker).

treadmill walking have reduced metabolic cost of transport in unimpaired adults [28,41,56,57]. In a feasibility study with CP participants, powered plantarflexion assistance provided by an untethered exoskeleton during treadmill walking improved net metabolic cost of transport in CP participants by 19 ± 5% compared to walking without wearing the device [47].

To improve mobility, exoskeletons, by definition, must be able to effectively improve efficiency and speed while walking over-ground. Reducing metabolic cost via robotic assistance while walking over-ground is seemingly more challenging than during controlled treadmill walking. Very few exoskeleton studies have assessed energy cost during over-ground walking, and only in a limited number of unimpaired participants; the magnitudes of the reported reductions have been lower compared to treadmill studies. For example, in unimpaired individuals, untethered hip exoskeleton assistance reduced net metabolic cost by 2.7% during over-ground walking and by 3.9% during running compared to no exoskeleton [58]. A similar study with an untethered hip and ankle exoskeleton demonstrated an average 12.1% reduction in net metabolic cost of transport during assisted over-ground walking compared to no exoskeleton for two unimpaired participants [59]. Prior testing of tethered knee exoskeleton assistance demonstrated improved over-ground gait kinematics in children with CP [60]. However, to our knowledge, no published studies have

reported the effects of untethered exoskeleton assistance on net metabolic cost of transport or walking speed during over-ground walking in the CP population.

The overarching goal of this study was to assess the potential for adaptive plantar-flexor assistance from an untethered ankle exoskeleton to improve over-ground mobility outcomes in individuals with CP. We hypothesized that acclimated over-ground walking with the exoskeleton would decrease net metabolic cost of transport, increase self-selected walking speed, and reduce soleus muscle activity compared to walking without the device and walking with the device unpowered.

Methods

This research was approved by Northern Arizona University's Institutional Review Board under protocol #986744. Written informed consent for each adult participant, or written consent from a parent of each minor, was obtained prior to enrollment.

Recruitment

Six ambulatory individuals with CP of varying age, sex, disease severity, and prescription/use of walking aids (e.g. AFO) participated in the study (Table 1). Inclusion criteria included diagnosis of CP, age between 5 and 75 years old, at least 10° of passive ankle plantarflexion, the ability to walk over-ground for at least 6 minutes with or without walking aids, and the ability to understand and follow simple directions. Exclusion criteria included orthopedic surgery within 6 months of participation and any health condition other than CP that could affect participant safety.

Mechanical System

We developed a battery-powered, lightweight ankle exoskeleton capable of providing bilateral plantar- and dorsi-flexion assistance (Fig. 1A). A waist-mounted actuation assembly transmitted force through Bowden cables to pulleys at the ankle joints that rotated footplates relative to rigid shank cuffs (Fig. 1B). This exoskeleton was an improved version of the device used in our previous validation and pilot treadmill walking studies [25,47,61]. To minimize weight and improve long-term functionality, carbon fiber replaced aluminum components for the actuation housing, footplates, calf cuffs, and uprights (Fig. 1A). Reducing weight, particularly of the ankle assembly, is necessary as the metabolic detriment of increased distal leg mass is significant [62,63] and could outweigh any benefit due to powered assistance. Exoskeleton mass, including electronics and battery, was 1.73 kg for a "small" assembly (12 Nm peak torque) and 2.07 kg for a "larger" assembly (18 Nm peak torque); mass was reduced by 6.5% and 5.9%, respectively, compared to the previous design [47]. Participants wore the lightest exoskeleton capable of providing the required personalized torque.

Torque sensors (TRT-500, Transducer Techniques) at the ankle provided feedback to the control system to ensure proper tracking and force-sensitive resistors on the footplate detected transitions between stance and swing phases during gait (Fig. 1B). A custom printed circuit board housed motor drivers (ESCON Module 50/5, Maxon), circuitry for sensor measurements, a Bluetooth module for communication with a MATLAB (R2018b) graphical user interface, and a 32-bit ARM microprocessor (Teensy 3.6, PJRC) for control implementation (Fig 1A).

Adaptive Exoskeleton Control System

There are several difficulties to address when transitioning from treadmill walking at constant, controlled speeds to over-ground walking, particularly step-to-step variability. Changes in terrain,

walking speed, and the added complication of variable walking patterns amongst impaired individuals require an adaptive torque control scheme that parallels and supplements biological gait patterns. We recently developed an instantaneously adaptive proportional joint-moment control scheme (PJMC) that provides assistance proportional to a user's estimated ankle joint moment [64].

To summarize Gasparri *et al.* 2019, the biological ankle joint moment, which can vary between steps, legs, and participants, can be estimated using readings from custom force sensor mechanisms on each footplate. Operation of the controller incorporated a calibration procedure that determined the peak sensor force (F_{ref}) during walking at preferred speed. Forces measured during a step (F_{sen}) were normalized by the calibrated value, resulting in an in an instantaneous sensor force ratio ($R_F = F_{sen}/F_{ref}$). A regression equation used R_F to estimate the instantaneous ankle joint moment ratio $M_{rel}(t)$ used to calculate plantarflexion ankle assistance torque $\tau(t) = \tau_0 M_{rel}(t)$, where τ_0 is the prescribed torque set point (e.g. 10 Nm). The result is exoskeleton torque provided as a ratio of the biological ankle moment at the preferred walking speed. Provided assistance adapts to walking speed changes; can vary between steps, legs, and participants; and supplements biological ankle moment (Fig. 1B).

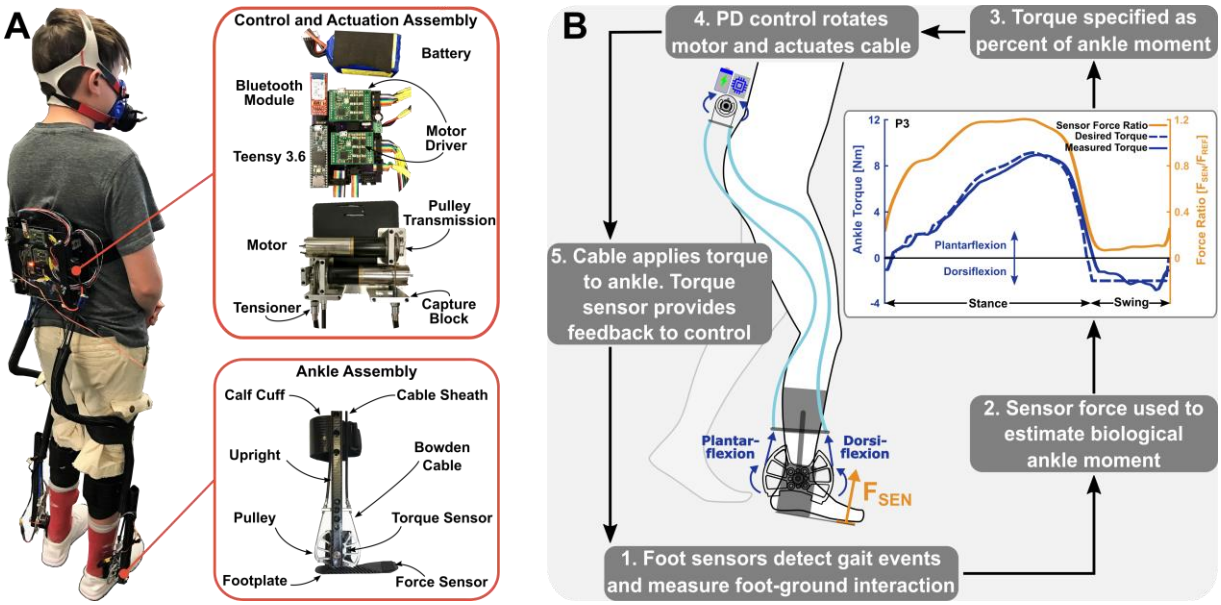

Fig. 1. Mechanical and control system overview. (A) The exoskeleton consisted of the ankle, control, and actuation assemblies. (B) The actuation assembly transmitted force through Bowden cables to rotate the ankle pulley and footplate and provide plantar- or dorsi-flexion assistance. Custom force sensors controlled state transitions and served as input into the adaptive force controller. The proportional joint-moment control scheme adapted to each participant's gait patterns as demonstrated by P3's averaged experimental force sensor ratio, desired torque, and measured torque profiles.

Heel and toe force sensors detected transitions between stance and swing phase of gait (Fig. 1B). Proportional plantarflexion assistance was provided during stance, whereas either dorsiflexion assistance or no assistance was provided during swing.

Experimental Data Collection

All walking trials took place on a 60.96 m (200 ft.) oval track. An operator controlled the exoskeleton through a MATLAB user interface. A trigger sent in MATLAB each time a participant passed through the starting line recorded the duration of the lap and initiated PJMC reference calibration. The operator provided 1-2 Nm dorsiflexion assistance to participants that exhibited foot-drop during swing.

A portable metabolic system (K5, COSMED, Rome, Italy) collected O_2 and CO_2 volume data during all walking trials (Fig. 1A). A technician, walking behind the participant, held the K5 transmitter unit to limit added mass to that of the exoskeleton and metabolic mask. At the start of each visit, prior to walking trials, we measured metabolic rate during quiet standing. Wireless electromyography (EMG) sensors (Trigno, Delsys) collected soleus muscle activity bilaterally.

We evaluated three general walking conditions. "Baseline": each participant's typical daily walking condition that included any physician-prescribed or required aids (e.g. AFOs, walkers); "Unpowered": walking while wearing the exoskeleton with the footplates disconnected from the ankle assembly to isolate the effects of added mass; and "Assisted": walking while the exoskeleton provided powered assistance.

On a pre-study screening visit, a licensed physical therapist completed a history and physical assessment and a technician took exoskeleton-fitting measurements.

On the first intervention visit, participants completed baseline, unpowered, and exoskeleton-assisted walking assessments and exoskeleton walking practice. Exoskeleton walking practice continued for two additional sessions, during which we tuned the torque set point in an attempt to maximize walking economy. The total exoskeleton acclimation time was 96.7 ± 8.2 minutes (mean ± standard error).

During the final visit, a comparison of baseline, unpowered, and three exoskeleton-assisted conditions took place in a randomized order (Table 2). The three assistance levels included "low", "training-tuned", and "high" torque magnitudes. The range spanning "low" to "high" assistance was informed from our prior treadmill study [47], and included to account for variation in walking speed on the final assessment. The average low assistance torque level was 0.225 ± 0.014 Nm/kg.

The average training-tuned assistance torque level was 0.264 ± 0.012 Nm/kg. The high assistance torque level for all participants was 0.300 Nm/kg.

Table 2. Final visit condition testing order.

Order	**P1**	**P2**	**P3**	**P4**	**P5**	**P6**
1	Baseline	Unpowered	Baseline	Baseline	Unpowered	Baseline
2	Training-Tuned	High	Training-Tuned	Low	Training-Tuned	High
3	Low	Low	Low	Training-Tuned	Low	Training-Tuned
4	High	Training-Tuned	High	High	High	Low
5	Unpowered	Baseline	Unpowered	Unpowered	Baseline	Unpowered

Metabolic measurement problems on the final visit for P1 (erroneous readings) and P4 (non-compliant caffeine intake) necessitated reassessment of net metabolic cost of transport on a supplemental visit for the final comparison of baseline, unpowered, and tuned assistance conditions, which happened to be 0.300 Nm/kg. Therefore, P1 and P4's results were included in both the training-tuned and high assistance condition group comparisons, but not in the low condition group. Walking speed analysis was completed from the trials collected on the post-training visit for consistency in speed assessment immediately following the back-to-back acclimation/practice.

Data Analysis

Walking speed was calculated by dividing the lap distance in meters by the average lap time in seconds. Metabolic data were processed using Brockway's standard equation [65] and averaged across the 6th minute of each walking condition. To calculate net metabolic cost of transport, we subtracted each participant's standing metabolic rate from the metabolic rate of each walking condition, and normalized the result by the average walking speed of that condition.

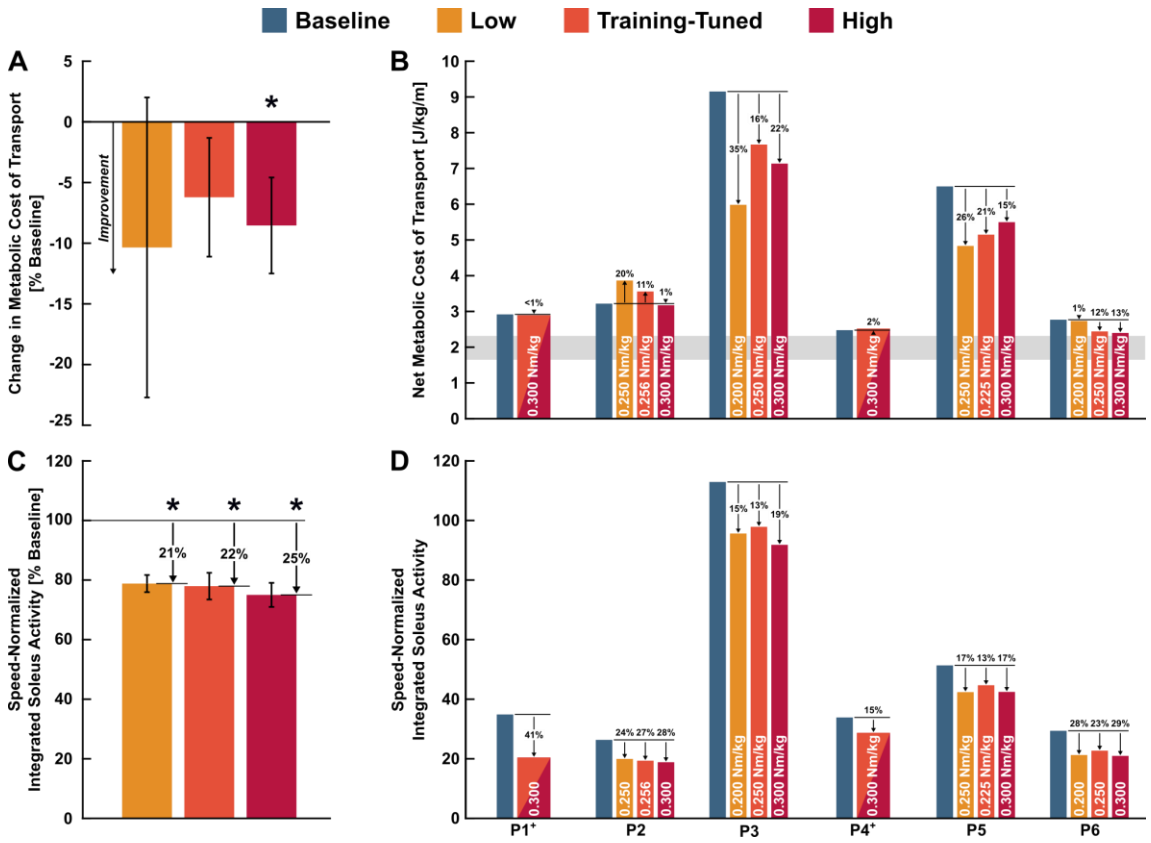

Fig. 2. Net metabolic cost of transport and soleus muscle activity results. Net metabolic cost of transport (top) and soleus muscle activity (bottom) across baseline and assisted over-ground walking conditions. Average ± standard error. * indicates a significant reduction relative to baseline at 95% confidence. White text indicates torque level. (A) Change in group level metabolic cost of transport for low, training-tuned, and high assistance conditions relative to baseline. (B) Participant level net metabolic cost of transport. Gray bar indicates typical range of net metabolic cost of transport reported for unimpaired individuals from 9 years old to adulthood [67]. (C) Change in group level speed-normalized integrated soleus muscle activity for low, training-tuned, and high assistance conditions relative to baseline. (D) Participant level speed-normalized integrated soleus muscle activity. + For P1 and P4, the supplemental visit results were included in both training-tuned and high condition analyses, but not in the low condition analysis.

We analyzed EMG data from an entire lap during the 6th minute of each walking condition. EMG data were band-pass filtered between 15 and 380 Hz, rectified and low-pass filtered at 7 Hz [66]. Filtered EMG data were normalized by the peak value of the baseline condition. The area under the averaged EMG - percent cycle curve during the stance phase was integrated for the baseline and best assistance conditions [66]. Integrated stance phase soleus EMG (iEMG) was averaged

across both legs for each participant and normalized by the average walking speed of that condition.

We performed all calculations and statistical comparisons in MATLAB. Percent change in net metabolic cost of transport, walking speed, and soleus iEMG relative to baseline was calculated for the unpowered and all assisted conditions.

Statistics

Net metabolic cost of transport, walking speed, and soleus iEMG for each walking condition were checked for normality using Kolmogorov-Smirnov tests; all tests confirmed normality. To assess our hypothesis that walking with assistance would improve outcomes over baseline and unpowered conditions, one-tailed *t*-tests assessed significance of percent improvement in net metabolic cost of transport and walking speed between assisted vs. unpowered and baseline conditions. To assess our hypothesis that walking with assistance would reduce speed-normalized plantar-flexor muscle activity, a one-tailed *t*-test assessed significance of percent reduction in speed-normalized soleus iEMG for assisted vs. baseline conditions.

To assist with the design of future intervention protocols, we used linear regression to investigate if a relationship existed between an easily assessed participant characteristic, normalized baseline walking speed, and the maximum observed change in net metabolic cost of transport during exoskeleton-assisted walking. We also used linear regression to assess the relationship between the anticipated detriment to net metabolic cost of transport due to wearing the exoskeleton (unpowered) and the anticipated improvement in net metabolic cost of transport during exoskeleton-assisted walking.

We performed statistical analyses for this feasibility study at 95% confidence; $p \leq 0.05$ indicates significance. Results are reported as mean ± standard error (SE). Data points 1.5 times beyond the inter-quartile range past the first quartile were considered outliers and excluded from the analysis.

Results

All participants had baseline metabolic costs of transport that were generally greater that what is typical for unimpaired individuals [67]. There was an 8.5 ± 4.0% (p=0.042) reduction in net metabolic cost of transport during high assistance compared to baseline (Fig. 2A), and a 17.6 ± 3.2% (p=0.001) reduction compared to the unpowered condition (Fig. 3).

Net metabolic cost of transport did not change during the low (p=0.232) and training-tuned (p=0.130) exoskeleton-assisted walking conditions compared to baseline (Fig. 2A). Compared to

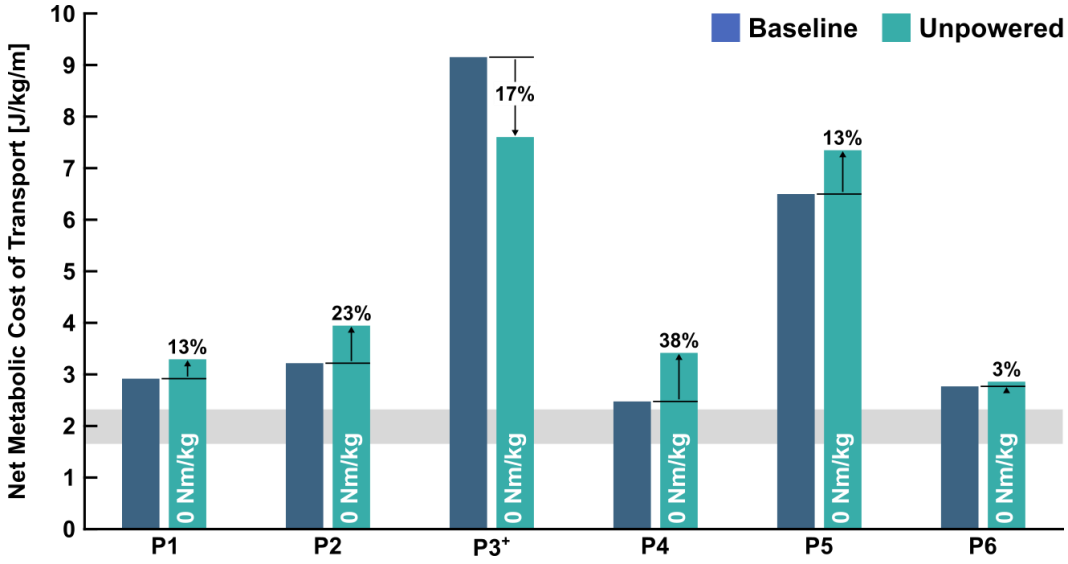

Fig. 3. Net metabolic cost of transport for baseline and unpowered conditions tested during the post-training or supplemental visit. Gray bar indicates typical range of net metabolic cost of transport reported for unimpaired individuals from 9 years old to adulthood [67]. + P3 wore AFOs heavier than the ankle sub-assembly during the baseline condition and consequently experienced a reduction in energy expenditure during the unpowered condition.

the exoskeleton-unpowered condition, metabolic cost of transport did not change with low assistance (p=0.066) but decreased by 15.3 ± 4.6% (p=0.010) with training-tuned assistance.

Participants had increased net metabolic cost of transport when walking with the exoskeleton unpowered compared to baseline with the exception of P3, who wore prescribed AFOs that were heavier than the exoskeleton's ankle assembly (Fig. 3). Omitting P3, the metabolic detriment of walking with the unpowered exoskeleton was 18.0 ± 5.9% (p=0.019) compared to baseline.

Walking speed increased by 5.9 ± 2.5% (p=0.034) with low assistance, by 3.9 ± 1.9% (p=0.050) with training-tuned assistance, and by 6.9 ± 2.4% (p=0.018) with high assistance compared to baseline (Fig. 4). Strong responders to ankle assistance had speed improvements of 17% (P3), 10% (P6), and 6% (P5) over baseline with high assistance. Walking with the exoskeleton unpowered did not significantly affect speed vs. baseline.

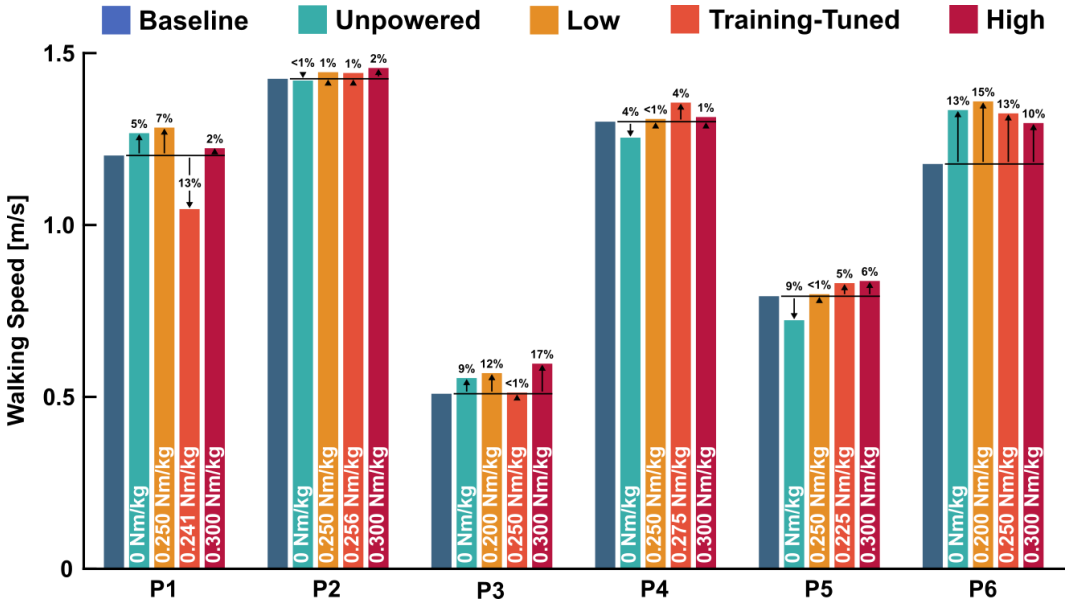

Fig. 4. Self-selected walking speed for baseline, unpowered, and assisted conditions tested during the post-training visit.

Speed-normalized soleus iEMG decreased by 21.2 ± 2.8% (p=0.003) with low assistance, by 22.0 ± 4.5% (p=0.002) with training-tuned assistance, and by 25.0 ± 4.0% (p<0.001) with high assistance compared to baseline walking (Fig. 2CD).

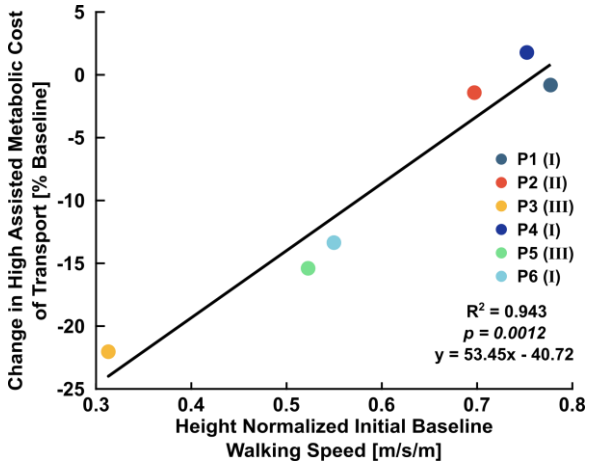

Fig. 5. Relationship between the percent change in high assistance vs. baseline metabolic cost of transport and normalized pre-acclimation baseline walking speed. Normalized walking speed explained 94% of the variance in the change in metabolic cost of transport during walking with high assistance relative to baseline. Roman numerals in parentheses indicate participant GMFCS level.

There was a significant relationship between the height-normalized first visit baseline walking speed and the change in final visit net metabolic cost of transport with high assistance compared to baseline walking (Fig. 5). Participants with slower pre-training baseline walking speeds had greater reductions in final visit net metabolic cost of transport during the high assistance condition (R^2=0.94, p=0.001). There was a significant relationship (R^2=0.75, p=0.025) between the percent change in high assistance vs. baseline net metabolic cost of transport and the percent change in unpowered vs. baseline metabolic cost of transport (Fig. 6).

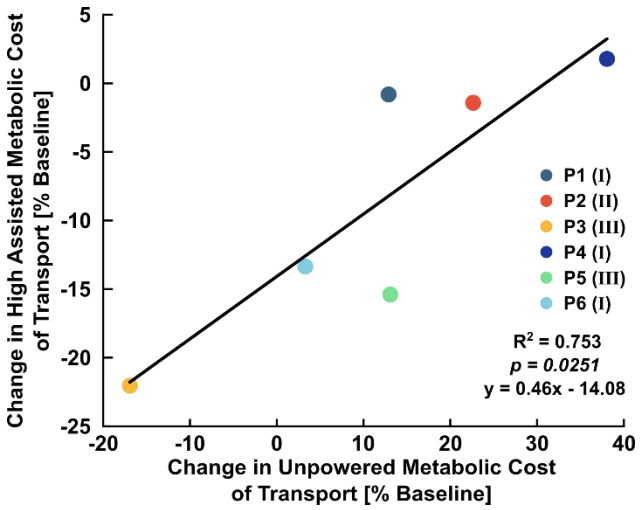

Fig. 6. Relationship between change in net metabolic cost of transport during high assistance condition walking and change in metabolic cost of transport during walking with the exoskeleton unpowered. The metabolic cost associated with wearing the exoskeleton explained 75% of the variance in the change in metabolic cost of transport during walking with assistance relative to baseline. Roman numerals in parentheses indicate participant GMFCS level.

Discussion

We partially accept our primary hypothesis that net metabolic cost of transport would decrease, self-selected walking speed would increase, and soleus muscle activity would decrease during assisted walking compared to unpowered and baseline conditions. While reduction in metabolic cost of transport was significant for only the high assistance condition, all assisted conditions increased self-selected walking speed and reduced soleus muscle activity at the group level. Reduced soleus muscle activity appears to contribute to the improvement in exoskeleton-assisted walking economy. The results show that it is possible, but not guaranteed, to improve mobility-related outcomes with powered plantar-flexion assistance.

We asked our participants which general walking condition they preferred to assess whether participant perception supported our quantitative results. Five of the six participants conveyed a preference for walking with powered assistance to walking without an exoskeleton (Table 1).

Our prior treadmill study demonstrated improved walking mechanics during walking with ankle exoskeleton assistance, including increased total ankle power and improved posture [47]. Anecdotal observation from the present over-ground study suggests that improved gait mechanics combined with our measurement of reduced muscle activity to facilitate the improvement in walking economy. In general, outcomes from this over-ground study were more variable than our prior treadmill study, and improvement in net metabolic cost of transport was more modest (8.5% vs. 19%) [47].

An interesting observation is that all assistance conditions resulted in similar reductions in soleus activity even when metabolic cost of transport relative to baseline was unchanged (Fig. 2C). This result suggests that the motor system "slacks" in an attempt to decrease muscle activation during repetitive tasks [68]. Slacking could partially explain why participants experienced greater improvements in energy expenditure during treadmill walking with a static, on-off controller in our previous study [47] as opposed to over-ground walking with a dynamic, adaptive controller in the present study.

We anticipate that our findings of the potential for untethered ankle exoskeleton assistance to improve over-ground walking economy and speed have clinical relevance and justify continued exoskeleton intervention research in individuals with CP. Reduced energy expenditure during ambulation could facilitate greater accumulation of walking exercise and improve mobility, particularly for highly impaired individuals. Impairment-oriented therapy has proven to largely ineffective [19,69] while modern, more successful approaches to improving motor learning involve task-oriented training specific to the desired outcome [70–72]. In short, gait-specific training has proven most successful in improving walking outcomes. The results of this study

suggest that exoskeleton assistance may be a viable approach to maximizing walking exercise duration.

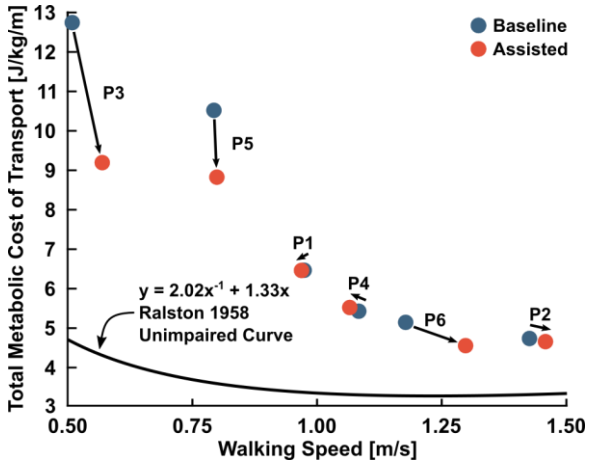

Fig. 7. The effect of exoskeleton assistance on participant energy cost and speed. The Ralston 1958 curve is the energy-speed relationship for unimpaired participants [75]. Powered assistance generally increased walking speed and decreased net metabolic cost of transport in the cohort. The assistance condition that resulted in each individual's greatest reduction in energy cost are depicted.

The presented results should be carefully interpreted. Improvements in over-ground walking economy and speed outcomes remained generally unchanged during walking with assistance for our less impaired participants. The potential for reducing net metabolic cost of transport during assisted walking compared to baseline depends on several device and participant characteristics. For example, finding an optimal magnitude of assistance for each participant remains challenging, particularly for over-ground walking. In most cases for this cohort, the training-tuned assisted condition did not reduce energy expenditure, but other improvements in mobility outcomes were detected. Human-in-the-loop optimization techniques may help address this challenge [28,73].

The metabolic detriment of wearing the device unpowered accounted for 75% of the variance in the maximum change in net metabolic cost of transport with high assistance compared to baseline (Fig. 6). A previous study demonstrated that the metabolic detriment due to wearing the device

depends heavily on the relative body mass [47]. That is, if the exoskeleton is a small fraction of an individual's mass the metabolic detriment of wearing the device is mitigated.

We found that baseline walking speed is a simple predictor of improvement in walking economy from ankle exoskeleton assistance for people with CP. Pre-acclimation baseline walking speed accounted for 94% of the variance in the potential benefit in net metabolic cost of transport with high assistance (Fig. 5). Slower walking speed is associated with greater level of neuromuscular impairment where there may be more capacity for improvement during walking with powered assistance [10,54]. Improvements in propulsion symmetry were found during exoskeleton-assisted walking for stroke survivors, and, similar to our findings, individuals that walked more slowly benefitted the most from assistance [16]. It is possible that our more impaired participants exhibited the greatest reduction in metabolic cost of transport with assistance because they had the most to benefit in terms of posture and ankle function [47,66].

Participants with slow baseline walking speed, moderate-to-severe impairment, and reduced ankle joint function stand to benefit the most from powered assistance but only if the ratio of exoskeleton mass to participant mass is small. P3, P5, and P6 benefited the most from exoskeleton assistance because of slow baseline walking speeds and low metabolic detriments when wearing the device unpowered. More impaired participants could use an exoskeleton in conjunction with forearm support walkers for even greater improvement in metabolic cost of transport [74].

The nonlinear convex relationship between net metabolic cost of transport and walking speed may contribute to our understanding of the effect of exoskeleton assistance during over-ground walking at self-selected speeds. Ralston 1958 suggests a theoretical optimal speed at which energy expenditure is minimized [75]. The impaired participants from this study do not fall on the energy-

speed curve proposed by Ralston, even during assisted walking, but assistance generally reduces deviation from metabolically optimal walking economy (Fig. 7).

Consistent with prior research, we found that baseline metabolic cost of transport generally scaled with GMFCS level [76]. There is limited research on energy-speed relationships for individuals with CP, but one study found that energy expenditure index (EEI) for children with CP decreases with increasing walking speed [77]. However, the EEI-speed curve for CP children is incomplete due to the tendency of impaired individuals to transition to running when asked to walk at high speeds.

The primary limitation of this exploratory study was the small sample size and high variability of age, mass, walking aids, and impairment level, although the variability in participant characteristics may demonstrate translation of presented results to a wider population. Furthermore, we did not perform multiple comparisons correction with the intention that the actual p-values can be interpreted to determine relevance and significance of the presented results.

In conclusion, the presented results support continued research on the development and testing of ankle exoskeletons to improve over-ground mobility for individuals with gait disorders. Lightweight untethered ankle exoskeletons with adaptive control have the potential to reduce net metabolic cost of transport, increase over-ground walking speed, and reduce soleus muscle activity when an appropriate assistance level is used. Exoskeleton-assisted gait training may prove effective as task-specific exercise to improve mobility and motor skills in individuals with neuromuscular impairment. Future studies in this patient population should investigate the effects of long-term functional gait training with ankle exoskeleton assistance.

Chapter 3: Closing the Loop on Exoskeleton Motor Controllers: Benefits of Regression-Based Open-Loop Control

Authors: Greg Orekhov, Jason Luque, and Zachary F. Lerner

Abstract

Lower-limb exoskeletons are widely researched to improve walking performance and mobility in several patient populations. Low-level sensor-less exoskeleton motor control is attractive for consumer applications due to reduced device complexity and cost, but complex and variable transmission system configurations make the development of effective open-loop motor controllers that are responsive to user input challenging. The objective of this study was to develop and validate an open-loop motor control framework resulting in similar or greater performance vs. closed-loop torque control. We used a generalized linear regression to develop two open-loop controllers by modeling motor current during exoskeleton-assisted walking; a "complex" model used desired torque and estimated ankle angular velocity as inputs, while a "simple" model used desired torque alone. Five participants walked at 1.0-1.3 m/s on a treadmill with closed-loop and both open-loop controllers providing ankle exoskeleton assistance. Both open-loop current controllers had similar root-mean-squared torque tracking error ($p=0.23$) compared to the closed-loop torque-feedback controller. Both open-loop controllers had improved relative average torque production ($p<0.001$ complex, $p=0.022$ simple), lower energy consumption ($p<0.001$ for both), and reduced operating noise ($p=0.002$ complex, $p<0.001$ simple) over the closed-loop controller. New control models developed for a different ankle exoskeleton configuration showed similar improvements (lower torque error, greater average and peak torque production, lower energy consumption) over closed-loop control during over-ground walking. These results demonstrate

that our empirical modeling framework can produce open-loop motor controllers that match closed-loop control performance during functional exoskeleton operation.

Index Terms—Adaptive control, ankle assistance, exoskeleton, closed loop, open loop, statistical modeling.

Introduction

Wearable exoskeletons provide mechanical assistance to human joints and seek to augment the user's function or task performance [31]. Most exoskeleton research and commercial development has focused on assisting mobility in patient populations with neuromuscular impairment caused by spinal cord injury, stroke or cerebral palsy [16,24,26,60]. Despite considerable effort, only a few commercially-available devices have measurably improved user performance [78]. Effective high- and low-level control of exoskeleton assistance are two critical components of wearable systems that require special attention, particularly when translating wearable exoskeleton technology from research environments to free-living environments [78]. Research and commercial exoskeleton devices have employed both open- and closed-loop low-level controllers to varying levels of success [56,79].

Torque sensor-less (i.e. low-level open-loop) exoskeleton control is attractive for research- and commercial-grade devices alike due to lower cost and reduced mechanical and software complexity, which may limit the potential for system instability and bodily harm [80,81]. However, adequate performance of open-loop controllers depends on proper system and disturbance characterization. Methods involving disturbance observers typically require an inverted mechanical plant model [80,82] but modeling user-generated disturbances in functional exoskeleton use cases is difficult. Accurate analytical models for cable-driven robot control are

difficult to develop because cable routing and tension affect friction compensation [83]. For lower-extremity exoskeletons designed to conform to each user, variable cable lengths, positions, and routing that change over the gait cycle and are difficult to quantify pose considerable challenges for generalizing characterization of analytical model parameters. Once established, open-loop controllers may require considerably less tuning than closed-loop controllers but, by definition, they may also be less adaptive or responsive. Open-loop characterization of system disturbances can improve exoskeleton performance [82] but the viability of open-loop exoskeleton controllers depends on their responsiveness to user intent across variable walking conditions.

We previously developed a high-level ankle exoskeleton control scheme that provided adaptive assistance proportional to the biological joint moment [64]. We subsequently demonstrated the ability of this controller, implemented on an untethered ankle exoskeleton, to improve over-ground walking economy in individuals with cerebral palsy [26]. In our prior research, the control signal from this high-level algorithm was prescribed via a closed-loop proportional-derivative (PD) torque-feedback controller. While the high-level algorithm nicely adapted the torque set points to variable ankle demand, we observed high battery energy consumption, loud operating noise, and occasional difficulty with tracking peak torque values that were within the mechanical capabilities of the device. These findings, coupled with a desire for a simpler, more reliable system, motivated

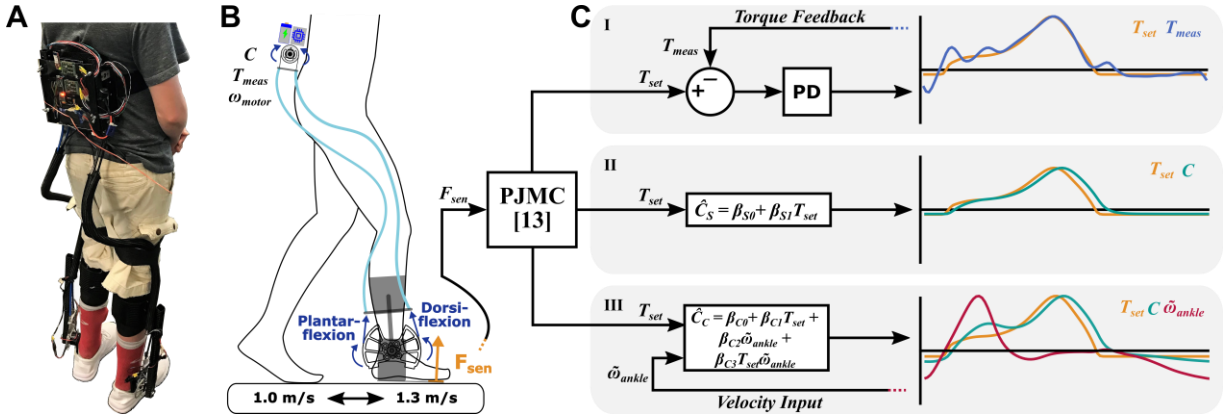

Fig. 8. Mechanical and control system overview. (A) A user wearing our bilateral ankle exoskeleton. (B) Simple visualization of exoskeleton function and experimental setup utilizing a treadmill at typical adult walking speeds [22-24]. Force-sensitive resistors in the footplate detect state transitions and the proportional joint moment control (PJMC) defines the assistance profile T_{set} from the instantaneous force reading F_{sen} [64]. Motors mounted at the hip actuate Bowden cables and rotate a pulley to plantar- or dorsi-flex the ankle joint. A torque sensor at the ankle measures applied torque T_{meas}. On-board sensing and calculations yield motor current C and estimate ankle angular velocity $\tilde{\omega}_{ankle}$ from measured motor velocity ω_{motor}. (C) Simplified block diagrams of closed- and open-loop control schemes. Closed-loop torque control (I) minimizes error between T_{meas} and T_{set} using a PD controller. Simple open-loop current control (II) predicts a current setpoint $\hat{C}_S$ from T_{set} only. Complex open-loop current control (III) predicts a current setpoint $\hat{C}_C$ from T_{set}, real-time velocity input $\tilde{\omega}_{ankle}$, and the interaction of the two signals. β_i are coefficients determined from generalized linear regression and can be found in equations 4-7 of the text. Desired assistance profiles for all control schemes were communicated to motor drivers via pulse width modulation. Plots of experimental data demonstrate the variability in control objectives, input, and output signals for the three control modes.

a renewed investigation into low-level exoskeleton control. Surprisingly, we were unable to find any published work that compared the performance of open-loop vs. closed-loop control during exoskeleton-assisted walking trials.

The objective of this study was to develop an effective empirical modeling framework for generating open-loop motor control schemes of cable-driven ankle exoskeletons that meet or exceed the performance of closed-loop torque-feedback control. We utilized regression-based system modeling to establish relationships between delivered torque and prescribed motor current during walking with the device at variable speeds. Our primary hypothesis was that an

appropriately modeled open-loop current controller could meet and potentially exceed the performance of closed-loop torque-feedback control. Our secondary hypothesis was that inclusion of estimated ankle velocity as a model input would increase the responsiveness and therefore performance of open-loop motor control. We assessed the performance of two regression-based open-loop motor current controllers (velocity- & torque-input and just torque-input) by comparing torque tracking error, average joint torque, energy consumption, and noise production to our standard closed-loop torque-feedback controller during exoskeleton-assisted treadmill walking at moderate speeds. To the best of our knowledge, this is the first study to use regression-based empirical methods to model open-loop exoskeleton dynamics in functional use cases.

Methods

Ankle Exoskeleton and High-Level Control Algorithm

For this study, we used a battery-powered and wireless ankle exoskeleton designed to provide both plantarflexion (PFX) and dorsiflexion (DFX) assistance [26,47]. To summarize exoskeleton design, which has been reported in extensive detail previously, brushless DC motors (EC4-Pole 30 200W, Maxon) worn around the waist actuated Bowden cables that subsequently rotated a pulley at the ankle joint (Fig. 8AB). The pulley was mounted to a carbon fiber footplate that rotated relative to a carbon fiber calf cuff. A torque sensor between the pulley and footplate measured applied torque and, in the case of closed-loop control, provided feedback to a control unit. The control unit included a microprocessor, motor drivers, signal processing chips, and Bluetooth module. Force-sensitive resistors (FSRs) on the footplate detected gait events and informed a simple state machine to appropriately shift between PFX and DFX assistance during the stance

and swing phases of walking (Fig. 8B). A 5-sample moving average filtered torque sensor and FSR analog readings.

The exoskeleton assistance profile was controlled by an instantaneously-adaptive Proportional Joint Moment Controller (PJMC) [64]. PJMC prescribed the desired torque (T_{set}) as in equation (1):

$$T_{set} = T_0 \frac{F_{sen}}{F_{ref}} \quad (1)$$

where F_{sen} was the real-time FSR reading and F_{ref} was the average peak FSR reading during a baseline calibration. The instantaneous sensor force ratio scaled the desired peak torque setpoint T_0 (e.g. 15 Nm) so that it adapted assistance based on the ankle demand across variable walking conditions [64]. The PJMC controller was calibrated once during steady-state walking conditions so that any change in speed was reflected in the real-time FSR reading F_{sen}, which automatically adjusted the desired torque profile [64].

In the case of closed-loop control, a PD controller tracked T_{set} based on the ankle torque (T_{meas}) measured from the embedded torque sensor (Fig. 8C, I). The PD gains for this controller were carefully tuned to track the desired PFX torque while limiting resonance (i.e. oscillation amplitude amplification) and overshoot. This closed-loop controller and these PD gains were used in previous studies that demonstrated clinically significant improvements in joint kinematics, positive ankle joint power, and metabolic cost of transport in people with cerebral palsy [25,26] – outcomes that depended on an appropriately tuned control system.

Open-Loop System Modeling for Low-Level Control

Developing an open-loop motor controller capable of accurately prescribing the high-level adaptive assistance torque from PJMC required precisely characterizing exoskeleton interaction with the user during walking. Instead of attempting to develop and validate an analytical model of the exoskeleton system dynamics coupled with complex human interaction, we sought to develop an empirical model to characterize the system experimentally. We first used a basic open-loop current controller to collect the experimental data for empirically predicting motor current as a function of ankle torque alone or both ankle torque and motor velocity during walk across a range of speeds and PFX assistance levels. The basic open-loop current controller specified motor current (C_{set}) as in equation (2):

$$C_{set} = T_{set}\left(\tau_m R_{gb} R_p \varepsilon_{mgb}\right)^{-1} \qquad (2)$$

where the torque setpoint (T_{set}) was divided by the motor torque constant (τ_m), gearbox and pulley gear ratios (R_{gb} and R_p, respectively) and motor and gearbox efficiencies (ε_{mgb}). The gearbox and pulley ratios were 103:1 and 2.3:1, respectively. The microcontroller recorded the motor current (C) and the average motor angular velocity (ω_{motor}) from the motor drivers (ESCON 50/8, Maxon). Maxon motors use hall sensors to detect shaft velocity. Ankle angular velocity ($\widetilde{\omega}_{ankle}$) was estimated using motor and exoskeleton gear ratios assuming no transmission losses, as in equation (3):

$$\widetilde{\omega}_{ankle} = \omega_{motor}\left(R_{gb} R_p\right)^{-1} \qquad (3)$$

Collecting data during functional use cases ensured that system characteristics, such as energy lost due to friction, and human disturbances, such as walking speed and assistance profile variability, were sufficiently captured and subsequently modeled. Motivated by the critical role of positive

mechanical ankle joint power for efficient locomotion [23,34,47,84] and based on the rationale that DC motors operate with an inverse relationship between motor torque production and output velocity [85], we hypothesized that motor current could be accurately modeled using the measured torque (T_{meas}) and the estimated ankle angular velocity ($\widetilde{\omega}_{ankle}$).

We developed a generalized linear model (GLM) of motor current in MATLAB using T_{meas} and $\widetilde{\omega}_{ankle}$ as inputs assuming normal distributions and a unity link function [86]. Positive $\widetilde{\omega}_{ankle}$ values correspond to ankle PFX. All coefficients of the fitted model, including the interaction of T_{meas} and $\widetilde{\omega}_{ankle}$, were significant at 95% confidence. The complex current model ($\hat{C}_C$) coefficients are summarized below (Eq. 4).

$$\hat{C}_C = -0.124 + 0.282\,T_{meas} + 0.0578\,\widetilde{\omega}_{ankle} + 0.002\,T_{meas}\,\widetilde{\omega}_{ankle} \quad (4)$$

We also developed a simple motor current model ($\hat{C}_S$) with only T_{meas} as an input (Eq. 5) for the purpose of testing our secondary hypothesis that ankle velocity is important for modeling exoskeleton responsiveness.

$$\hat{C}_S = -0.055 + 0.291T_{meas} \quad (5)$$

To employ the regression equations for open-loop control, we replaced T_{meas} with T_{set} such that both models predict current using the adaptive desired assistance profile defined by PJMC (Fig. 8C).

The parameter coefficients of both GLMs can be interpreted to make informed predictions about exoskeleton performance when using these regression-based open-loop current controllers. Since both models are dominated by the torque term, the predicted motor current profile will closely match the desired torque assistance profile. We also expect that the complex (velocity- & torque-

input) open-loop controller will be more responsive than the simple (just torque-input) open-loop controller because the velocity term in Eq. 4 will increase current in response to high ankle angular velocity (Fig. 8C), such as during heel strike and toe-off regions of gait. Furthermore, the interaction term in the complex model represents mechanical ankle joint power; this term likely favorably increases current production when torque and ankle angular velocity have the same direction.

Table 3. Participant characteristics. Experience refers to familiarity walking in the exoskeleton prior to data collection. Preference of controller (closed-loop, simple open-loop, or complex open-loop) was surveyed after data collection. SP1 completed the over-ground experiment.

User	**Age [Years]**	**Sex**	**Mass [kg]**	**Experience**	**Controller Preference**
P1	30	F	59.4	Advanced	Simple open
P2	27	M	69.5	Beginner	Closed
P3	25	M	86.6	Advanced	Complex open
P4	21	F	77.2	Beginner	Closed
P5	31	M	65.8	Advanced	Complex open
SP1	25	M	81.6	Advanced	Simple open

Exoskeleton Motor Controller Comparison Experiment

We evaluated the low-level exoskeleton motor controllers during a treadmill walking experiment approved by Northern Arizona University's Institutional Review Board under protocol #986744. Five unimpaired individuals participated in the study (Table 3). Written informed consent for each participant was obtained prior to enrollment. Exclusion criteria included any health condition that could affect walking ability or participant safety. An operator controlled the treadmill and exoskeleton through a MATLAB graphical user interface. Participants wore the exoskeleton and walked on a treadmill at 1.0 m/s for PJMC baseline calibration; the same participant-specific FSR

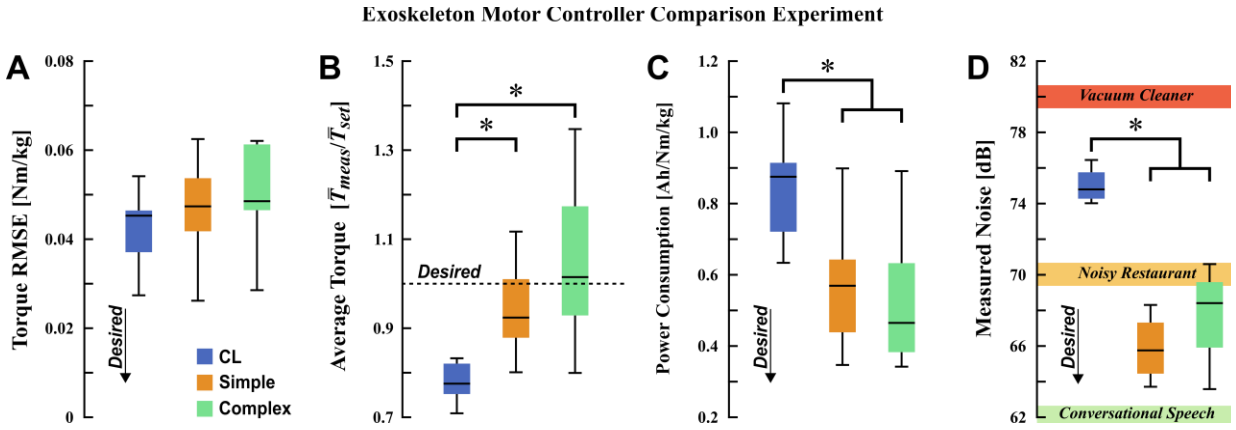

Fig. 9. Summary of treadmill controller performance metrics and statistical analyses. Minimum, first quartile, median, third quartile, and maximum values shown. * indicates a significant difference between control modes at 95% confidence. Desired trends are indicated with arrows and dashed lines. Closed-loop (CL), simple open-loop, and complex open-loop controller results shown. (A) Total stance phase exoskeleton torque root-mean-square error (RMSE). Torque RMSE quantifies overall controller effectiveness in tracking the desired torque T_{set}. (B) Measured torque averaged across each stance phase, $\bar{T}_{meas}$, normalized by the average desired torque of the same step, $\bar{T}_{set}$. The ratio of measured to desired torque quantifies controller overshoot and general system torque capacity. (C) Energy consumption normalized by average measured torque $\bar{T}_{meas}$. (D) Measured exoskeleton noise during operation. Some typical noise scenarios present a sense of volume scale.

sensor calibration was used for all trials. All participants were prescribed 0.25 Nm/kg peak PFX torque assistance.

Participants walked with closed-loop torque control, simple (torque-input) open-loop current control, and complex (velocity- & torque-input) open-loop current control in single-blind randomized order. Participants were told to walk normally prior to the experiment. No coaching or instructions were provided during walking trials. Treadmill speed was set to 1.0 m/s, then 1.3 m/s, and back to 1.0 m/s; these speeds are within the typical ranges for children and adults with cerebral palsy [10,26], stroke victims [16], and unimpaired adults [28,87,88]. The acceleration/deceleration between speeds was set to 0.02 m/s^2. The time spent at each steady-state speed interval was 3 minutes.

We recorded the desired torque set point (T_{set}), measured torque (T_{meas}), motor current (C), and motor angular velocity (ω_{motor}). Exoskeleton state transitions separated signals into PFX and DFX regions corresponding to stance and swing phases of gait, respectively [26]. Controller performance analysis and assessment, performed across the entire stance phase, was completed using MATLAB.

Primary controller performance outcome measures included deviance from the desired control signal, overall torque and power generation capacity, battery energy consumption, and noise. We calculated root-mean-squared error (RMSE) between T_{set} and T_{meas} to quantify assistance profile tracking performance. Average stance phase measured torque $\bar{T}_{meas}$ was calculated and normalized by corresponding average demand torque $\bar{T}_{set}$ to assess average torque capacity and overall assistance potential. Similarly, peak torque tracking was quantified by the ratio of maximum demanded torque T_{set} and corresponding measured torque T_{meas}.

Battery energy consumption was calculated by numerically integrating motor current C with respect to time and is reported in typical units of battery capacity in Ah. We normalized energy consumption by $\bar{T}_{meas}$ to evaluate power use relative to torque produced. Noise levels were calculated by averaging measured sound recordings over the course of each trial.

The demand assistance profile T_{set} is generated in real-time to instantaneously adapt the torque profile to variations in speed and terrain [64]. Additionally, angular velocity is an important contributor to ankle power [23,34] and a controller must be able to provide torque assistance without limiting joint range of motion. To assess controller kinematic adaptability, motor peak PFX (toe-off) angular velocities for each stance phase were also collected and averaged.

Framework Verification Experiment

To verify the effectiveness of our controller design framework and demonstrate utility beyond treadmill walking, we recruited an additional participant SP1 (Table 3) to perform over-ground exoskeleton walking experiments. The same general protocol was followed to build new open-loop GLMs and compare closed-loop and open-loop controllers. We purposefully used a different exoskeleton mechanical assembly, including different motors (EC4-Pole 22 120W, Maxon), gearbox and pulley ratios (123:1 and 2.9:1, respectively), and actuation cable lengths than the exoskeleton used for treadmill experiments. The resulting complex and simple models for this exoskeleton are summarized in equations (6) and (7), respectively. As before, we replaced T_{meas} with T_{set} when implementing the open-loop controllers (Fig. 8C, II and III).

$$\hat{C}_C = 0.343\, T_{meas} + 0.0236\, \widetilde{\omega}_{ankle} + 0.004\, T_{meas}\, \widetilde{\omega}_{ankle} \quad (6)$$

$$\hat{C}_S = 0.373\, T_{meas} \quad (7)$$

SP1 walked one lap around a 60 m track with 0.25 Nm/kg PFX assistance and 1 Nm DFX assistance for each controller. Additionally, SP1 walked one lap with no assistance or resistance using the closed-loop controller (i.e. zero-torque control [47]) to capture motor behavior under minimal-load conditions. All trials utilized the same PJMC baseline calibration. During each lap, we captured T_{set}, T_{meas}, C, and ω_{motor}. Each lap contained between 37 and 38 complete strides and each stride was treated as an individual observation. Average walking speed, estimated from individual lap speeds, was 1.25 ± 0.03 m/s.

Similar data processing as for the treadmill experiment was used to calculate performance metrics. In addition to the previously mentioned metrics, we also compared motor velocity during toe-off

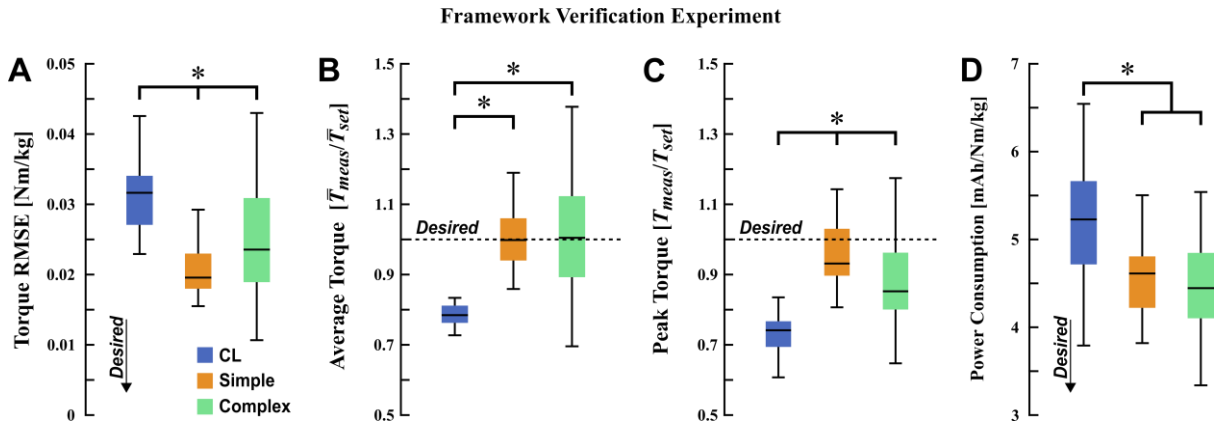

Fig. 10. Summary of over-ground controller performance metrics and statistical analyses. Minimum, first quartile, median, third quartile, and maximum values shown. * indicates a significant difference between control modes at 95% confidence. Desired trends are indicated with arrows and dashed lines. Closed-loop (CL), simple open-loop, and complex open-loop controller results shown. (A) Stance phase exoskeleton torque root-mean-square error (RMSE) per step. Torque RMSE quantifies overall controller effectiveness in tracking the desired torque T_{set}. (B) Measured torque averaged across each stance phase, $\bar{T}_{meas}$, normalized by the average desired torque of the same step, $\bar{T}_{set}$. The ratio of measured to desired torque quantifies controller overshoot and general system torque capacity. (C) The ratio of measured to peak demanded torque T_{meas}/T_{set} quantifies peak torque tracking and capacity. (D) Energy consumption per step normalized by the average measured torque of that step $\bar{T}_{meas}$.

between the three controllers and the closed-loop zero-torque control trial. Noise data was not collected during these experiments.

Statistics

Samples from each walking speed were pooled together for statistical analysis to collectively quantify performance across all experimental conditions. The typical number of strides (mean ± standard deviation) averaged and analyzed was 311.8 ± 14.1 strides for closed-loop control, 312.2 ± 9.1 strides for simple open-loop control, and 313.4 ± 14.2 strides for complex open-loop control. All experimental data were tested for outliers in MATLAB within and across participants. Outliers 1.5 times the interquartile range past the first or third quartiles for the data set were removed from further analysis. Each performance metric (e.g. torque RMSE, energy consumption, etc.) was

treated as an independent set of samples when testing for outliers. When an outlier was removed, corresponding observations were also removed from each control mode within the specific metric to maintain a balanced study design. One-way repeated measures analyses of variance (ANOVAs) were used to detect differences in performance metrics between the closed-loop torque control, simple open-loop current control, and complex open-loop current control schemes. Significantly different means detected by ANOVAs were further analyzed with *post-hoc* Tukey tests with corrections for multiple comparisons. All statistical analyses were performed at 95% confidence.

Results

During the main controller comparison experiment, all three controllers had statistically similar torque RMSE during stance phase assistance (p=0.23, Fig. 9A). Both open-loop controllers had a significantly improved average relative torque ratios (T_{meas}/T_{set}) compared to the closed-loop controller (p=0.022 for the simple model, p<0.001 for the complex model, Fig. 9B); average torque ratio was similar between the two open-loop controllers (p=0.46). Both open-loop controllers had a similar peak relative torque ratio vs. the closed-loop controller (p=0.21). The simple and complex open-loop controllers had lower energy consumption (p<0.001 for both, Fig. 9C) and noise generation (p<0.001 for the simple controller, p=0.002 for the complex controller, Fig. 9D) compared to the closed-loop controller. Participants were asked to state their controller preference (Table 3) and provide a qualitative comparison of the three control modes.

During the framework verification experiment, all three controllers had significantly different torque RMSE during stance (Fig. 10A). Closed-loop torque control had the highest torque RMSE (p<0.001 vs. both) whereas simple open-loop control had the lowest overall torque RMSE (p=0.010 vs. complex open-loop). Both open-loop controllers had significantly improved average

relative torque ratios compared to the closed-loop controller ($p<0.001$ for both, Fig. 10B). All three controllers had significantly different peak torque ratios ($p<0.001$ closed-loop vs. both open-loop controllers, $p=0.009$ simple vs. complex open-loop, Fig. 10C); simple open-loop had the highest ratio whereas closed-loop control had the lowest. Closed-loop torque control had the highest energy consumption per step ($p<0.001$ vs. both open-loop controllers, Fig. 10D). Simple and complex open-loop controllers had similar energy consumption ($p=0.74$).

Discussion

We accept our primary hypothesis that an appropriately modeled open-loop current controller can meet or exceed the performance of closed-loop torque-feedback control for providing adaptive cable-actuated ankle exoskeleton assistance during walking. Specifically, both open-loop current controllers had similar torque profile RMSE and peak relative torque ratios vs. the closed-loop torque controller, and both open-loop controllers also had greater average measured to demanded torque, better (lower) battery energy consumption relative to torque output, and quieter function than the closed-loop controller during treadmill walking (Fig. 9). Both open-loop controllers adapted well to changes in walking speed and torque demand, consistently producing good profile tracking. We accomplished this by modeling human-robot interactions using generalized linear regression during functional use cases, thereby capturing exoskeleton and human dynamics including inefficiencies due to friction and transmission losses. This empirical method was quick (<15 minutes) and effective in modeling two different cable-actuated exoskeletons. The framework verification experiment corroborated the treadmill results and provided evidence that our proposed empirical method for developing open-loop controllers can be generalized to other cable-actuated exoskeletons. Though promising, the results should be interpreted with care as this

preliminary study involved few, unimpaired participants under controlled conditions. Future work will expand the quantity and variety of participants and walking scenarios.

We asked participants to identify their preferred controller to assess whether perception matched the quantitative performance results. Controller preference was varied: two participants preferred the closed-loop torque controller, two preferred the complex model open-loop controller, and one preferred the simple model open-loop controller (Table 3). The supplemental participant also preferred the simple open-loop controller, splitting preference evenly among the three controllers. The two participants that preferred closed-loop torque control stated that they liked the responsiveness compared to the open-loop controllers that felt "stiffer" and "less responsive". On the other hand, most participants commented that open-loop control felt more "consistent" and "assistive", particularly in regards to peak torque, which supported the results showing improved relative torque production when walking with open-loop controllers.

We are unable to prove or disprove our secondary hypothesis that the inclusion of motor velocity as a model input would result in improved open-loop controller performance. There were no statically significant differences between the simple and complex open-loop controller performance metrics during the main treadmill experiment (Fig. 9), while the simple open-loop controller had lower torque RMSE vs. the complex controller during the framework verification experiment (Fig. 10). Prompted by these surprising results, we completed a post-hoc bench-top analysis to verify our ability to estimate ankle velocity from motor velocity (i.e. Eq. (3)). We observed considerable compliance in the ankle joint's angular position (~15°) when the motors were stalled, confirming our suspicion that motor angular velocity cannot be used to accurately estimate ankle angular velocity due to mechanical elasticity and deformation of the Bowden cable transmission system at high torque. While including scaled motor velocity (i.e. estimated ankle

velocity) as a model input was ineffective at improving open-loop motor control, future work should evaluate the use of an angular velocity sensor in-line with the ankle joint.

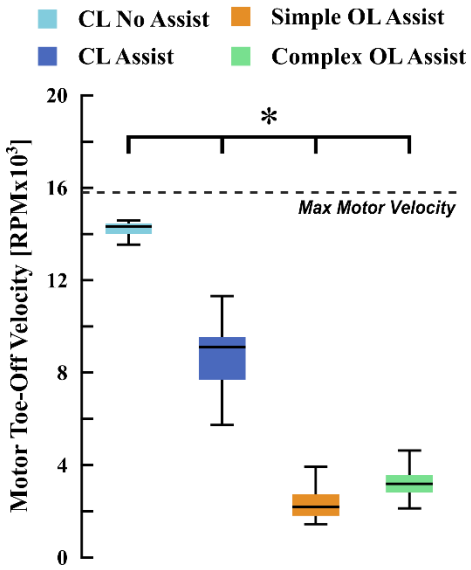

Fig. 11. Comparison of motor toe-off velocity during over-ground walking. The closed-loop controller operating in zero-torque control offers a "no-load" velocity target. The open-loop (OL) controllers and the closed-loop (CL) controller with assistance were all significantly different from each other and from the no-load velocity target. The maximum permissible motor velocity is 15800 RPM.

We initially planned to analyze peak ankle angular toe-off velocity and compare PFX power production for each controller. Peak ankle joint mechanical power typically occurs during the late stance phase of walking when the ankle produces large plantar-flexor angular velocity and moment during push-off [34,84,89]. User comments that the open-loop controllers felt "stiffer" encouraged a closer look at motor behavior during assistance. We discovered that all three controllers significantly underestimated peak biological ankle velocity during toe-off [90]. This was likely the result of series elasticity across the transmission system and ankle assembly, but also the inverse relationship between torque production and angular velocity for DC motors [85]. For example, the

closed-loop controller had reduced toe-off velocities when providing assistance vs. when operating in zero-torque control ($p<0.001$, Fig. 11, 12B).

Open-loop control had lower toe-off velocity than closed-loop control, which may have contributed to user perception of "stiffness" but also improved torque production efficiency (Fig. 11, 12). The open-loop controllers may have utilized transmission friction and elastic deformation of carbon fiber exoskeleton components to "build" torque during early-mid stance that subsequently was "released" during toe-off, requiring less motor power. The closed-loop controller, though appropriately tuned, suffered from low peak torque and high energy consumption due to resonance in early stance (Fig. 12). User perception was that assistance was much stronger with open- vs. closed-loop control. We plan to conduct a more-detailed biomechanical analysis using motion capture and explore methods for improving responsiveness in the open-loop controllers; a direct measurement of ankle joint velocity may improve the complex (velocity- & torque-input) controller performance and provide an opportunity to modify closed-loop control to reduce oscillation.

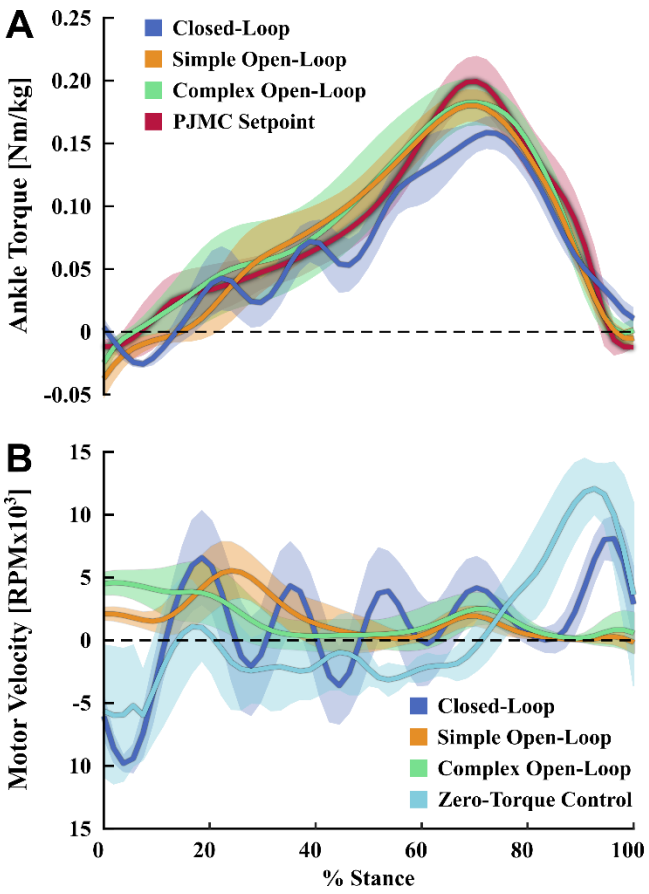

Fig. 12. Stance phase ankle torque and motor velocity profiles during over-ground walking. Lines designate the mean profile and shaded regions show standard deviations. (A) The proportional joint moment controller (PJMC) prescribed a target ankle torque [63]. The closed-loop controller was tuned to track the PJMC target but struggled to reach peak demanded torque (Fig. 8C, I). The open-loop controllers used the PJMC target torque to prescribe motor current (Fig. 8C, II and III) and reached similar peak torques. (B) Zero-torque control offers a no-load velocity reference. The region beyond 70% stance phase demonstrates the deviation between assisted and un-assisted motor angular velocities.

Future work should quantify the effects of closed-loop vs. open-loop motor controllers upon human biomechanics and energetics. Several previous studies demonstrated clinically significant improvements in joint kinematics, positive ankle power, muscle activity, and metabolic cost of transport in impaired populations using the closed-loop torque-feedback controller [25,26,47]. There is evidence that humans entrain (i.e. adapt biomechanics) to the frequency of external stimuli such as mechanical perturbations [91,92]. While torque tracking was similar between open- and

closed-loop motor control, user perception of "more consistent" assistance for open-loop control suggests that it may be more effective than closed-loop controllers at improving gait mechanics in individuals with neuromuscular impairment as the rhythmic nature of open-loop control may encourage a consistent step cadence and a reduction in muscle firing pattern variability.

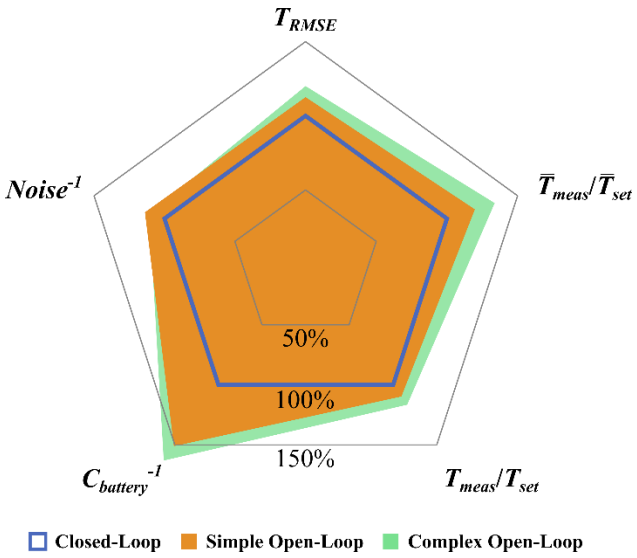

Fig. 13. A radar plot of the primary controller performance metrics. Treadmill results from the simple and complex open-loop controllers are reported as a percentage of the results from closed-loop control indicated with a blue dashed pentagon. The open-loop controllers had reduced noise and energy consumption $C_{battery}$, increased average stance torque ratio $\bar{T}_{meas}/\bar{T}_{set}$, and similar torque tracking T_{RMSE} and peak stance torque ratio T_{meas}/T_{set}.

Open-loop control may be attractive for commercialization because it produced significantly reduced noise generation and had more efficient torque production. The open-loop controllers averaged 127% of the closed-loop average torque output with 64% of the battery consumption and only 89% of the audible decibel readings (Fig. 13). The 11% reduction in decibel measurement, or around 8 dB, means that the open-loop controllers were nearly half as loud as the closed-loop

controller due to the logarithmic scale; noise level went from close to that of a vacuum cleaner for closed-loop control to close to that of conversational speech for open-loop control.

In summary, the results of this study show that a simple empirical modeling framework can be effective for developing sensor-less motor controllers for cable-actuated robotic exoskeletons. Both simple (torque-input only) and complex (velocity- and torque-input) open-loop controllers matched or exceeded the torque tracking and capacity of our finely-tuned closed-loop torque-feedback controller with significantly lower noise and energy consumption during walking (Figs. 9, 10, 12A, & 13). It remains unclear whether velocity input is beneficial for open-loop controller performance, though the high variability in performance of the complex controller suggests better sensitivity to different gait patterns than the simple controller. Low-level open-loop exoskeleton motor controllers hold potential to improve exoskeleton performance and reduce cost, weight, and complexity by eliminating the need for torque-feedback sensors. The resulting improvements in energy consumption and noise generation may facilitate commercialization, long-term intervention studies, and out-of-lab use. Future work will address the limitation of estimating ankle velocity using motor hall sensors and elucidate exoskeleton-user interaction.

Chapter 4: Usability and Performance Validation of an Ultra-Lightweight and Versatile Untethered Robotic Ankle Exoskeleton

Authors: Greg Orekhov[1], Ying Fang[1], Chance F. Cuddeback[1], Zachary F. Lerner[1,2]*

Affiliations: [1]Department of Mechanical Engineering, Northern Arizona University, Flagstaff, AZ, USA
[2]College of Medicine – Phoenix, University of Arizona, Phoenix, AZ, USA

Abstract

Background

Ankle exoskeletons can improve walking mechanics and energetics, but few untethered devices have demonstrated improved performance and usability across a wide range of users and terrains. Our goal was to design and validate a lightweight untethered ankle exoskeleton that was effective across moderate-to-high intensity ambulation in children through adults with and without walking impairment.

Methods

Following benchtop validation of custom hardware, we assessed the group-level improvements in walking economy while wearing the device in a diverse unimpaired cohort (n = 6, body mass = 42-92 kg). We also conducted a maximal exertion experiment on a stair stepping machine in a small cohort of individuals with cerebral palsy (CP, n = 5, age = 11-33 years, GMFCS I-III, body mass = 40-71kg). Device usability metrics (device don and setup times and System Usability Score) were assessed in both cohorts.

Results

There was a 9.9 ± 2.6% (p=0.012, range= 0-18%) reduction in metabolic power during exoskeleton-assisted inclined walking compared to no device in the unimpaired cohort. The cohort with CP was able to ascend 38.4 ± 23.6% (p=0.013, range= 3-133%) more floors compared to no device without increasing metabolic power (p=0.49) or perceived exertion (p=0.50). Users with CP had mean device don and setup times of 3.5 ± 0.7 minutes and 28 ± 6 seconds, respectively. Unimpaired users had a mean don time of 1.5 ± 0.2 minutes and setup time of 14 ± 1 seconds. The average exoskeleton score on the System Usability Scale was 81.8 ± 8.4 ("excellent").

Conclusions

Our battery-powered ankle exoskeleton was easy to use for our participants, with initial evidence supporting effectiveness across different terrains for unimpaired adults, and children and adults with CP.

Trial registration

Prospectively registered at ClinicalTrials.gov (NCT04119063) on October 8, 2019.

Keywords

Ankle, exoskeleton, incline walking, stair ascent, metabolic power, cerebral palsy, dorsiflexor assistance, plantarflexor assistance

Background

Ankle exoskeletons hold potential to augment walking performance in unimpaired individuals and in individuals with neurological conditions [16,30–32]. The ankle joint is a frequent target for powered assistance due to its critical role in efficient bipedal locomotion [33–35] and because it is

a commonly affected joint in individuals with neurological deficits [36,37]. Individuals with cerebral palsy (CP), for example, typically have ankle plantarflexor weakness and limited push-off power that contributes to slow, inefficient walking, particularly on graded terrain, like stairs [38–40].

Unburdened by the need to carry motors and a power supply, users walking with tethered ankle plantarflexor assistance have consistently demonstrated improved walking economy for nearly a decade [28,35,44,45]. However, achieving improvements in walking economy with untethered ankle exoskeletons has apparently been more challenging, with only a small number of studies reporting activity performance benefits compared to walking without the device [16,22,25,26,31]. Untethered ankle exoskeletons capable of mobility augmentation outside of the laboratory follow two general design approaches: placing motors on the shank close to the joint or placing motors at the waist. Opting to minimize mass and the physical profile added to the lower-limb, Awad et al. [16,22] developed a soft exosuit with waist-mounted motors that improved paretic limb function, walking speed and walking economy in stroke survivors. Mooney et al. [31] took a shank mounted motor approach instead, and addressed the metabolic detriment of adding mass distally on the leg by incorporating a clever mechanical design achieving high torque and power output, and demonstrated improvements in loaded and unloaded walking in healthy adults; this appears to be the only published work demonstrating a group-level improvement in energy efficiency in unimpaired individuals when walking with an untethered, battery-powered ankle exoskeleton compared to no device.

For several years, our group has worked on untethered, low-torque ankle exoskeletons for children and young adults with CP. We have demonstrated that bilateral assistance proportional to the user's biological ankle moment during stance phase ([61,64]) can improve key metrics such as energy

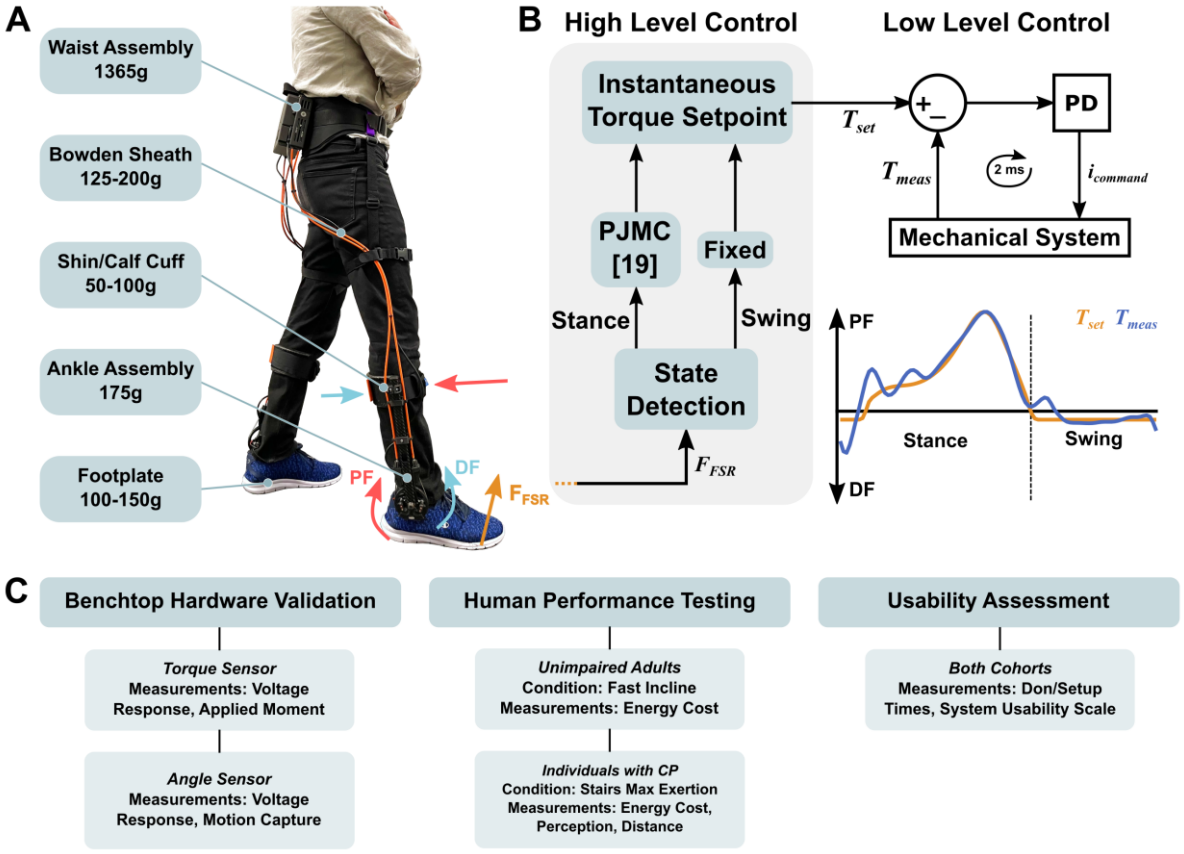

Fig. 14. Exoskeleton mass breakdown, exoskeleton control overview, and protocol summary. A. Device components and mass. Values are mass per leg except for the waist assembly. B. High- and low-level control layers. The high-level controller was responsible for gait event detection (i.e., toe-off and heel strike) and assistive torque profile generation. During stance, a forefoot force sensor signal was an input to a proportional joint moment controller (PJMC) that generated an adaptive plantarflexor torque profile in real time [64]. During swing, a constant dorsiflexor torque was prescribed. The low-level controller tracked the plantarflexor and dorsiflexor torque profiles using a closed-loop PD controller. C. A summary of the experiments, cohorts, conditions, and measurements analyzed in this study.

expenditure and walking speed in small cohorts with CP during level walking [26,27]. However, early prototypes had poor reliability and durability, and proved ineffective for individuals of body mass greater than approximately 45 kg because of limited torque production and significant motion of the ankle assembly relative to the shank and foot. Additionally, these prior exoskeletons were cumbersome to don and doff, designed without consideration for usability, and control was limited to a computer-based researcher interface. Usability factors are important yet under-researched

aspects of wearable lower-limb exoskeleton design that hold practical implications for real-world deployment. Devices intended to augment mobility in the community should be easy to don and operate, with portable and intuitive user interfaces. The ability of individuals with CP to put on and operate an ankle exoskeleton without researcher or technician intervention remains unknown.

The first goal of this study was to design a novel cable-driven ankle exoskeleton, validate custom torque and angle sensors, and evaluate electromechanical performance during ambulation (Fig. 14). Our second objective was to highlight the relevance and versatility of this device by demonstrating its ability to reduce the energy cost of fast incline walking in healthy adults, and on distance achieved during a maximal exertion stair-stepping exercise in CP. We selected these moderate- to high-intensity activities for these human performance experiments because we believe such activities reflect the real utility of ankle exoskeletons in both unimpaired and impaired populations, namely, augmenting ambulatory activities that have elevated ankle plantarflexor demand. We hypothesized both cohorts would have significant improvements while walking with vs without the device. Our final objective was to complete a usability assessment, quantifying the time for users or their caretakers, if applicable, to don and set up the device without researcher intervention. We hypothesized that individuals could don, calibrate, and receive assistance from the device in less than five minutes.

Methods

Exoskeleton Design

We designed a lightweight bilateral, bidirectional battery-powered ankle exoskeleton (Fig. 14AB). Waist mounted motors actuated a pulley assembly at the ankle via a chain-to-cable transmission system. The instrumented ankle joint pulley was mounted within a carbon fiber tube that also

supported cable housing reaction forces. Carbon fiber footplates and shank cuffs provided rigid yet comfortable load transfer interfaces. Sensors on the footplate informed a high-level controller used to provide adaptive plantarflexor torque during stance phase and/or constant dorsiflexor torque during swing phase (Fig. 14B). A custom embedded torque transducer at the ankle provided feedback for low-level closed-loop torque control. The total bilateral mass of the device ranged from 2.4 to 2.6 kg, depending on the cable length, and size of the footplates and cuffs (Table 4). The exoskeleton's peak torque output was 30 Nm. Between 50 and 65% of the total exoskeleton mass (depending on the configuration) was contained within the waist assembly so that the detriment of distally added weight on metabolic power was minimized [63]. Mass minimization, modularity, comfort, and ease of donning and operation were important criteria that guided the design.

Table 4. Exoskeleton mass breakdown.

Component[1]	**Mass (kg)**	**Location on Body**
Waist assembly	1.37	Waist
Cable transmission (x2)	0.31	Thigh
Ankle assembly and cuff (x2)	0.55	Shank
Footplate (x2)	0.28	Foot
Total Bilateral Exoskeleton Mass	2.51	

[1] The mass corresponding to components indicated with (x2) is bilateral. The exoskeleton mass breakdown presented was for a medium-sized exoskeleton sized for users between 160 and 185 cm tall.

Waist Assembly and Cable Transmission

The waist assembly housed the exoskeleton actuation and control hardware including the motors, custom printed circuit board (PCB), and battery (Fig. 15). A padded harness system fastened the assembly to the waist (Fig. 14A). A modular fiber-reinforced 3D-printed assembly casing was designed to mount two motors (EC4-Pole 90W with 89:1 GP 22HP gearbox, Maxon) via cartridges and house the electronics module and battery (Fig. 15B). 18 mm sprockets were welded onto the

gearbox output shafts and moved chains within the cartridge to actuate the cable transmission that rotated the ankle assembly, transmitting torque and power from the motor to the user. Steel cables looped through the chain ends and were held in place by a guide and swage (Fig. 15C). Nylon webbing restraints held the cable transmission system to the thighs (Fig. 14A). Each motor mounting cartridge was removable, allowing for quick and easy replacement of each exoskeleton leg assembly independently. The cartridges were designed for ease of maintenance and to house different motor configurations and sizes. They could be quickly swapped for taller or shorter cable configurations depending on the user. Transmission cable configurations were made in set sizes to span set sizes of user heights (<160 cm, 160-185 cm, >185 cm). The custom PCB interfaced with sensing, control, and wireless communication hardware including a microcontroller (Teensy 3.6, PJRC), motor drivers (ESCON Module 50/8, Maxon), Bluetooth module, and other components to regulate battery voltage and amplify measurement signals (e.g., INA125P, Texas Instruments). A 5V cooling fan provided airflow through the motor assembly (Fig. 15A). A 24 V, 2000 mAh Li-Ion battery (KamPing) for this study was selected to provide an ambulatory duration equal to or greater than the typical physical therapy session (20-35 minutes [93,94]) when walking near the peak torque rating.

Ankle Assembly

The ankle assembly was designed to minimize distal mass and lateral protrusion from the shank, support cable transmission reaction forces, and provide a rigid interface to support and assist a user during activity. Mass added distally on the body increases the metabolic cost of walking more than when it is placed more proximally [63] and limits an exoskeleton's theoretical potential for benefit [29]. Components placed on the medial portion of the lower limb increase the risk of inter-limb

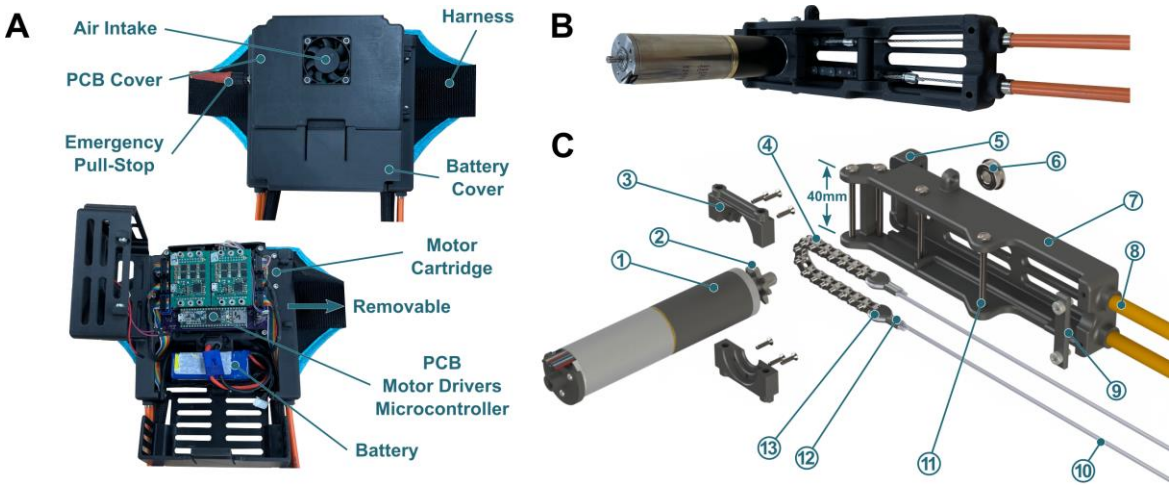

Fig. 15. Waist assembly overview. A. Closed and open pictures of the waist assembly module and harness system. The waist assembly module housed the motors, motor cartridges, PCB, battery, and wiring harness. B. Assembled view of a motor cartridge assembly. C. Exploded view of a motor cartridge assembly. 1) A 90W Maxon motor with an 89:1 gearbox. 2) An 8-tooth sprocket welded onto the gearbox output shaft. 3) Reinforced motor blocks were the interface between the motor and cartridge. 4) A chain driven by the sprocket actuated the cable transmission. 5) A sliding cover on each cartridge permitted easy access to the chain assembly 6) A thrust bearing supported the motor shaft to prevent tip deflection during operation. 7) The cartridge was 3D-printed and reinforced with carbon fiber aligned with the long axis. 8) The Bowden sheaths guided steel cables down to the ankle assembly. 9) Wire strain relief. 10) Steel cable looped through final link on each side of the chain and passed through the Bowden sheath. 11) Steel bolts held the motor subassembly in place within the cartridge and attached the cartridge to the rest of the motor assembly. 12) A crimped swage held the steel cable looped through the chain. 13) A small guide component prevented cable stress concentrations and failure.

collisions, while posterior or lateral protrusions may cause collisions with the environment. Our previous prototypes suffered from a lack of assembly stiffness due to a large moment arm between the user and the lateral upright and the absence of out-of-plane stiffening geometry [25,26,48]. We addressed these issues through mechanical design and material selection specifically intended to maximize assembly stiffness, such as using a square carbon fiber tube for the upright, incorporating stiffening ridges to the footplate and cuff, and reducing lateral protrusion of the ankle assembly by designing a low-profile ankle joint with custom sensors (Fig. 16).

The ankle assembly incorporated a single degree of freedom rotational joint and interfaced with the user via a shank or calf cuff and a footplate (Fig. 16A). The steel cables rotated a torque- and

angle-measuring pulley assembly (Fig. 16B). The pulley was placed within a carbon fiber tube and was supported on both ends by flanged bearings (Fig. 16B). The pulley was 80mm in diameter and formed a 5:1 gear reduction with the motor sprocket. While the pulley design permitted 120 degrees of motion before colliding with the upright, the chain assembly limited the motion to 80 degrees which was sufficient to capture the biological ankle range of motion [95]. We designed a custom low-profile in-line torque transducer for low-level motor control and torque measurement (Fig. 16B) with the goal of minimizing the physical profile of the assembly and lateral lever arm. The lateral lever arm in this design was 3 cm measured from the center axis of the upright to the edge of the footplate vs. 5 cm for a previous prototype [25,26,47]. The lateral lever arm, and consequently both the coronal bending and axial twisting moments, were 40% smaller than on our previous devices. We also designed a custom embedded angle sensing unit that resided above the pulley within the carbon fiber tube to provide a platform for the development of new angle- or velocity-dependent control strategies, patient monitoring of ankle angle or range of motion, and measurement of the device's mechanical power. The footplate was designed to be rigid but lightweight and had a curved feature to match the shape of the foot and metatarsals during toe-off [48]. Cuffs and footplates were made in set sizes, were easily swappable, and each footplate size spanned several shoe sizes [48]. A force-sensitive resistor (FSR, Flexiforce A502, Tekscan) placed on the footplate spanning the 1st through 3rd metatarsal heads under the ball of the foot was used by the micro controller to detect gait events and generate real-time stance torque profiles.

The following subsections detail specific experiments related to the hardware validation, human performance testing, and usability assessment portions of the experimental protocol summarized in Figure 14C.

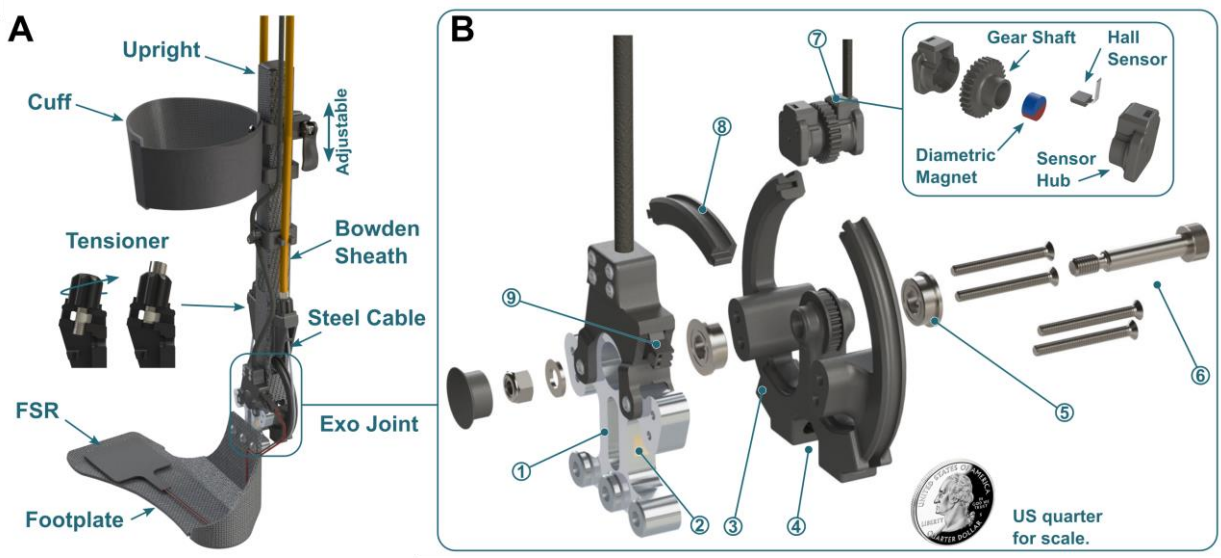

Fig. 16. Ankle Assembly. A. Assembled view of an entire ankle assembly, including calf cuff, machined carbon fiber upright, tensioners, instrumented pulley, and footplate. Tensioners compressed the Bowden sheath via a pull-and-twist knob and kept the cable transmission taut. B. Exploded view of the exoskeleton joint. 1) Torque transducer 2) Strain gage. 3) Carbon fiber-reinforced pulley. 4) Steel cable transmission crimping site. 5) Thrust ball bearings. 6) 6mm shoulder bolt. Four steel bolts fixed the torque sensor to the pulley. 7). Angle sensor assembly and exploded view. A gear shaft meshed with the pulley rotated a diametric magnet underneath a stationary Hall sensor. The resulting voltage was used to calculate joint angle and angular velocity. 8) Removable pulley bridge allowing assembly within the carbon fiber tube. 9) FSR connection.

Torque Sensor Design

Our custom torque transducer was a machined 7075-T651 aluminum part instrumented with strain gages designed to bi-directionally measure up to 30 Nm of torque (Fig. 16B, Fig. 17A). The width of the transducer was 10 mm and the mass was 30 g. For comparison, commonly used low-profile commercial sensors are over 25 mm wide and weigh over 50 g (e.g., Transducer Techniques TRT-500, [25,26,47,60,66]). The transducer measured the sagittal bending moment generated between the cable-driven pulley and footplate (Fig. 16, additional information in Supplemental Material section). The full Wheatstone bridge strain gage configuration minimized the effects of temperature and out-of-plane loading [96], isolating sagittal-plane torque applied to the user's ankle joint. The Wheatstone bridge voltages were measured, summed, and amplified using a

differential op-amp and a 1-kOhm resistor (INA125P, Texas Instruments) on our custom PCB. Refer to the Supplemental Material section for methods and figures related to the experimental setup for validating the torque sensor measurement and assessing its ability to isolate sagittal plane moments.

Angle Sensor Design

An angle sensor was located above the pulley axis of rotation, residing within the carbon fiber tube to minimize the lateral protrusion of the assembly. The assembly consisted of a 3D-printed plastic gear shaft enclosed in hubs that meshed with a gear on the pulley (Fig. 16B). The gear shaft rotated a diametric magnet underneath a Hall Effect sensor (SS49E, Honeywell) in the lateral hub. A rotating diametric magnet in this configuration induced a repeatable sinusoidal voltage response from the Hall sensor [97]. The angle measurement was then used to estimate joint angular velocity in real time by numerical differentiation. Refer to the Supplemental Material section for methods and figures related to the experimental setup for validating the sensor angle and velocity measurements.

Software and Control

The FSR signal was used to detect transitions between stance and swing, and determine an assistive torque profile during stance. A software threshold defined as a percentage of the total FSR signal range could be increased or decreased to adjust the initiation of stance phase and swing phase assistance. We used a high-level proportional joint moment controller (PJMC [64], Fig. 14) to generate an adaptive torque profile ($T_{set}(t)$) proportional to a real-time estimate of the biological ankle moment during stance phase, as in Equation 1:

$$T_{set}(t) = T_0 \frac{F_{FSR}(t)}{F_{cal}} \qquad (1)$$

where $F_{FSR}(t)$ was the instantaneous FSR reading, F_{cal} was the reference calibration value defined by the average of the peak FSR reading over three steps for each leg, and T_0 was the desired peak exoskeleton torque (e.g., 30 Nm). The footplate FSR captured the shape and magnitude of a signal that served as an estimate of the total biological ankle moment [64,98]. F_{cal} normalized the FSR signal, so any variance in the signal magnitude due to FSR placement on the footplate or foot contact with the FSR was eliminated and didn't affect the real time torque profile $T_{set}(t)$. Nominal constant dorsiflexor assistance could be applied during swing phase. A low-level PD controller tracked the generated torque profile using measurements from the torque sensor at the ankle joint (Fig. 14B). PJMC was recently validated across variable terrain including inclined treadmill walking and stair ascent [98], and allows users to seamlessly transition between terrains. The same PJMC parameters were used for all participants and terrains in this study.

Unimpaired Cohort Experiments

We recruited six healthy adults spanning a range of body sizes with the goal of demonstrating applicability of our device to unimpaired moderate-intensity walking performance augmentation (Table 5). During the experiment, participants walked for six minutes with and without exoskeleton assistance on a treadmill with a five-degree incline. We used a five-degree incline to mimic the maximum allowable ramp angle from Americans with Disabilities Act (ADA) guidelines [99]. We selected moderate intensity incline walking for our unimpaired performance testing experiment primarily because we believe it reflects the real utility of ankle exoskeleton in unimpaired populations, namely, augmenting moderate- to high-intensity ambulatory activities

that have elevated ankle plantarflexor demand. Additionally, this condition satisfied our goal of demonstrating a potential benefit beyond the most commonly investigated terrain (level ground). Participants used the shortest exoskeleton configuration that allowed them to walk without limiting step length. Participants were also sized for footplates and cuffs that fit snugly and were comfortable. Proper footplate fit was qualified by contact between the ball of the foot and the footplate FSR and by close alignment (within 3 cm) of exoskeleton and biological ankle joint centers. Footplate mounting hole patterns allowed for easy joint center alignment. Extra foam padding was added to footplates and cuffs as needed for comfort and fit.

Prior to the first trial, participants were given 10-15 minutes of exoskeleton acclimation time during which an operator tuned the exoskeleton assistance and treadmill speed. After a standing torque sensor zero calibration, participants walked at 1.0 m/s with 0.35 Nm/kg of nominal peak stance phase assistance and 0.05 Nm/kg of swing phase assistance while the dynamic FSR calibration was performed. Torque levels were chosen from our prior works [26,27,47] and pilot tests. Then, the operator increased the treadmill speed until the participant confirmed that the activity was of moderate intensity (Table 5). The operator re-calibrated F_{cal} to ensure good torque tracking at the faster walking speed, modified the FSR state transition threshold to ensure timely transitions between stance and swing (if needed), and adjusted swing phase assistance until the participant confirmed that the dorsiflexor torque was helpful after toe-off but did not impede the following heel strike. Most participants were comfortable with exoskeleton assistance after about 5-10 minutes of acclimation time. The calibrated exoskeleton parameters were saved and used during the shod-exoskeleton comparison experiment.

Each participant was assigned one shod and one assisted trial; trial order was alternated across the cohort (Table 5). We collected metabolic data using an indirect calorimetry unit (K5, COSMED).

Oxygen and carbon dioxide volumes were used to calculate metabolic power using Brockway's equation [65] for the last three minutes of each trial [23,100]. Prior to each trial, the participant stood quietly for 2-3 minutes or until respiratory data were steady. The last minute of respiratory data during standing prior to each trial was used to calculate basal metabolic rate. The metabolic power for each walking trial was offset by the basal rate and normalized by body mass to calculate net metabolic power [101]. Between trials, participants sat and rested for 10 minutes.

We streamed exoskeleton signals, including motor current and velocity, desired and actual joint torques, and exoskeleton joint angle and angular velocity, to a custom MATLAB (R2018b, MathWorks) interface at 100 Hz. Exoskeleton joint power was calculated as the product of the measured joint torque and angular velocity for each leg. The net metabolic powers between the

Table 5. Unimpaired participant information.

Participant	**Sex**	**Age [years]**	**Mass [kg]**	**Height [cm]**	**Stance Torque [Nm]**	**Swing Torque [Nm]**	**Walking Speed [m/s]**	**Trial Order**
P1[1]	F	24	50.0	160.0	17.5	2.5	1.25	Exo-Shod
P2	F	22	57.5	152.5	20.5	3.0	1.25	Shod-Exo
P3	M	26	91.6	173.0	30.0	3.0	1.25	Shod-Exo
P4	M	22	65.0	162.6	23.0	3.0	1.25	Exo-Shod
P5	F	23	45.7	155.0	16.0	2.5	1.35	Exo-Shod
P6	M	20	72.6	178.0	25.0	2.5	1.15	Shod-Exo

[1]This participant also completed a short exoskeleton-assisted walk on a step mill. Her typical exoskeleton torque, angular velocity, and power for inclined walking and stair ascent are shown in Fig. 5. Additional participant torque, velocity, and power curves are available in the Supplemental Material section.

shod and exoskeleton trials were compared to assess the impact of powered exoskeleton assistance on energetics.

Impaired Cohort Experiments

We recruited seven individuals with CP spanning a range of ages and impairment levels with the goal of demonstrating that our device can be effective at improving aerobic capacity during a maximal exertion test in this patient population (Table 6). Moving beyond our prior research that focused on augmenting walking on level ground in CP, we sought to explore application of ankle exoskeleton assistance to improve maximum exertion performance, which has not been previously explored in the literature. We designed an experiment to test performance on a stair-climbing machine as a way to expanding our understanding on the use of ankle assistance across different terrains and ambulatory intensities. Individuals with CP have difficulty with stair ascent [102] and are acutely susceptible to lower leg muscle fatigue [103], so we sought to demonstrate that our device was effective at prolonging the duration of this high-intensity activity. Inclusion criteria for this experiment included diagnoses of CP; the ability to walk on a stair machine for at least 5 minutes; Gross Motor Function Classification System (GMFCS) level I, II, or III; at least 20° of passive ankle plantarflexion range of motion; no knee extension or ankle dorsiflexion contractures greater than 15°; no orthopedic surgery completed in the prior 6-month period; and the absence of any medical condition other than CP that would affect safe participation. Participants were fitted with an ankle exoskeleton, footplates, and cuffs as described in the previous section. The same exoskeleton calibration procedure as in the previous section was conducted prior to exoskeleton-assisted trials.

Table 6. Impaired participant information

Participant	Sex	Age [years]	Mass [kg]	Height [cm]	GMFCS[1] Level
CP1	M	33	71.4	170	II
CP2	M	11	48.4	150	I
CP3	M	15	57.2	165	I
CP4	F	25	47.4	147	III
CP5[2]	M	14	39.5	148	II
CP6[2]	M	12	37.7	141	II
CP7	M	14	55.8	165	II

[1]GMFCS: Gross Motor Function Classification System.
[2]Two participants did not perform the maximal exertion portion of the experiment because of minimum mass requirements on the stair-stepping machine.

The maximal exertion test protocol was as follows. The stair stepping rate was increased from each participant's comfortable rate by one intensity level (0.3-0.4 floors/min) every thirty seconds until the participant indicated they wanted to stop. All participants wore a safety harness and were surrounded by researchers ready to stop the machine and support the participant to prevent harm. Participants completed one shod and one exoskeleton-assisted maximal exertion trial (Supplemental Video 1: https://doi.org/10.6084/m9.figshare.14810574). Participants took a 20-minute break between trials and confirmed that they were fully rested. Two of the seven participants were too light to trigger an increase in stair stepping rate and were unable to complete the experiment. We prescribed 0.30 Nm/kg of nominal peak plantarflexor assistance and 0.03 Nm/kg dorsiflexor assistance. During each trial, we recorded duration, step rate, and metabolic rate. We calculated the total distance travelled in number of floors (1 floor = 16 steps). After each trial, we recorded each participant's perceived exertion using standard scales [104]. We compared the floors ascended between the shod and exoskeleton conditions. We also compared net metabolic power between the conditions over the duration of the shortest trial because intensity increased as

the trials continued and we sought to make a direct comparison of metabolic power for the same duration and intensity. For example, if the shod trial was five minutes long and the assisted trial was seven minutes long, we compared the average net metabolic power across the first five minutes of both trials.

Usability Assessment

All seven participants with CP performed a device usability assessment with the goal of demonstrating that time to don and operate the device improved with practice and could be completed in less than 5 minutes. Our usability experiments were motivated by our interest in conducting future evaluations of ankle exoskeleton assistance for augmenting mobility in free-living scenarios. The cohort included a wide range of participants, as we were interested in receiving a variety of feedback from both children and adults on the usability and effectiveness of our exoskeleton. We recorded the time of each step of the donning process and the total app setup time (from powering on the device to walking with full torque magnitude) for each participant, including time spent reading instructions. Participants completed the exercise three times. Three individuals from the unimpaired cohort (P1, P3, and P4) were selected to perform the same assessment as a reference. Donning our device was a three-step process. Participants 1) prepared the device by placing it on a chair and placing footplates within shoes, 2) inserted their feet into the shoes, tied the shoes tightly, and strapped the cuffs in place on each shank, and 3) clipped and adjusted the waist assembly straps (Supplemental Video 2: https://doi.org/10.6084/m9.figshare.14810598). We designed a custom iOS application that would automatically connect to the exoskeleton and guide the user through steps needed to start walking with assistance. Controlling the device using the iOS app was a quick three-step process that included: 1) user weight input in pounds, 2) static torque transducer calibration during quiet

standing, and 3) dynamic controller calibration (state detection and ankle moment normalization) while walking in zero-torque mode. When ready, participants were instructed to walk and the firmware automatically completed the walking calibration and provided 0.30 Nm/kg of nominal peak stance torque and 0.03 Nm/kg swing torque, building in magnitude from zero over the course of three steps per leg. Refer to this link to the donning instructions on our website (https://biomech.nau.edu/don/). The most affected participant (CP4) received parental assistance due to severe upper-extremity disability. To assess subjective user experience and quantify the usability of the exoskeleton, each participant completed the System Usability Scale questionnaire [105]. Briefly, the System Usability Scale includes 10 statements rated by means of a 5-point Likert scale, from 1 (strongly disagree) to 5 (strongly agree), and the scores have a range of 0 to 100 that is divided into five scales: score of 0–25: worst, score of 25–39: poor, score of 39–52: OK, score of 52–85: excellent, and score of 85–100: best imaginable [106].

Statistics

All data sets were tested for normality using Shapiro-Wilk tests at the 5% significance level [107] and all samples were normally distributed. We compared net metabolic power for the unimpaired

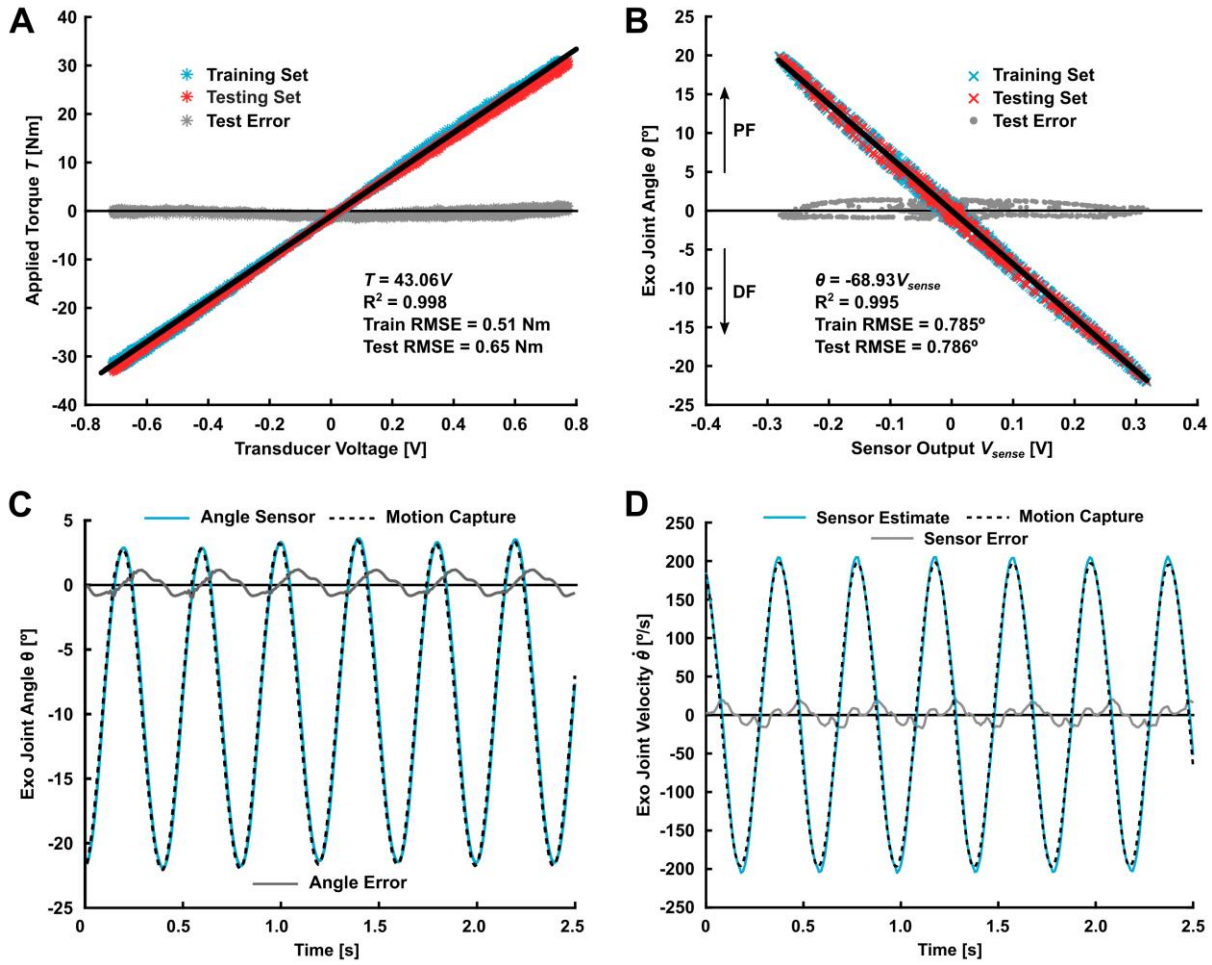

Fig. 17. Torque (A) and angle sensor (B-D) validation results A. Linear regression for estimating torque applied to the transducer given a voltage measurement with root-mean-squared error (RMSE). Refer to the Supplemental Material section for torque sensor sensitivity to out-of-plane loads. B. Linear regression relating angle sensor output to motion capture with RMSE; a positive angle corresponds to plantarflexion (PF). C. Time series angle measurement with RMSE. D. Comparison of sensor-estimated joint velocity to the motion capture result. Refer to the Supplemental Material section for a comparison of sensor and motor velocity estimates during validation.

cohort and net metabolic cost of transport and distance travelled for the impaired cohort between shod and exo-assisted trials. For the usability section, we compared time needed to don and setup the device across three attempts. Two-tailed paired t-tests were used to assess differences at 5% significance for all group-level comparisons. Cohen's d (d) was used to calculate effect size as the difference of group means divided by the pooled standard deviation, where 0.2 was considered a

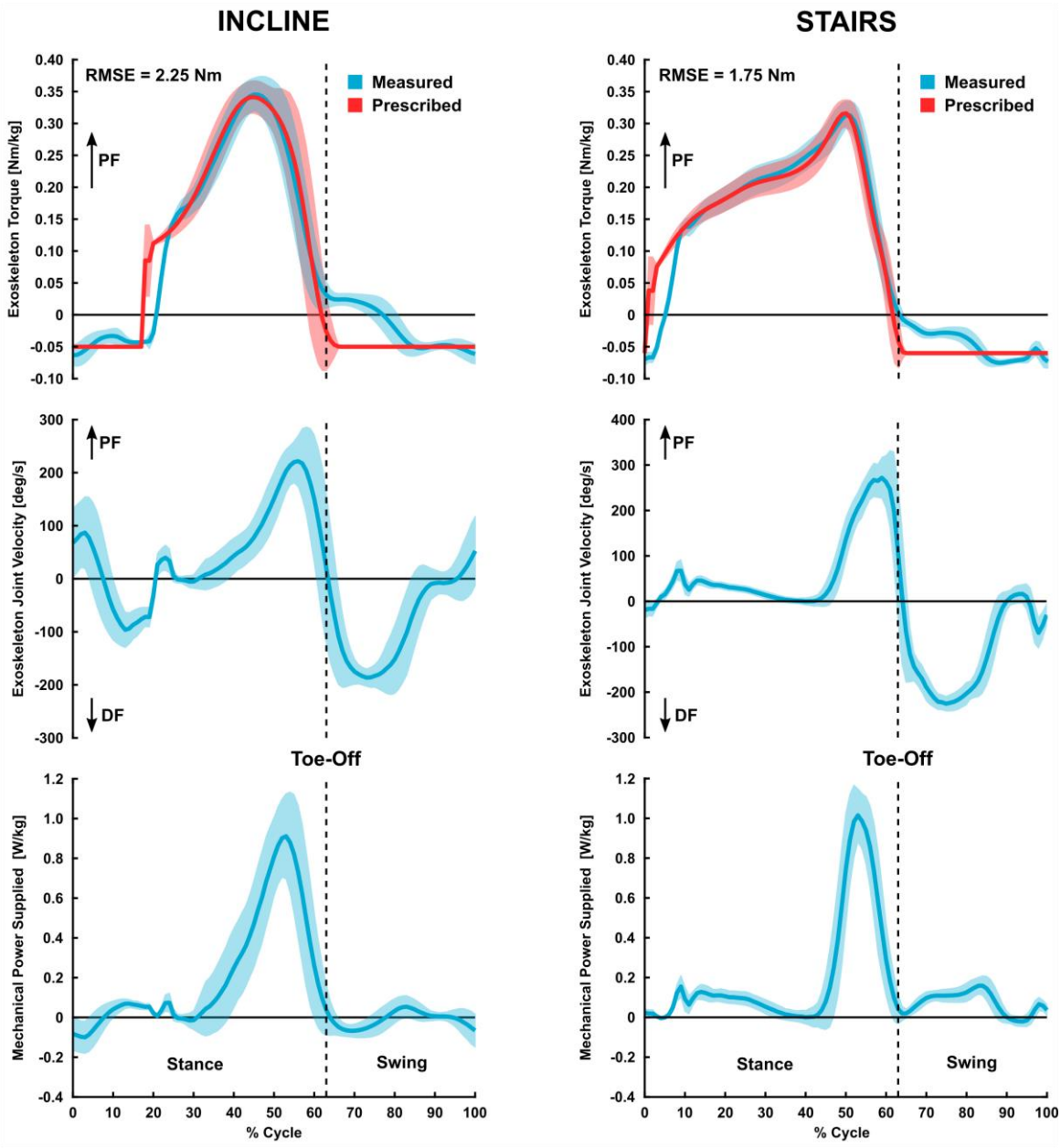

Fig. 18. Representative exoskeleton measured (blue) and prescribed (red) torque (top row), velocity (middle row), and power (bottom row) profiles (mean ± standard deviation) from a single subject (P1, Table 5) during assisted walking on a 5-degree incline (left column) and on a stair-stepping machine (right column). Mechanical power (bottom row) was calculated by multiplying measured exoskeleton torque (Nm) and angular velocity (radians per second). Torque and power were normalized by the participant's body mass. Torque tracking error during early stance and immediately after toe-off are due to motor torque rate and speed limitations. Refer to the Supplemental Material section for additional participant torque, velocity, and power curves and for a short section on energy consumption and electrical to mechanical power efficiency.

small effect, 0.5 a medium effect, and 0.8 a large effect [108]. All analyses and statistical comparisons were done in MATLAB. Simple statistical comparisons were used without p-value corrections so that the reader may judge the significance and impact of the group-level comparisons for themselves.

Results

Torque Sensor Validation

The linear model relating our custom torque sensor's voltage output to applied torque explained 99% of the data variance and had low overall mean testing error and variance between predicted and actual torques (Fig. 17A). The torque absolute test root-mean-squared error (RMSE) was 0.65 Nm. We assessed the ability of the torque sensor to isolate sagittal plane moments and confirmed that out-of-plane sensitivity was between 5.2% and 15.5% of the sagittal bending moment sensitivity (see Supplemental Material section). No evidence of fatigue or offset drift has been observed. Refer to the Supplemental Material section for torque sensor stress analysis and uncertainty estimates.

Angle Sensor Validation

The linear model relating our custom angle sensor's voltage output to the motion capture angle explained 99% of the data variance and had low overall mean testing error and variance between predicted and actual pulley angles (Fig. 17B). The angle and angular velocity absolute RMSE computed from the ankle joint sensor relative to motion capture was 0.67 degrees and 9.01 deg/s, respectively, for a 2.5-second sample (Fig. 17CD). Estimating the exoskeleton joint velocity using

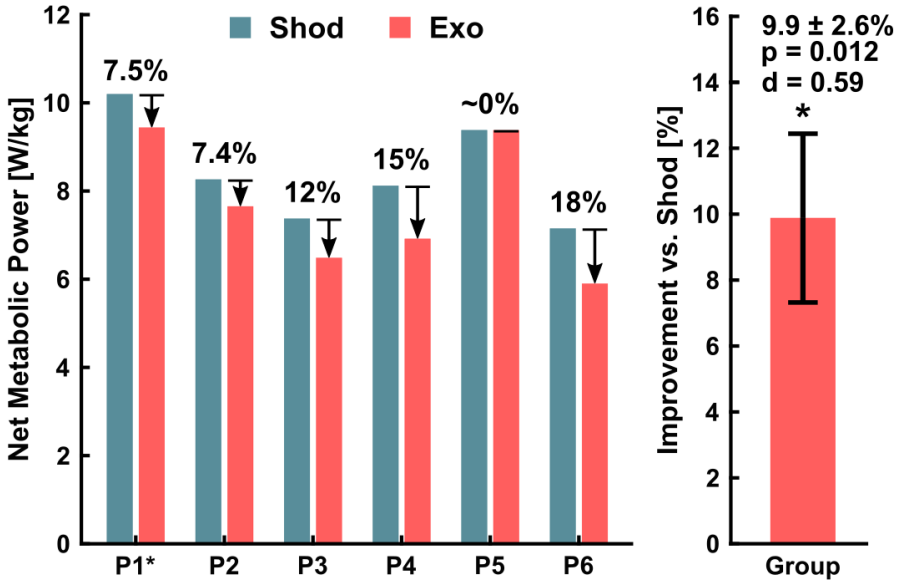

Fig. 19. Unimpaired cohort metabolic results during incline treadmill walking with and without the exoskeleton. Five of the six participants responded well to exoskeleton assistance and showed a reduction in net metabolic power compared to no device. Refer to Table 5 for participant information and trial order. *Significant at 95% confidence.

measured motor velocity and the transmission system gear reductions yielded large error compared to motion capture (RMSE = 17.85 deg/s, see Supplemental Material section).

Unimpaired Cohort Experiments

Five of the six unimpaired participants responded well to exoskeleton assistance during inclined treadmill walking (Fig. 19). Improvements in energy cost during the last three minutes of the trial ranged from 7.4% to 18%, with one participant (P5) showing no change when walking with assistance. Our cohort had a 9.9 ± 2.6% (mean ± standard error) improvement in metabolic power when walking with vs without the device ($p = 0.012$, $d = 0.59$, Fig. 19). Exoskeleton torque, angular velocity, and mechanical power were captured for five of the six unimpaired participants (Fig. 18, also see Supplemental Material section).

Impaired Cohort Experiments

All participants were able to safely complete the maximal exertion stair-climbing test without incident. The number of floors climbed during the maximal exertion experiment increased by 38.4 ± 23.6% with exoskeleton assistance compared to shod ($p = 0.013$, $d = 0.25$, Table 7, Fig. 20A). Despite the increase in distance ambulated, the net metabolic powers for assisted and unassisted maximal exertion tests were not significantly different ($p=0.49$, Fig. 20B), and perceived exertion on a scale of 1-10 was similar (6.8 ± 0.8 with the device vs 7.2 ± 1.5 without the device, $p = 0.50$).

Usability Assessment

The usability assessment results showed that total don time and app setup time generally decreased with practice (Fig. 20DE). Placing the footplates into the shoe and donning the ankle assembly was the most time- consuming step. The third attempt time (3.5 ± 0.7 minutes) was significantly different from the first attempt (down 100 ± 30s, $p = 0.018$, $d = 0.66$) and from the second attempt (down 58 ± 14s, $p = 0.006$, $d = 0.51$). Refer to Supplemental Video 2 in Additional File 3 for an example of the usability assessment. For reference, the average unimpaired final don time was 1.5 ± 0.2 minutes. The final app setup time (28 ± 6s) was significantly different from the second attempt (down 24 ± 8s, $p = 0.016$, $d = 1.26$). For reference, the average unimpaired final app setup

Table 7. Maximum exertion speed and distance results.

Participant	**Stair Speed [floors/min][1]**			**Floors Ascended**		**Improvement over Shod [%]**
	Start	**Shod End**	**Exo End**	**Shod**	**Exo**	
CP1	2.7	5.2	5.2	13.37	13.77	3
CP2	3	4.1	4.6	11.97	13.85	15.7
CP3	2.7	4.1	4.6	6.95	8.89	27.9
CP4	1.2	1.6	2	0.92	2.13	131.5
CP7	2.7	3.7	3.7	5.97	6.81	14.1

[1]Increasing exercise intensity on the step mill increased the ascent speed incrementally.

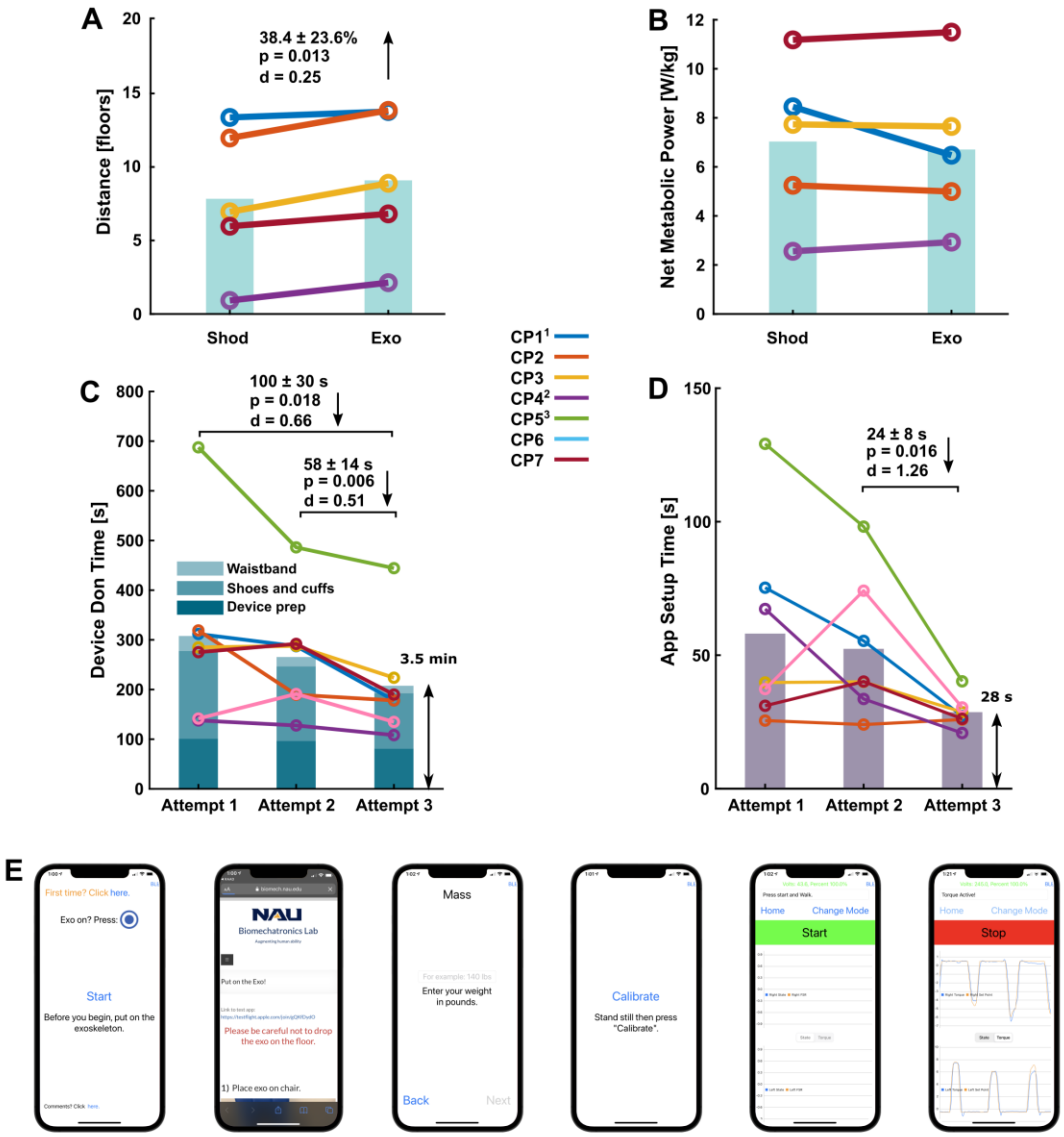

Fig. 20. Maximal exertion stair-climbing results (top row) and usability assessment (bottom row). A. Number of floors climbed during the maximal exertion experiment. B. Average net metabolic power during the max exertion experiment. In general, participants had little change in energy cost but climbed more floors when walking with the device. [1]CP1 had a large reduction in net metabolic power without a change in floors travelled suggesting that he likely could have climbed higher. C. Device don time. The final attempt time was significantly lower than both the first and second attempts. [2]A caregiver assisted CP4 throughout the assessment. [3]CP5 had spastic hemiplegia of the upper and lower-extremities and had difficulty handling the device, but had a nearly three-minute improvement with practice. D. App setup time. Setup time decreased with practice to ~30 seconds. E. App at each step. From left to right: 1) start screen checks to see if a device is in range, 2) optional donning instructions (link available in Additional File 2), 3) mass input, 4) torque sensor calibration, 5) screen for adjusting parameters and starting trial, 6) example of an active trial.

time was 14 ± 1s. The average System Usability Scale questionnaire score of the impaired cohort was 81.8 ± 8.4 (“excellent”).

Discussion

The goal of this study was to design a highly useable lightweight ankle exoskeleton with custom sensing and provide an initial indication of its effectiveness across a range of terrains and users. Our design utilized a modular motor assembly mounted at the waist to provide ankle torque via interchangeable Bowden cables, calf cuffs, and footplates in standard sizes that spanned a wide range of users from children to adults. We validated our in-line sensing modules that provided direct, real-time measurement of ankle angle, torque and power; these sensors provide an opportunity for the development of new control strategies (e.g., velocity-dependent muscle force prediction), patient monitoring (e.g., ankle range of motion), closed-loop torque control, and assessment of mechanical performance (e.g., torque tracking). The device was able to provide up to 30 Nm of peak torque with a mass 2.3-2.6 kg depending on size and battery selection. We developed a custom iOS application allowing users to control the device themselves. We accept our primary hypotheses that 1) improvements in ambulatory performance (economy or distance) for both unimpaired and impaired cohorts are detectable during diverse exoskeleton-assisted tasks, and 2) users can don and control the device in less than five minutes. While the improvements in walking economy and distance are motivating, we caution the reader to interpret the results with care due to the small cohort sizes.

Our battery-powered device improved moderate-intensity incline walking efficiency by 10% compared to without wearing the device in an unimpaired cohort of adults of diverse body masses and statures (Fig. 19). Compared to untethered and even tethered systems, our device had

competitive peak torque capability when normalized to the mass added onto the shank (Fig. S2 in Additional File 3) and demonstrated similar improvements in energy expenditure. For example, the seminal untethered, shank-mounted exoskeleton from Mooney et al., weighed 1.06 kg per leg, produced up to 45 Nm (0.5 Nm/kg) peak torque during unloaded, level walking for a small cohort of heavy unimpaired adults (n = 6, mass = 89 ± 8 kg, mean ± SD) and induced a group-level reduction in energy expenditure of 11 ± 4% (mean ± SE) compared to walking without wearing the device [31]. On the other side of the spectrum, an untethered soft exosuit from Awad et al. with a peak torque of about 15 Nm (0.15 Nm/kg) and a distal mass of 0.42-0.50 kg was successful in preliminary and clinical trials during unilateral assistance with stroke survivors [16,22]; we are not aware of bilateral unimpaired metabolic results for this system. A tethered ankle exoskeleton from Galle et al. had a peak torque of 36.6 Nm (0.6 Nm/kg), a distal mass of 0.445 kg per leg, and induced a group-level reduction of 12.3 ± 2.9% compared to shod (n = 14, mass = 61.0 ± 4.5 kg) [45]. A high-powered tethered exoskeleton from Zhang et al. with distal mass 0.875 kg induced a 21% improvement in a single subject during walking at a 10-degree incline [28] whereas, in the present study, the maximum observed reduction in energy cost during 5-degree incline walking was 18%. Compared to the aforementioned exoskeletons, our device produced up to 30 Nm, had a distal mass of 0.415 kg per leg, and induced a similar group-level reduction in energy consumption in an unimpaired cohort with greater mass variability than the aforementioned studies (mass range of 46-96 kg). As far as we are aware, our device had one of the lightest ankle assemblies of any research or commercial powered device at the time of this writing. The light distal mass likely contributed significantly to the observed benefits in energy reduction based on the augmentation factor, an estimate of potential benefit that balances positive power production with detriments to energy consumption due to added mass [29,109]. Though our exoskeleton

provided less torque and power than the device described in Mooney et. al. [31], it had a similar augmentation factor due to its reduced distal mass (between 28 and 56 W vs. 44 W in [109] and 33 W in [29]). Augmentation factor was calculated as described in Mooney et. al. [29] using our in-line joint sensors. Refer to the Augmentation Factor Calculation section at the end of this chapter for example calculations.

Maximal exertion tests are commonly used to assess functional capacity, with individuals with CP having lower maximal oxygen consumption compared to unimpaired individuals [110]. In this study, we demonstrated that children and young adults with CP were able to ascend almost 40% more steps on a stair stepping machine while using the device during a maximal exertion test. This provides new insight into the potential for wearable ankle assistance to provide both psychological and physiological benefits during high-intensity activities (Fig. 20CD). For example, average metabolic power or perceived exertion remained the same despite the encouraging group-level increase in distance. One of the most promising findings was that our most impaired participant (CP4) ascended nearly twice as far with exoskeleton assistance compared to no device (2.1 vs. 0.9 floors, respectively). An interesting result at the individual level was that while CP1 had only a very small improvement in distance when using the device, there was a sizeable reduction in metabolic cost compared to no device (~23%, Fig. 20B), suggesting that he opted to decrease his effort while using the device as opposed to maintaining the same level of effort when not using the device like most participants. While additional research is needed, our results suggest that lightweight untethered ankle assistance may allow for increased and task-oriented training in individuals with CP, which has been proven successful at improving mobility in both CP and post-stroke patients [70–72].

To the best of our knowledge, this is the first study to report on the design of an untethered exoskeleton that allows individuals with physical disabilities to don and operate the device without researcher intervention. Individuals with CP were able to don and control the device to the point of walking with assistance (either on their own or with caregiver aid) in an average of just 4 minutes, suggesting that future deployment in clinical and home settings may be realistic. While the mobile app allows the user to modify exoskeleton tuning parameters, we envision that the user would not need to adjust tuning parameters after the initial device fitting and tuning process with a trained physical therapist or researcher. The rate of improvement over three attempts suggests that donning and setup time would likely decrease further with continued use. For example, one participant (CP5), a determined teen with upper- and lower-extremity spastic hemiplegia, had considerable difficulty donning the device on his own but improved his time by almost 3 minutes with practice (Fig. 20D). When prompted for feedback on the design, comfort, and control of the exoskeleton, users and caregivers tended to comment favorably on the low hardware profile on the shank and waist, low device weight, shank and waist interface comfort, quick don and doff times, and intuitive torque assistance. Donning the shoes and cuffs was similar to typical AFOs and the waist straps only needed to be adjusted once. The System Usability Scale questionnaire score of 81.8 ± 8.4 (excellent) was comparable to a commercial robotic device (Ekso GT, score: 83) and better than another pre-market devices (PASfinal, score: 59.5) [111].

While small cohort exoskeleton studies are common [29,31,44,45,56], we acknowledge that a limitation to this study was the small sample sizes used for statistical analysis and encourage the reader to interpret group-level results and statistical significance with caution. Another limitation of this study was that the battery used during the experiments provided just 37 minutes of walking duration at the average torque used across both cohorts (~22 Nm). While we met and exceeded

our goal of completing performance testing with a battery meeting the typical ambulatory duration of a standard physical therapy session (20-35 minutes [93,94]), the battery used in this study would be insufficient for all day use. However, we theorize that in the future deployment of this or similar commercial exoskeleton systems, users may prefer to minimize adding mass to the body by interchanging multiple batteries throughout the day.

Conclusion

This study reported on the design and initial testing of a new, lightweight ankle exoskeleton. We validated custom low-profile joint-level sensing and achieved one of (if not) the lightest reported distal mass placements of any tethered or untethered powered ankle exoskeleton. The device performed well across a range of ambulatory conditions, walking abilities, and body sizes, reducing incline walking energy consumption in unimpaired adults and improving maximal exertion stair climbing distance in children and adults with CP. Our device was effective for children with CP as light as 38 kg and unimpaired adults as heavy as 92 kg, suggesting that 0.30-0.35 Nm/kg peak plantarflexor assistance and 0.03-0.05 Nm/kg dorsiflexor assistance was sufficient to improve ambulatory performance. All of our unimpaired participants and most of our participants with CP were able to don and initiate user-calibrated ankle assistance in under 5 minutes without researcher intervention. Future work will continue to explore the effectiveness of adaptive ankle exoskeleton assistance across a multitude of challenging terrains for unimpaired and impaired participants.

Abbreviations

CP – cerebral palsy; PCB – printed circuit board; GMFCS - Gross Motor Function Classification System; RMSE – root-mean-squared error; PF – plantarflexion (refers to angle); DF – dorsiflexion (refers to angle).

Declarations

Funding

This work was supported in part by the Eunice Kennedy Shriver National Institute of Child Health and Human Development of the National Institutes of Health under award numbers 1R01HD107277 and 1R44HD104328. The content is solely the responsibility of the authors and does not necessarily represent the official views of the National Institutes of Health.

Ethics approval and consent to participate

All human subjects experiments were approved by Northern Arizona University's Institutional Review Board under protocol #986744-27 as a part of NCT04119063. All participants 18 and over read and signed informed consent forms. For all minors, we obtained assent and informed written consent from a parent.

Consent for publication

All participants 18 and over read and signed photo and video release forms. For all minors, we obtained assent and written consent from a parent.

Availability of data and materials

The datasets used and analyzed during the current study are available from the corresponding author on reasonable request.

Competing interests

ZFL is a co-founder with shareholder interest of a university start-up company seeking to commercialize the device used in this study. ZFL and GO hold intellectual property inventorship rights.

Authors' contributions

GO designed the exoskeleton device, led the mechanical and performance validation experiments, analyzed and interpreted data, generated figures, and wrote the manuscript. YF designed and led the maximal exertion and usability experiments, analyzed data, and generated figures. CFC designed the iOS app for controlling the exoskeleton. ZFL was the principal investigator, designed the exoskeleton device and iOS app, conceived, designed, and led the study, interpreted data, and wrote the manuscript.

Acknowledgements

This work was supported in part by the Eunice Kennedy Shriver National Institute of Child Health and Human Development of the National Institutes of Health under award numbers R15HD099664 and R44HD104328. The content is solely the responsibility of the authors and does not necessarily represent the official views of the National Institutes of Health. We thank James Babers and Leah Liebelt for their design and manufacturing contributions. We also thank Jeff Yows and Samuel Maxwell for their help with exoskeleton assembly and experiments. We also thank Ben Conner for his help with participant recruitment and experiments.

Supplemental Material

Torque Sensor Stress Analysis

Several of our early torque sensor prototypes experienced sudden failure after a short period of use. In most cases, the failure was characterized by shifts in the zero-load voltage in response to loading within the calibrated range of sagittal torque which suggested that the material experienced plastic deformation. The sudden nature of the failures coupled with the short life span suggested that the material yielded due to over-stress as opposed to fatigue. These failures necessitated a closer examination of the loading conditions and refinement of the basic stress analysis simulations performed during the initial design phase.

The sensors were initially designed with a small factor of safety against 30 Nm sagittal bending with no consideration of out-of-plane loading. We sought to refine the design the withstand up to 50 Nm sagittal bending and corresponding ratios of out-of-plane forces and bending moments. We had limited understanding of the out-of-plane loading conditions due to an inability to measure such loads directly, so we estimated the out-of-plane forces and moments under a simple 50 Nm sagittal bending load (M_{SAG}, Fig. 21). During assistance, the exoskeleton pushes against the ground to support the user vertically and to aid with propulsion as the ankle plantarflexes. A vertical reaction force F_Z under the ball of the footplate and an anterior reaction force F_A oppose the exoskeleton assistance. The footplate and cuff reaction force positions were such that a coronal bending moment M_{COR} and axial twisting moment M_{AX} were applied to the torque sensor (Fig. 21). For an adult wearing a US size 10-11 shoe size, F_Z was about 15 cm anterior of the pulley center and 7.5 cm medial of the torque sensor centerline. F_A was about 28 cm above pulley center and also about 7.5 cm medial of the torque sensor centerline (Fig. 21). The estimated forces and

moments for the 50 Nm sagittal loading condition are summarized in Table 8. The forces and moments were treated as loads applied to the torque sensor during stress analysis.

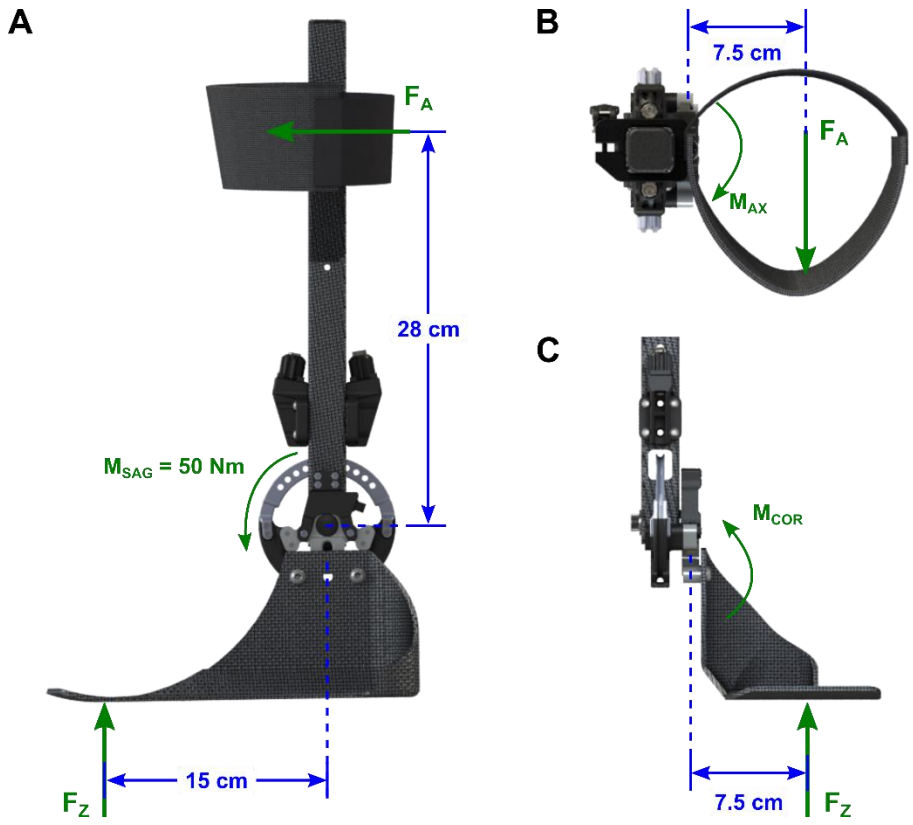

Fig. 21. Estimated reaction forces and out-of-plane bending moments applied to the torque sensor during 50 Nm of assistive sagittal torque. A. In the sagittal plane, a vertical force FZ under the footplate and anterior force FA at the cuff oppose the exoskeleton torque. B. The anterior force produces a twisting moment in the axial plane. C. The vertical force produces a bending moment in the coronal plane.

Table 8. Summary of estimated forces and moments applied to the torque sensor.

F_Z [N]	F_A [N]	M_{SAG} [Nm]	M_{COR} [Nm]	M_{AX} [Nm]
340.0	178.6	50.0	25.5	13.4

The torque sensor was redesigned to withstand the estimated loads with a factor of safety (FS) of 1.0 against yield for an overload condition of 50 Nm. Specific design changes in version 2 (V2) of the torque sensor included shortening the sensor height to withstand M_{COR}, widening the central columns to withstand M_{SAG}, and increasing the thickness of the sensor to withstand M_{AX}. Static

finite element (FE) simulations in Solidworks 2020 were conducted to verify that the design changes between V2 and the original torque sensor design (V1) reduced the stress for each bending mode. The purpose of the simulations was not to obtain a true estimate of stress and strain but rather as a relative FS comparison for the same loading conditions between two designs. The manufacturer of our torque sensors offered a range of values for the material yield strength of which we used the lowest estimate (372 MPa, 7075-T651 plate, Protolabs). In short, we overestimated the loading conditions and underestimated the yield criteria to develop a conservative stress estimate of a combined loading scenario that may occur for one instance of time during each gait cycle.

Within the Solidworks FE environment, the torque sensor models were fixed at the interfaces with the pulley (Fig. 22). The estimated forces and bending moments for the 50 Nm overload condition were applied between two footplate mounting holes. That is, forces were applied evenly between appropriate faces of the sensor-footplate mounting holes such that the total between all surfaces equaled F_Z and F_A. Bending moments were applied as forces and pressures at each mounting hole such that, when accounting for the distance between the holes, the total bending moment in each plane equaled M_{SAG}, M_{COR}, and M_{AX} (Fig. 22). Forces and moments applied to the model mimicked the sensor-footplate interaction.

After loading conditions were applied, the Solidworks models were meshed using default element type and size settings. Mesh controls were applied on sharp corners, chamfers, and fillets to prevent excessive stress concentrations (Fig. 23). Elements in controlled regions were typically 0.1-0.5 mm wide. Other elements were typically 1 mm wide.

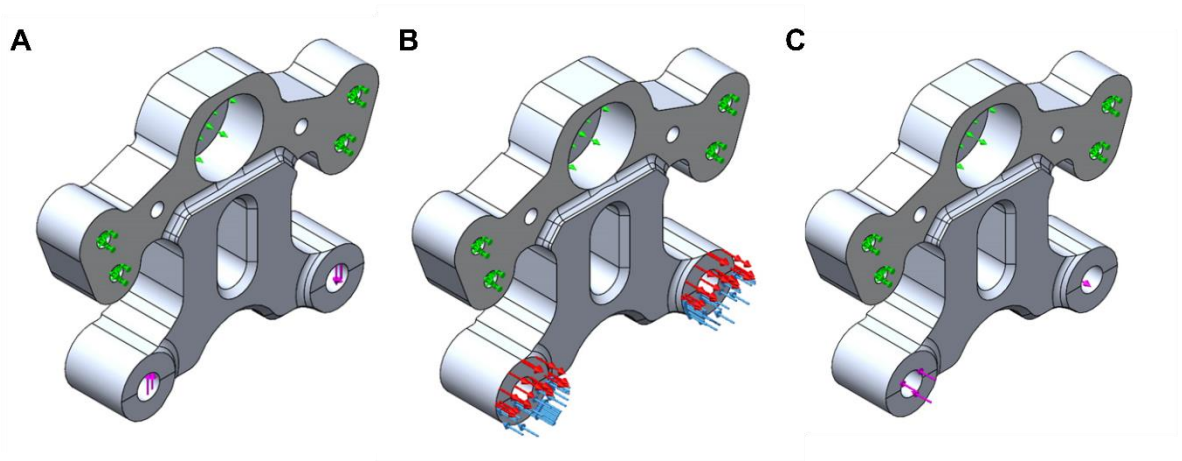

Fig. 22**.** Loading conditions applied in the Solidworks FE environment. The pulley-sensor interfaces were fixed and are indicated in green. A. Sagittal bending, vertical, and anterior forces were applied to internal faces of the sensor-footplate mounting holes and are indicated in purple. B. Coronal bending was applied as opposing pressures on the faces contacting the footplate. Red and blue indicate opposing coronal bending pressures. C. Axial twisting was applied as opposing forces on the cylindrical faces of each mounting hole.

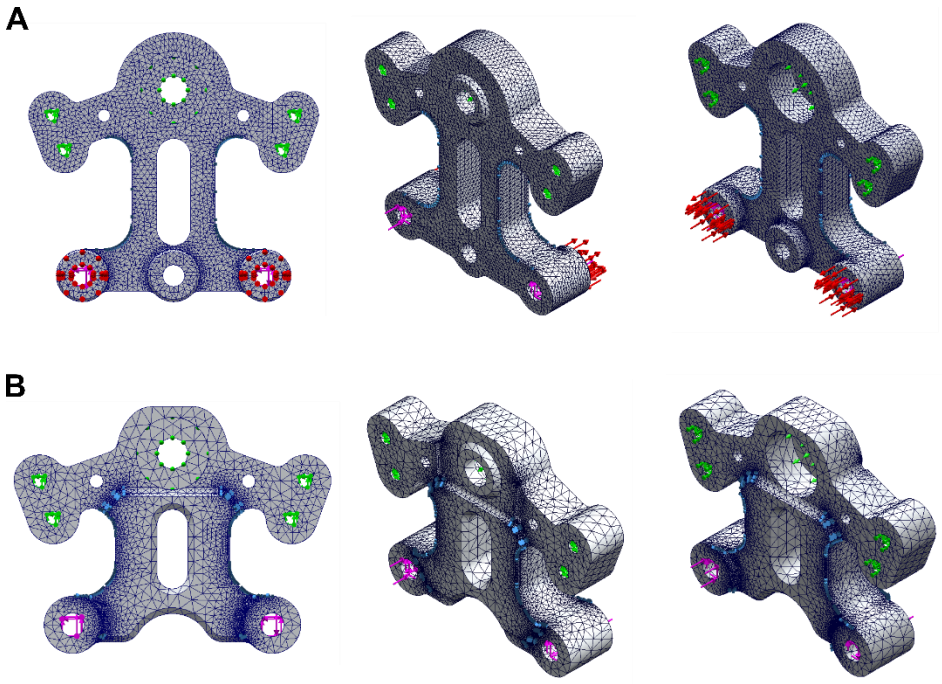

Fig. 23**.** Solidworks FE meshes for V1 (A) and V2 (B) torque sensor models. Mesh controls indicated with blue arrows were applied on regions with sharp corners, fillets, and chamfers to limit stress overestimation in regions with stress concentrations.

Static simulations were conducted for the combined loading condition with all forces and moments applied simultaneously. Additionally, simulations for each bending mode isolated were conducted to assess which modes were likely responsible for V1 torque sensor failures and to verify that V2 torque sensors would withstand the same conditions. Four simulations for each torque sensor model were conducted (Fig. 25). Solidworks FE calculated the maximum Von Mises stress and minimum yield FS for each simulation (Table 9). Additionally, a fatigue simulation was conducted to assess the minimum longevity of each sensor. For the fatigue analysis, the applied load varied between 60% and -33% of the full loading scenario from the static simulations. That is, the fatigue simulation was designed to mimic the alternating loads that would occur during walking with 30 Nm plantarflexor assistance and 10 Nm dorsiflexor assistance (Table 9, Fig. 24).

Table 9**.** Summary of static and fatigue FE simulations. [1]Full load refers to the combined loading scenario with all bending modes and reaction forces applied simultaneously. [2]The yield strength for 7075-T651 plate was 372 MPa.

Simulation	**Max Von Mises Stress (MPa)[2]**		**Minimum Yield Factor of Safety**		**Minimum Life at 30 Nm (cycles)**	
	V1	**V2**	**V1**	**V2**	**V1**	**V2**
Sagittal Bending	241.8	169.0	1.538	2.201	-	-
Coronal Bending	413.3	272.1	0.900	1.367	-	-
Axial Twist	241.1	0.91	1.543	4.090	-	-
Full Load[1]	595.7	391.7	0.625	0.950	10^5	10^6

To summarize the static results, the V2 torque sensor design was predicted to withstand material yield for each isolated bending mode. Conversely, the simulations predicted that V1 torque sensors likely failed due to yield from coronal bending (Table 9). Though V2 torque sensors were predicted to have a minimum yield FS of 0.95 during combined loading at 50 Nm, we accept that the V2

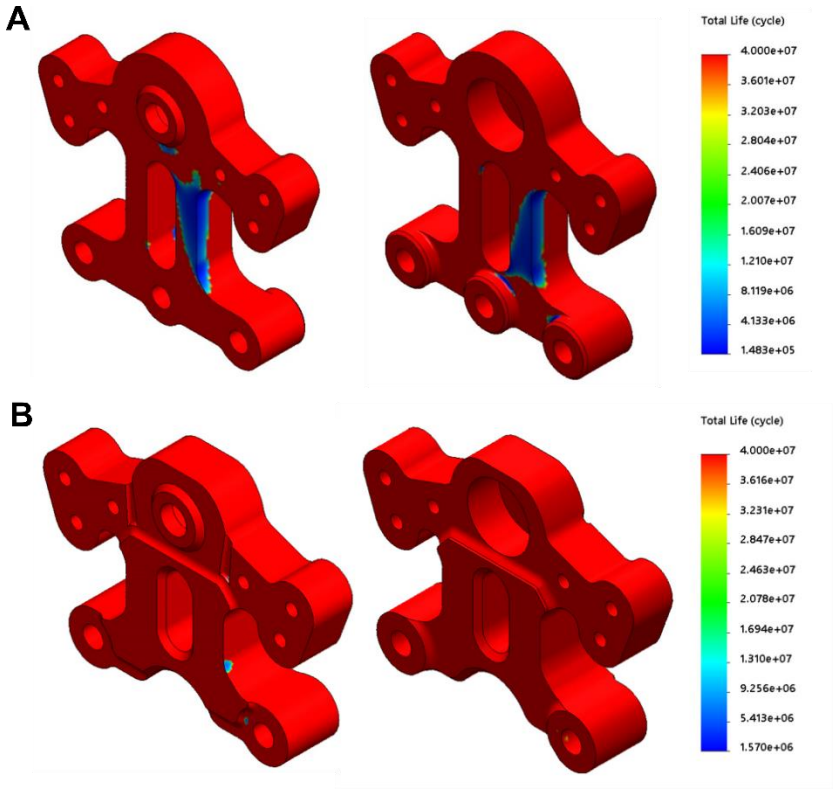

Fig. 24**.** Fatigue simulations for V1 (A) and V2 (B) torque sensor designs. The applied load for fatigue simulations was designed to mimic the alternating loads during exoskeleton-assisted walking. The color map corresponds to the minimum number of cycles. V1 torque sensors were predicted to have a minimum life of 10^5 cycles and accumulated significant damage on the sensing site where strain gages were placed. V2 torque sensors, on the other hand, had a minimum life of 10^6 cycles and accumulated no damage directly on the sensing site.

sensor design is a vast improvement over the original design. We overestimated the applied stresses during walking and underestimated the material yield strength and are confident that our torque sensors can withstand the typical loading conditions when the exoskeleton provides the maximum rating of 30 Nm plantarflexor assistance. The fatigue simulations predicted that V2 torque sensors would last at least 10 times longer than V1 sensors and would accumulate no damage directly on the sensing site where strain gages are placed. That is, fatigue simulations predict no material yield that would affect the critical torque measurement which would compromise the efficacy and safety of our exoskeletons.

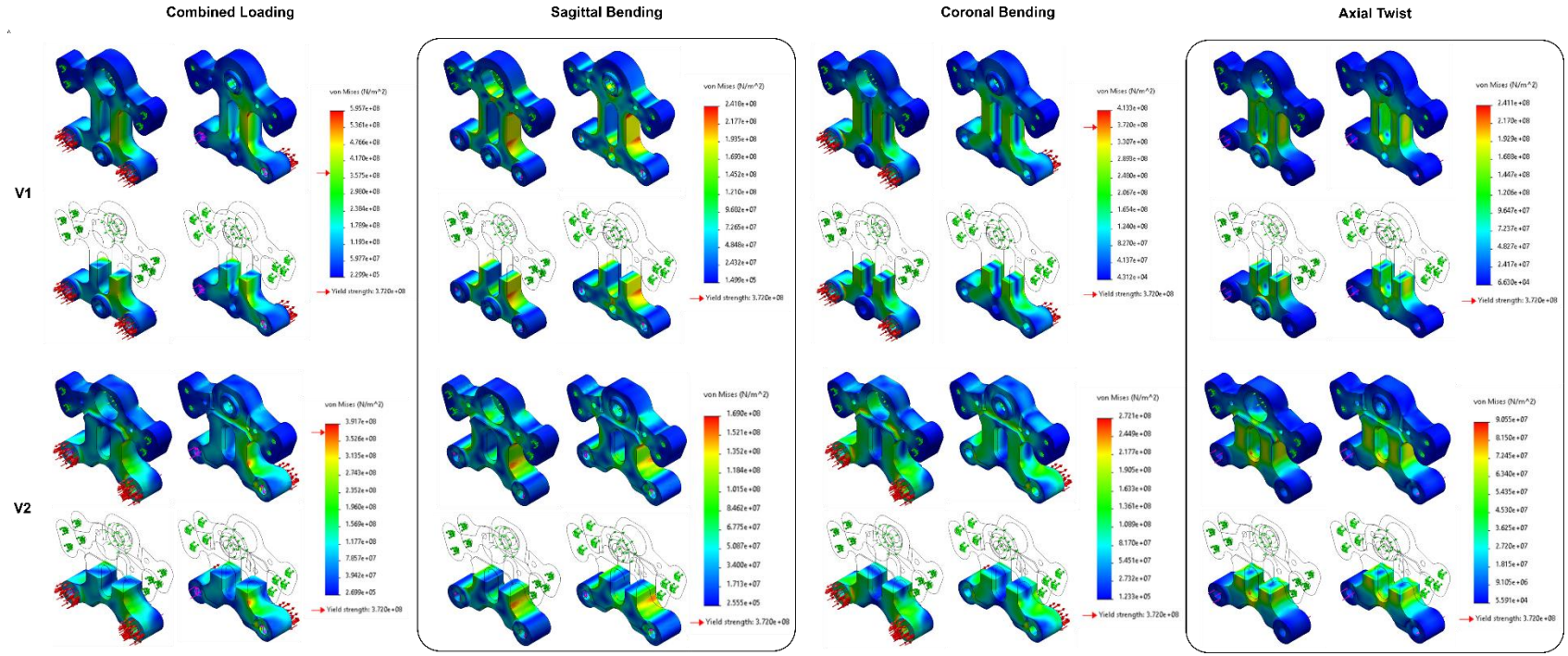

Fig. 25. Static simulation results for V1 (top row) and V2 (bottom row) torque sensor designs. The same loading conditions were applied for V1 and V2 torque sensor simulations. Solidworks FE calculated the von Mises stress for each loading scenario and indicated failure with a red arrow corresponding to the material yield strength of 372 MPa. To summarize, V1 torque sensors failed during coronal bending and combined loading corresponding to 50 Nm applied exoskeleton torque. V2 torque sensors failed during combined loading due to a stress concentration on a fillet. The factor of safety for V2 torque sensors for the overload condition of 50 Nm applied exoskeleton torque, which greatly exceeds the maximum repeatable assistive torque of 30 Nm, was 0.95. The V2 torque sensor design was a vast improvement over the V1 design.

Real testing verified that V2 torque sensors are a vast improvement over V1 torque sensors. To date, 14 torque sensors of the V2 design were machined, instrumented, calibrated, and actively used on exoskeleton devices in Flagstaff and other sites without issue. No failures have been reported. Furthermore, no evidence of plastic strain accumulation due to overload or fatigue has been observed in any torque sensors. One exoskeleton device, developed exclusively for durability testing, has experienced no zero-offset drift across over 17 cumulative hours of walking and over 62,000 assisted steps (Fig. 26).

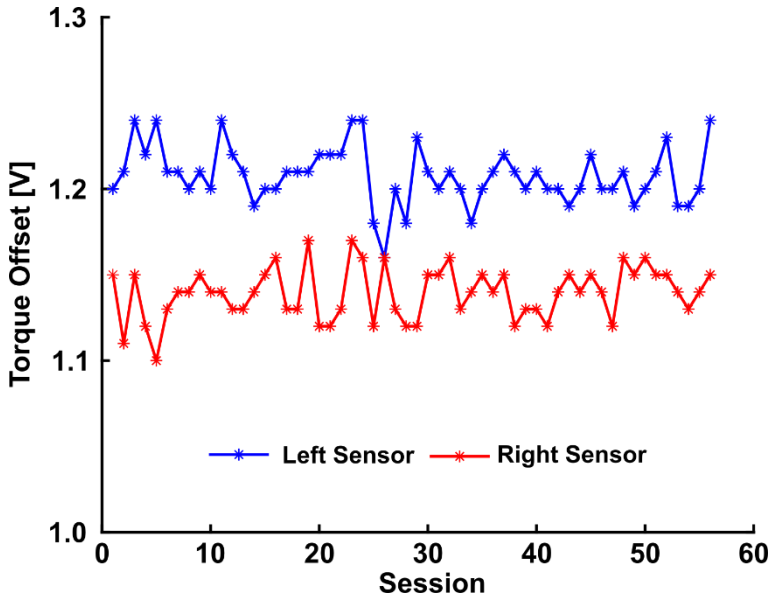

Fig. 26**.** Torque sensor zero-load offset over time. Each session was typically between 20 and 45 minutes. Prior to the start of each session, a zero-load offset calibration was acquired and saved. There is no evidence of a trend across sessions that would indicate material yield or fatigue. The variability in the zero-load offset is typical as different users of varying height, shoe size, and mass wore the device.

Torque Sensor Validation

The torque sensor was instrumented with a full Wheatstone bridge, which is a gage configuration that negates out-of-plane loads and temperature effects. The sensor measured the sagittal bending moment generated between the cable-driven pulley and footplate (Fig. 27).

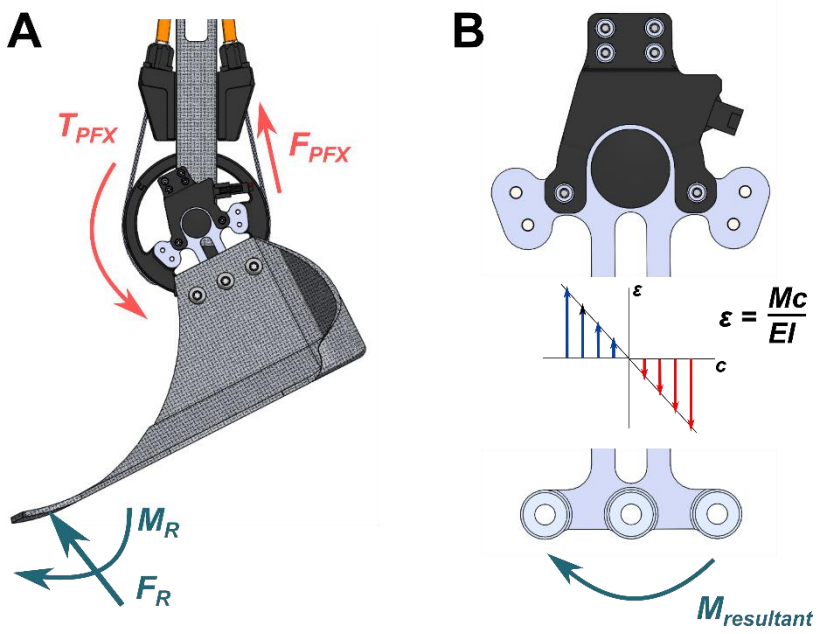

Fig. 27**.** Torque sensor function. **A.** The sensor transferred and measured torque between the pulley and footplate. **B.** The strain gauge configuration on the transducer measured the resultant sagittal bending moment between the footplate and pulley and negated out-of-plane bending and twisting.

We used a calibrated load cell (LCM200, Futek) attached to a known lever arm to relate the applied torque to the sensor's voltage response (Fig. 28). Four sensors were loaded to 30 Nm three times in each direction. Five-point moving average data were collected at 100 Hz and offset by a zero-load calibration value taken at the beginning of each loading repetition in MATLAB (R2018b, MathWorks). Loading repetitions for each sensor were averaged. Data from three sensor were used as training data for a linear model estimating applied torque given a voltage reading. Data from

the last sensor were used as a testing set to validate the model's performance. The results of this validation were presented in the manuscript (Fig. 17A).

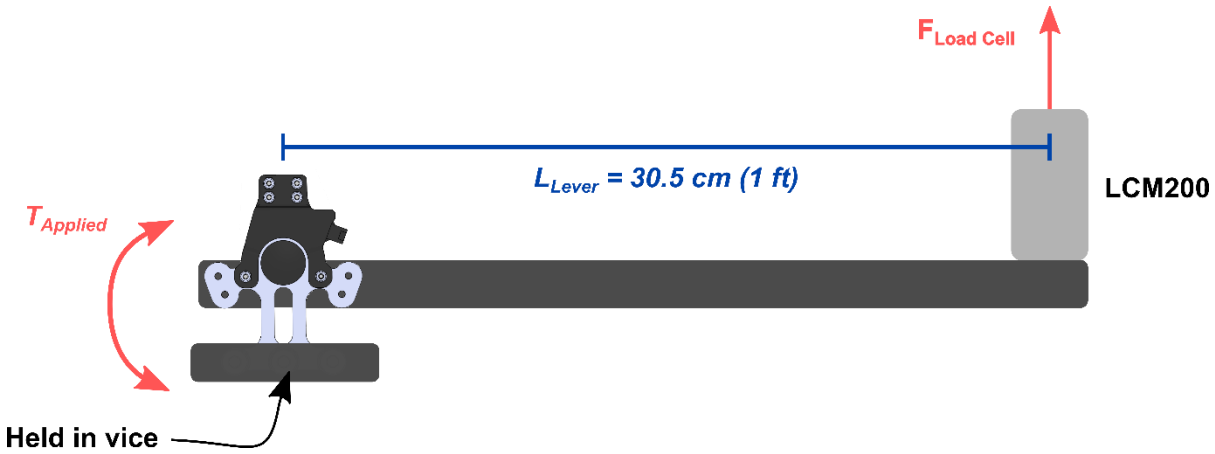

Fig. 28. Torque sensor validation setup. The LCM200 load cell was calibrated by the manufacturer and measured force. The torque sensor voltage response was related to the load cell force applied at the end of a lever using linear regression. Each sensor was loaded up to 30 Nm and unloaded three times in each direction.

As a final check of the torque sensor calibration procedure, we fixed a mass of a known weight onto the LCM200 load cell at the end of a 2-foot (0.6098 m) level arm and measured the torque applied to one custom, pre-calibrated sensor using the sensor's calibration curve and the LCM200 load cell. The mass weighed 4.28 kg measured using a digital scale with half-gram resolution and, when accounting for the mass of the calibration jig, induced an estimated torque of 27.59 Nm. After waiting for the harmonic response from the sudden torque to stabilize, 500 measurement samples from the torque sensor and the LCM200 load cell were captured and offset by a tare calibration taken prior to load application. The LCM200 load cell measurement was 27.72 ± 0.22 Nm and the torque sensor measurement was 27.59 ± 0.01 Nm (Fig. 29). The large standard deviation for the load cell was due to the high signal-to-noise ratio – the load cell is rated for up to 1000 lbs (454 kg) with an overall uncertainty of 1% full-scale output, so the desired signal magnitude to induce 30 Nm at our custom torque sensor was too small to be detected within the

resolution of custom data acquisition system. The load cell output signal had to be amplified with a gain of 304 V/V to place the signal range within the measuring bounds of the analog resolution of the Teensy 3.6 (0 – 3.3V with 1 mV resolution).

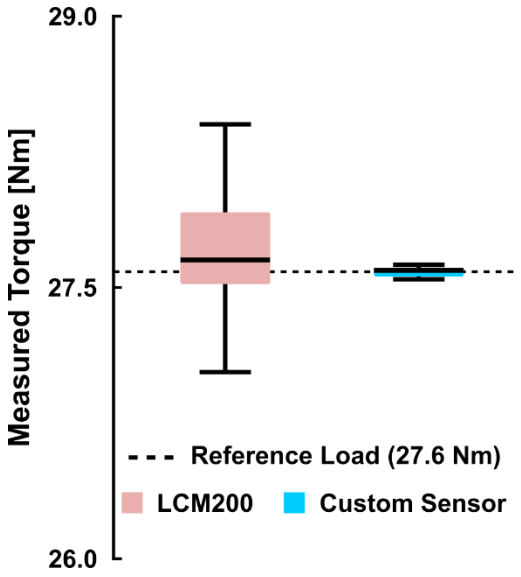

Fig. 29**.** Torque sensor measurement verification. A reference load was applied to the end of a known lever arm and measurements from the LCM200 load cell and a pre-calibrated custom torque sensor were acquired. Both measurements lay close to the reference, particularly for the custom torque sensor. The large standard deviation for the commercial load cell was due to high signal-to-noise ratio from signal amplification.

Torque Sensor Out-of-Plane Sensitivity

We also assessed the ability of the transducer to isolate sagittal plane moments. Strain coupling with bending modes other than the primary load direction (i.e., sagittal bending in our case) can alter the sensor output voltage. To ensure that our torque sensor's sensitivity to out-of-plane bending moments compared to the sagittal moment was low, we conducted an experiment to capture the sensor's voltage response to each bending direction individually. One sensor was precisely loaded to 10 Nm and released three times in each plane to simulate the application of a bending moment (sagittal and coronal bending and axial twist) using the LCM200 load cell and

calibration setup described in the previous section. The torque sensor voltage response to each bending moment was determined using simple linear regression (Table 10, Fig. 30). The torque sensor's sensitivity to axial twist and coronal bending was 15.5% and 5.2% of the sagittal bending sensitivity, respectively. The pooled uncertainty, calculated as the root-sum-square of the out-of-plane sensitivities, was 16.3%.

Table 10. Torque sensor sensitivity regression fit summary. The torque sensor sensitivity to coronal bending and axial twist is considerably less than for sagittal bending. Some error in the sensor voltage responses was likely due to the difficulty of perfectly isolating each bending mode.

Bending Mode	**Sensor Sensitivity (V/Nm)**	**R^2**	**Root-Mean-Squared Error (V)**	**Percent of Sagittal Sensitivity (%)**
Sagittal	0.0233	0.998	0.0122	-
Coronal	0.0012	0.792	0.0022	5.2
Axial Twist	0.0036	0.930	0.0047	15.5

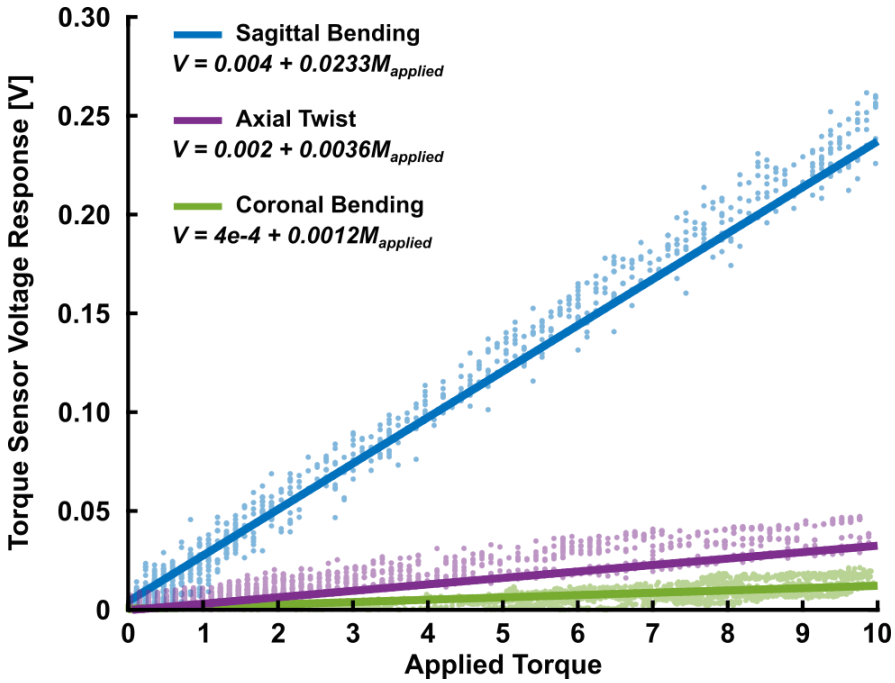

Fig. 30. Comparison of torque sensor sensitivity to different bending modes. The torque sensor was most sensitive to sagittal bending followed by axial twist and coronal bending.

Torque Sensor Measurement Uncertainty

It is important to identify and address sources of uncertainty and error in our sensors and calibration equipment to assess the validity of the torque measurement. In this short section, we will focus on a qualitative assessment of various sources of error that may impact the accuracy and precision of the torque measured by our custom sensors. Some sources of quantifiable and unquantifiable error are summarized in Table 11.

Table 11. Some possible sources of error in the torque sensor measurement.

Error Source	Estimated Relative Uncertainty (Unit)	Source of Relative Uncertainty Estimate
LCM200 load cell uncertainty	±1% full-scale output (kg)	Manufacturer (Futek)
Amplifier gain defined by resistor value (per measurement)	±1% of the gain (V/V)	Manufacturer (INA125P, Burr-Brown)
Teensy 3.6 analog read resolution (per measurement)	±0.03% of full-scale voltage (V)	Manufacturer (PJRC)
Torque sensor gage resistance tolerance (per side)	±0.5% (Ω)	Manufacturer (Sensing Systems)
Torque sensor gage placement tolerance (per side)	±5-8% of dimension (mm)	Manufacturer (Sensing Systems)
Torque sensor manufacturing tolerance (per dimension)	±1-2% of dimension (mm)	Manufacturer (Protolabs)
Misaligned load application during calibration	Not easily quantifiable	Torque Sensor Validation Section (Fig. 28)
Overall LCM200 noise using our system	±0.7% of full-scale voltage (V)	Torque Sensor Validation Section (Fig. 29)
Overall torque sensor noise using our system	±0.01 % of full-scale voltage (V)	Torque Sensor Validation Section (Fig. 29)
Torque sensor out-of-plane sensitivity	±16.3% of full-scale voltage (V)	Torque Sensor Out-of-Plane Sensitivity Section (Fig. 30)
Effect of using a single calibration value for all torque sensors	±6.5% of mean calibration slope (Nm/V)	Torque Sensor Measurement Uncertainty (Fig. 31)

To date, 14 sensors have been manufactured, instrumented, and calibrated using the procedure detailed in the Torque Sensor Validation section. A calibration slope at 95% confidence was obtained for each sensor using linear regression as described in the text of the present chapter. To assess the overall uncertainty in the calibration slope, the calibrated slopes of all 14 sensors were pooled together. The mean calibration value, used in converting the torque sensor bridge voltage (a voltage that is amplified by the excitation circuit and then measured by the microcontroller

analog-to-digital converter) to sagittal torque between the pulley and footplate, was 41.5 ± 2.7 Nm/V (Fig. 31).

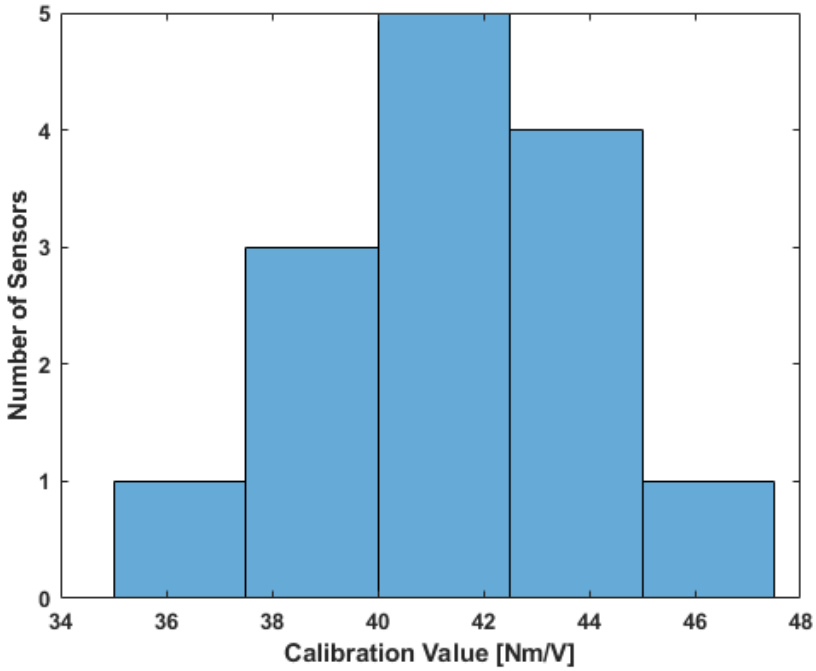

Fig. 31**.** Histogram of torque sensor calibration values. Calibration values for each sensor were obtained using the methods described in this chapter and in the Torque Sensor Validation section. The bin width is 2.5 Nm/V. The mean slope was 41.5 ± 2.7 Nm/V.

The effect of some error sources, particularly those as a result of the manufacturing and instrumentation process, on the actual torque measurement of our sensors is quite difficult to assess. There is also considerable coupling between some sources of error, such as between the out-of-plane sensitivity of our sensors and the possibility of misaligning the load cell during calibration or even during the sensitivity analysis itself. Future work should strive to minimize the effects of many of these sources of error. For example, it would be possible to limit or even eliminate the likelihood of misaligning the load cell during calibration with the addition of some simple hardware to fix the load cell in place relative to the lever arm. The largest sources of measured torque error include the out-of-plane sensitivity (up to 16.3% of full-scale voltage) and

the effect of using a single calibration slope for all torque sensors (up to 6.5% of the calibration slope). The overall uncertainty in the torque measurement, calculated as the root-sum-square of the aforementioned uncertainties, during exoskeleton-assisted walking may then be as high as 17.5% of the full-scale torque, or about 5.25 Nm. The uncertainty in the measured torque affects the closed-loop controller effort and may ultimately reduce the electro-mechanical efficiency of our system.

Angle Sensor Validation

We conducted a motion capture experiment to validate on-board angle and angular velocity measurement. 3D positions of retroreflective markers placed on bilateral ankle assemblies were recorded at 120 Hz in Vicon Nexus as the joints rotated in response to sinusoidal angular displacement driven by the motors (Fig. 32, 33). Motion capture data were filtered with a 4th order Butterworth low-pass filter with a 12 Hz cutoff, down-sampled to 100 Hz, and synchronized with a hardware trigger to the voltage data from each Hall sensor streamed over Bluetooth to MATLAB at 100 Hz. To validate the angular position measurement, 2/3 of the sensor voltage and corresponding motion capture angle data were randomly selected to generate a linear model. The training data spanned 40 degrees of exoskeleton joint motion split between plantarflexion and dorsiflexion regions. The remaining data were used to test the model and calculate the error between the sensor module measurement and the angles from motion capture. To validate on-board angular velocity estimation, the time derivative of the Hall sensor and motion capture angles were calculated by numerical differentiation. For comparisons and to confirm suspicions of mechanical delay due to the cable transmission, motor velocity was measured using the motor's internal Hall sensors.

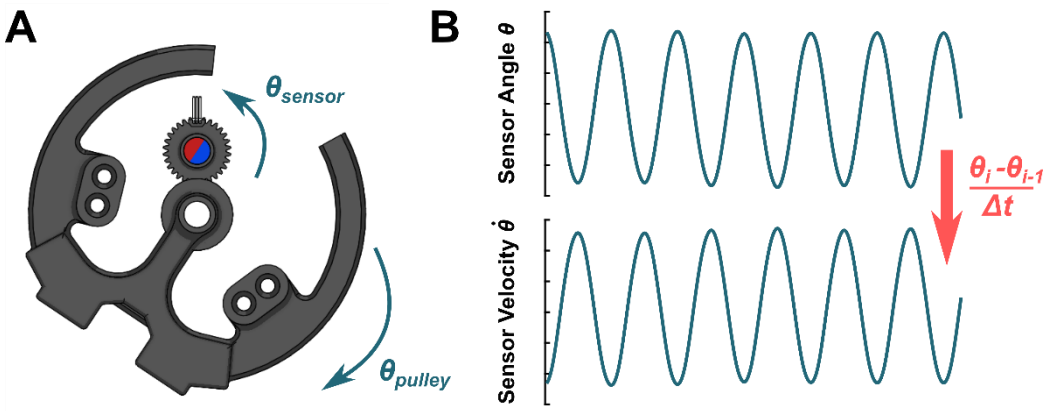

Fig. 32**.** Angle sensor function. A. Sagittal plane view of the angle sensor and pulley. The sensor shaft rotated opposite the pulley. A Hall sensor was held above the rotating diametric magnet. B. The Hall sensor output a repeatable voltage in response when the pulley was rotated. The pulley velocity was calculated in real time using a numerical derivative.

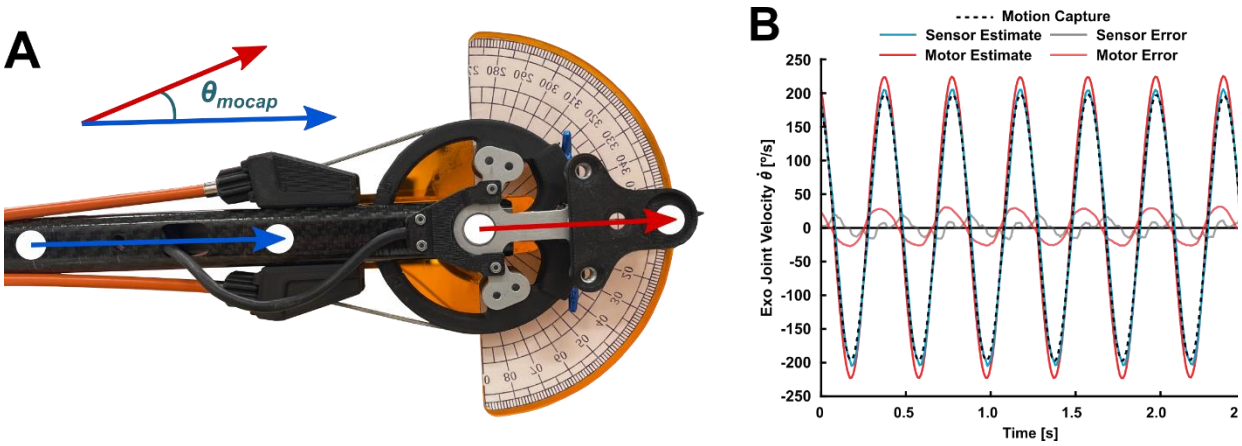

Fig. 33**.** Angle sensor validation setup. A. Reflective markers on the upright and exoskeleton joint defined two vectors in space such that angle between the vectors represented the angular position of the joint. The numerical derivative of the angle represented the angular velocity of the joint. B. A sample of angular velocity data from the validation experiment (same as Fig. 17 in the main text). The motors were commanded to move in a sinusoidal motion with velocity control while the custom angle sensor captured pulley angle and velocity. Some transmission losses between the motor and the pulley are evident as the motor estimate error is greater than the sensor estimate error (motor velocity RMSE = 17.85 deg/s, sensor velocity RMSE = 9.01 deg/s).

Exoskeleton Data Curves

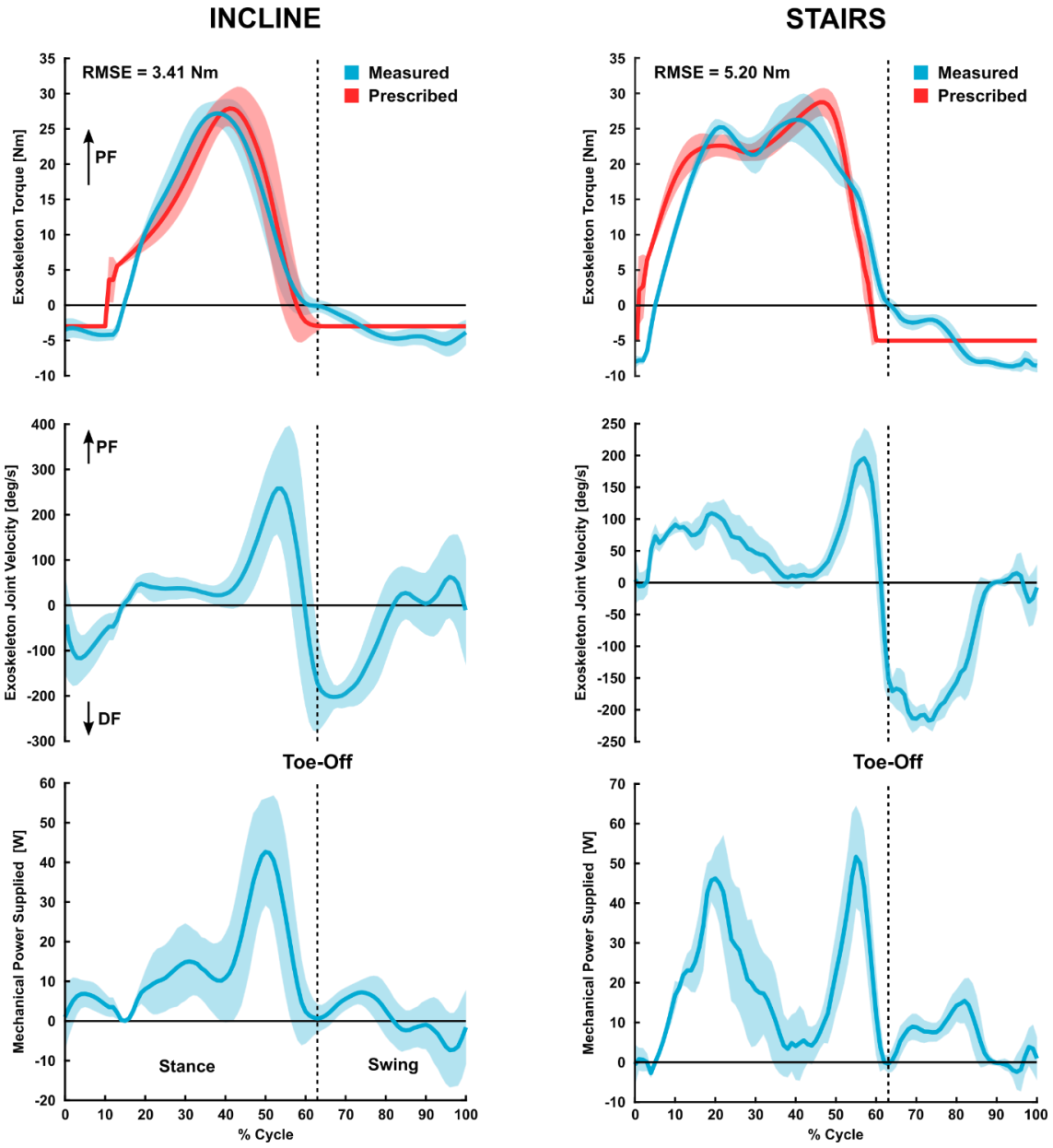

Fig. 34. Supplemental exoskeleton performance data. P3's exoskeleton joint torque (top row), angular velocity (middle row), and mechanical power (bottom row) for inclined walking (left column) and stair ascent (right column). Peak measured torque typically ranged from 25 to 30 Nm. The upper torque capacity of the exoskeleton is 30 Nm. Torque root-mean-squared error (RMSE) was largely due to motor power limitations. The adaptive nature of our high-level controller results in variable torque, velocity, and power profiles between users and terrain.

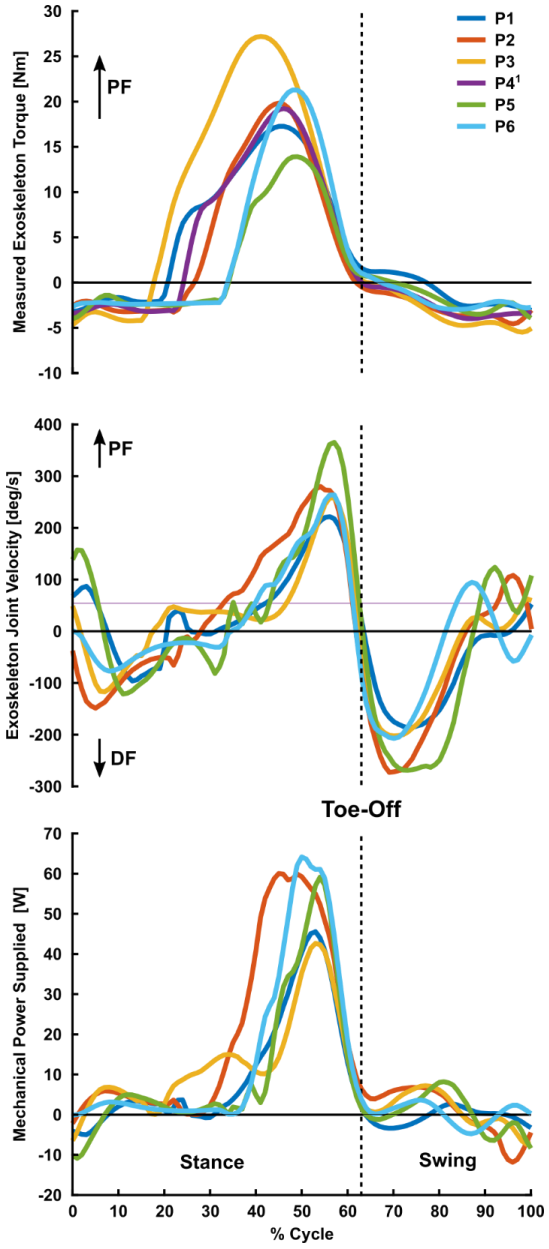

Fig. 35**.** Mean **e**xoskeleton measured joint torque (top), angular velocity (middle), and mechanical power (bottom) for each unimpaired participant. [1]P4 did not have available angular velocity or joint power data.

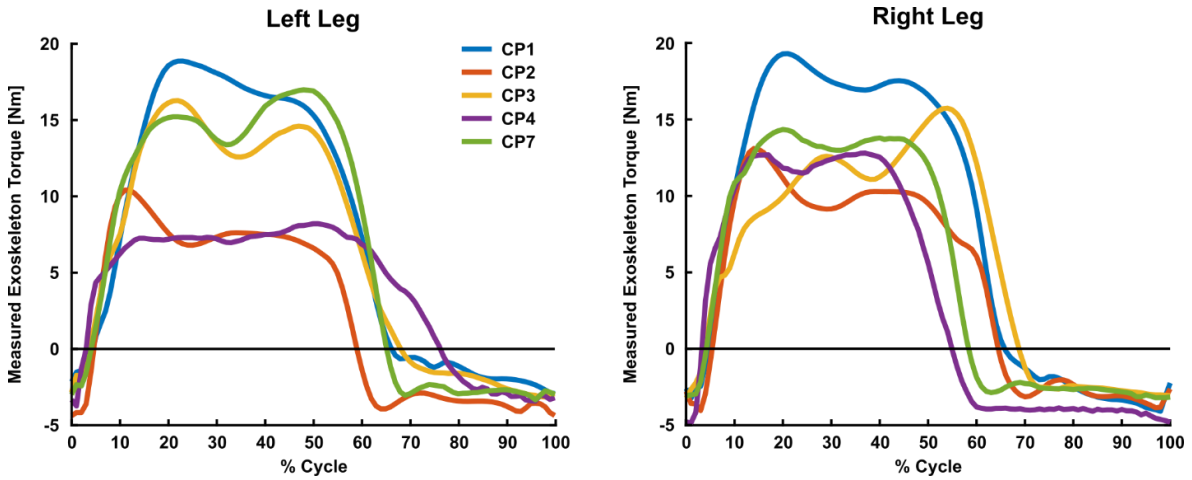

Fig. 36**.** Mean exoskeleton measured joint torque for the participants with CP that performed the stairs maximum exertion experiment. Joint angular velocity and mechanical power data were unavailable.

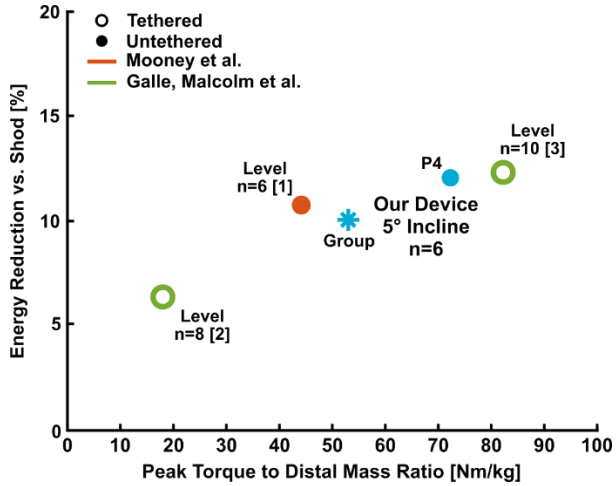

Fig. 37**.** Comparison of observed metabolic benefit for unimpaired users vs. peak exoskeleton torque to distal mass ratio. Data points with the same color represent the same exoskeleton design. Though our device had lower peak torque and power than some other devices, the low distal mass of our exoskeleton resulted in a high torque-to-weight ratio. The observed group-level reductions in metabolic power during assisted walking compared to no device was similar to other groups. Published studies demonstrating metabolic benefits during exoskeleton-assisted walking for unimpaired users are limited.

Energy consumption and Efficiency

The batteries used in this study had a capacity of 2000 mAh. To determine the effective battery life, overall energy consumption, and electrical-to-mechanical efficiency of our device, we conducted an experiment in which one person walked on a treadmill inclined 5 degrees at 1.5 m/s with the exoskeleton unilaterally providing 22 Nm peak plantarflexor torque and 2.75 Nm dorsiflexor torque (the mean torque levels for the present study). Battery voltage, motor current, motor velocity, exoskeleton joint torque, and exo joint velocity were collected for 50 steps. To assess overall device energy consumption, the motor current was integrated with respect to time for each step (Fig. 38A). Exoskeleton joint mechanical power was calculated as the product of joint torque and angular velocity measured using our validated in-line sensors. Electrical power consumed by the device was calculated as the product of battery voltage measured by a voltage monitor (INA219, Texas Instruments) on the PCB and motor current measured by Maxon motor drivers. Electrical-to-mechanical power efficiency was calculated as the ratio of mean exoskeleton joint power output to mean electrical power consumed (Fig. 38B).

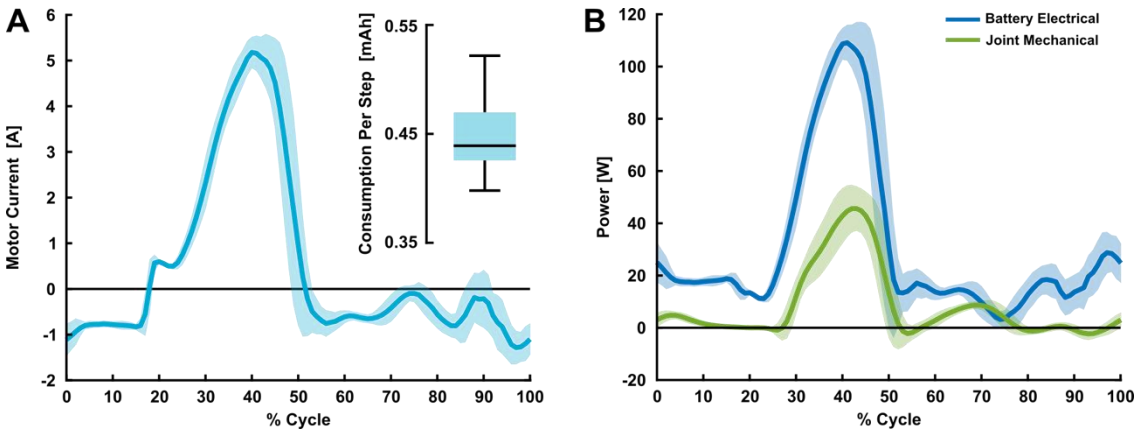

Fig. 38**.** A. Mean ± standard deviation motor current profile for one leg. In the corner, the distribution of energy consumption per step in mAh is shown. The average energy consumption per step was 0.45 ± 0.03 mAh which translates to about 2222 strides or 37 minutes if all 2000 mAh of the battery were used assuming a cadence of one stride per second. B. Electrical and mechanical power profiles for the battery and exoskeleton joint, respectfully. The electrical-to-mechanical power efficiency, calculated as the ratio of mean joint mechanical power to electrical power consumed during stance, was 35%.

Augmentation Factor Calculation

Augmentation factor (AF) is an estimate of the potential metabolic impact an exoskeleton may have on a user [29,109]. As described in [29], the AF was developed for an autonomous ankle exoskeleton and estimates a change in metabolic power depending on device characteristics such as positive mechanical power, dissipated and mass distribution on the body. AF, defined as

$$AF = \frac{p^{+} + p^{dis}}{\eta} - \sum_{i=1}^{4} \beta_i m_i \qquad (1)$$

where $p^{+}$was the mean positive power across the gait cycle, p^{dis} was zero if the positive power exceeded the negative power or otherwise was the absolute value of the difference between positive and negative power, η was the muscle-tendon efficiency, and β_i was the metabolic impact of wearing added mass m_i on body location i (Table 12). In short, AF balances the

impact the exoskeleton mechanical power contribution ($p^+ + p^{dis}$) has on a body based on muscle-tendon efficiency (η=0.41, [29,44,112]) with the overall detriment of wearing additional mass on the body ($\sum_{i=1}^{4} \beta_i m_i$). The metabolic detriment of wearing additional mass (m_i) varies by location on the body (β_i) with mass placed distally such as on the shank or foot having a greater impact on energetics than mass placed proximally on the pelvis (Table 12, [63]).

Table 12. Exoskeleton component mass breakdown.

Component[1]	**Mass (kg)**	**Location on Body**	**Metabolic Impact (W/kg)**
Waist assembly	1.37	Waist	3.33
Cable transmission (x2)	0.31	Thigh	5.55
Ankle assembly and cuff (x2)	0.55	Shank	5.62
Footplate (x2)	0.28	Foot	14.80
Total Bilateral Exoskeleton Mass[3]	2.51		

[1] The mass corresponding to components indicated with (x2) is bilateral. [2] The impact of added mass on metabolic power based on location was investigated in Browning et. al. 2007 [5]. [3] The exoskeleton mass breakdown presented was for a medium-sized exoskeleton sized for users between 160 and 185 cm tall.

All participants in the unimpaired cohort used the same exoskeleton with small differences in the mass of cuffs and footplates. For simplicity, the same mass distribution as in Table 12 was used in calculating AF for each unimpaired participant. The metabolic detriment of wearing our exoskeleton was estimated to be 13.5 W. A positive AF predicts a reduction in energy expenditure when wearing an exoskeleton. Mean exoskeleton positive power p^+ was calculated by averaging the positive mechanical power data collected during the unimpaired cohort experiment for each stride across both legs (including both stance and swing phases) and averaging again across strides for each participant. As described in [29], if the exoskeleton mean positive power exceeds the mean negative power, p^{dis} is zero. Refer to the exoskeleton joint power curves for each participant in Additional File 3 to observe that the positive mechanical power for each stride greatly exceeds any negative mechanical power. Components of the AF calculation in Eq. 1 are summarized in

Table 13 for each participant. Each participant's actual observed metabolic impact is also summarized.

Table 13**.** Summary of unimpaired participant characteristics, AF calculation components, and the predicted and actual metabolic benefit from the experiment in the main text.

Participant	**Mass (kg)**	**Peak Stance Torque (Nm)**	**p^+ (W)[1]**	**p^{dis} (W)**	**Mass Detriment (W)**	**Augmentation Factor (W)**	**Metabolic Impact (W)**
P1	50.0	17.5	17.1	0	13.5	28.1	38.0
P2	57.5	20.5	28.3	0	13.5	55.6	35.1
P3	91.6	30.0	20.8	0	13.5	37.2	81.5
P4[2]	65.0	23.0	-	-	-	-	78.3
P5	45.7	16.0	21.3	0	13.5	38.4	0.1
P6	72.6	25.0	20.1	0	13.5	35.4	90.9

[1]The mean positive power, dissipated power, mass detriment, and augmentation factor are bilateral. [2] Mechanical power data was not collected for P4.

For all participants, dissipated power p^{dis} was zero and the AF was positive, meaning that all participants should use less energy when walking with the exoskeleton. While all but one participant had a marked improvement in metabolic power when walking with exoskeleton assistance compared to shod, the agreement between the benefit predicted by AF and the actual observed benefit was poor.

Chapter 5: Design and Electromechanical Performance Evaluation of a Powered Parallel-Elastic Ankle Exoskeleton

Authors: Greg Orekhov and Zachary F. Lerner

Abstract

The widespread adoption of powered lower-limb exoskeletons for augmenting mobility requires energy-efficient actuation to provide meaningful assistance over relevant walking durations. We designed, modeled, and validated an ankle exoskeleton design with a parallel elastic element in the form of a carbon fiber leaf spring that stored and returned energy in parallel to a cable-drive ankle joint during stance phase. We assessed the impact of the parallel elastic element on the performance of the untethered robotic ankle exoskeleton at walking speeds of 0.75-1.25 m/s using a previously validated-controller, and a controller designed specifically to maximize the spring's benefit. The spring selected for our adult cohort had a stiffness of 97.2 Nm/rad, engaged best at 0-degrees ankle dorsiflexion, and produced 10-15 Nm assistive torque at all walking speeds. When tracking the previously validated exoskeleton controller, peak motor current was reduced by 14-20% and integrated current was reduced by 16-19% for parallel-elastic design vs. without spring engagement; this translated to 15-26% more assisted steps for the same battery capacity. When utilizing the controller designed to take advantage of the parallel spring torque, the number of assisted steps for the same battery capacity increased 46-76% compared to the no spring configuration depending on walking speed. Seeking to facilitate real-world adoption, this powered parallel elastic ankle exoskeleton design holds potential to significantly extend powered walking duration, and improve battery and motor life of operation by reducing peak and mean motor current requirements.

Introduction

Lower-limb exoskeletons have been extensively researched as tools for human performance augmentation in individuals with and without neurological impairments [16,30–32,47,113]. Specifically, lower-limb exoskeletons can reduce the burden of walking and maximize human performance via mechanical assistance provided in parallel to a user's biological joint. The ankle joint in particular is a typical target for exoskeleton assistance due to its dominant role in efficient bipedal locomotion [33–35].

Untethered exoskeletons must provide enough torque and power to both supplement joint mechanics and offset the metabolic burden from the added mass, otherwise the benefits of assistance are limited [49,109]. Only a few untethered exoskeletons have demonstrated improvements in walking efficiency due to the difficulty of designing a device that supplies enough positive power to supplement joint mechanics and counteract the burden of wearing actuators, batteries, and associated hardware [16,22,26,47,109,114]. Widespread adoption is hampered, in part, by the need for more energy-efficient designs that can deliver meaningful assistance over relevant walking durations.

Elastic elements are common components in robotic systems and can be placed in series or in parallel to motors or other actuators to reduce actuator burden and energy consumption [115–118]. Series elastic elements placed between the actuator and load can reduce actuator power requirements [119–121], but decouple the load from the actuator, complicating control. Elastic elements placed in parallel with the actuator affect the load directly, thereby also reducing power requirements, and potentially, actuator burden [117,121,122]. Simulated actuator energy and

power optimizations for exoskeletons have shown that springs in parallel with actuators may significantly reduce torque and power demand and were preferred over series elements [121].

Actuation design that improves electromechanical efficiency and performance could increase the ability of untethered exoskeletons to provide meaningful assistance in free-living settings. Important considerations for untethered lower-limb exoskeletons, whether for rehabilitation or mobility augmentation, include the added mass and duration of operation. Utilization of large batteries to increase assisted walking duration diminishes the physiological benefits for the user because additional mass offsets the benefits of exoskeleton assistance [49]. In prior work exploring the use of ankle exoskeleton assistance to improve walking efficiency in children and young adults with cerebral palsy, we found a strong negative relationship between device mass and assisted metabolic benefit [26]. Improved device efficiency would help minimize device mass (smaller actuators and batteries) to maximize benefit, particularly for children [26,47].

Despite the recommendations established from simulations, as far as we are aware, no untethered robotic ankle exoskeleton has experimentally evaluated the use of parallel elastic elements to improve electromechanical performance. This is likely a result of the significant design challenge related to adding mass and mechanical complexity to the lower leg. Another design challenge relates to proper spring engagement/disengagement during the stance and swing regions of the gait cycle; simply placing a spring in parallel with the joint would either limit range of motion or produce no net energy efficient benefit across the gait cycle. The overarching purpose of this work was to design an ankle exoskeleton with parallel elasticity and evaluate the parallel elastic element's ability to improve energy efficiency during walking. In the following sections, we summarize the design and function of our parallel-elastic actuation system utilizing a carbon fiber leaf spring and cable-driven pulley. First, we model the spring's behavior as a function of

displacement angle. Then, we evaluate the impact of spring engagement angle on motor current consumption. After establishing an optimal engagement angle, we then evaluate the benefits of parallel elasticity at different walking speeds in multiple adults. We hypothesized that parallel elasticity would significantly reduce motor current requirements at all walking speeds.

Methods

Parallel Elastic Element Design

We defined several requirements to guide the design of the parallel elastic element and its interaction with the rest of the exoskeleton assembly. The major design requirements included: (1) low distal mass to minimize metabolic detriment when wearing the device [63]; (2) a unidirectional elastic element that stores energy during early stance and releases energy during toe-off; (3) adjustable spring engagement angle to accommodate different anatomies and gait patterns; and (4) a target peak torque contribution from the elastic element of 10-15 Nm. This target peak torque was selected so that the design would be applicable for adolescents through adults by providing between 50-75% of the total external ankle torque [114,123].

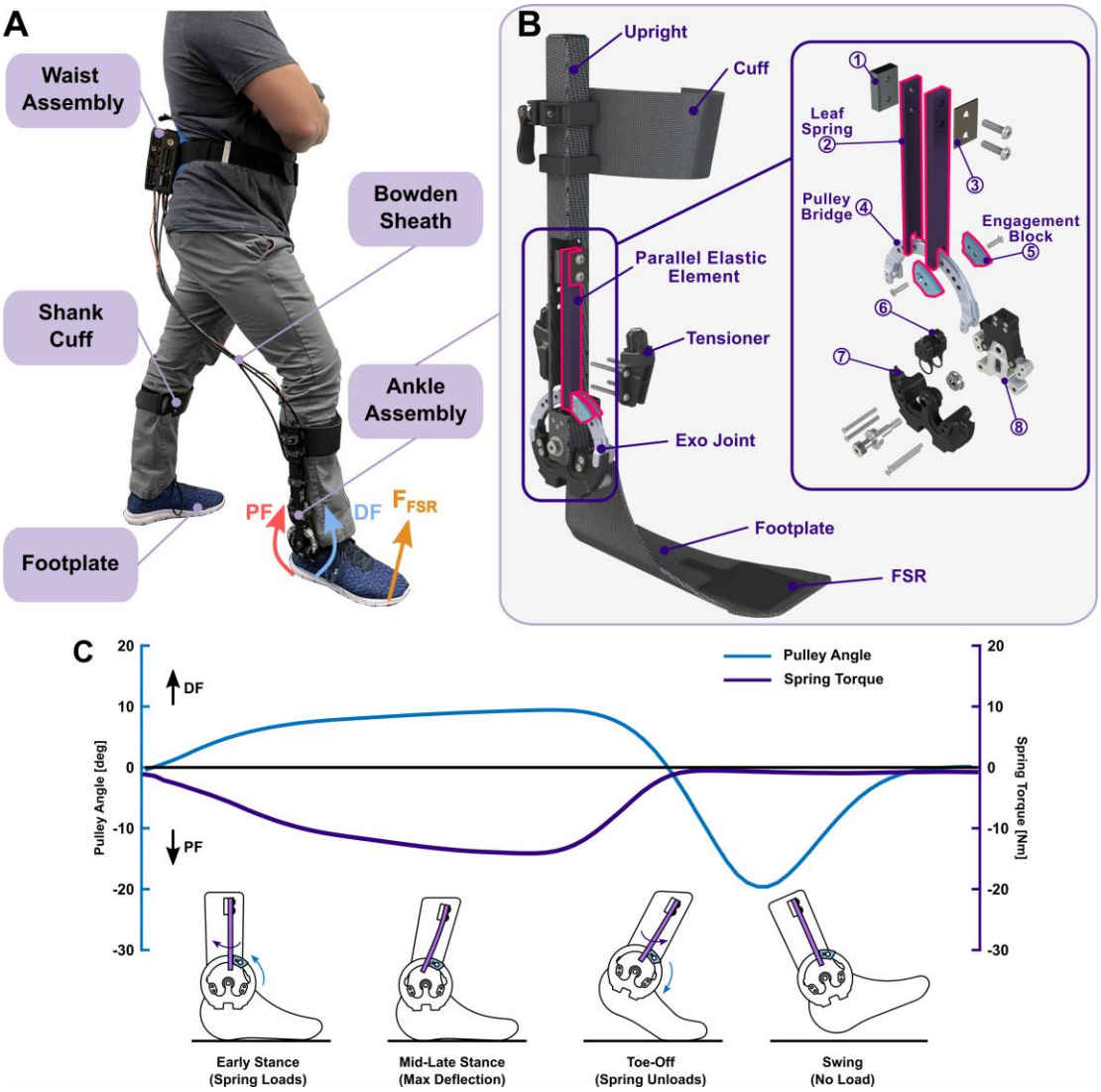

Fig. 39. Ankle exoskeleton overview and function. A. Picture of the untethered robotic ankle exoskeleton. B. Renderings of the ankle assembly with a cut-away showing the placement and a detailed view of the parallel elastic element and other hardware. The upright was a square carbon fiber tube to which all components were fixed. The parallel elastic element assembly was fixed to the upright and interfaced with the cable-actuated exoskeleton joint. Components from the detail view: 1) Spring capture block. 2) Carbon fiber leaf springs. 3) Custom washer. 4) An aluminum pulley bridge that accommodated several engagement angles. 5) Aluminum blocks that mounted to the pulley bridge and engaged the springs. 6) A custom angle sensor to measure the ankle angle. 7) Carbon fiber-reinforced pulley base actuated by the cable transmission. 8) A custom torque sensor. **C.** Schematic depiction of spring engagement across the gait cycle. The spring assembly (purple) was loaded by the pulley engagement blocks (blue) during regions of ankle dorsiflexion (DF) and stored potential energy. The energy was released as the spring was unloaded during toe-off in parallel with the exoskeleton providing plantar-flexor assistance to decrease required actuator torque. During swing, the spring remained unloaded so as to not counteract the exoskeleton function.

To meet our design requirements, we developed a novel exoskeleton ankle joint that incorporated a unidirectional carbon fiber leaf spring with a Bowden-cable-actuated pulley (Fig. 39). The leaf spring assembly consisted of one 1/4" thick 0/90 ply carbon fiber bar (8194K111, McMaster-Carr) and one 1/8" thick bar of the same ply (8194K16, McMaster-Carr). The functional length of the spring was 80 mm and the overall assembly length was 118 mm. An assembly of long, thin springs was used as opposed to a single short, thick spring to minimize strain on the spring assembly at maximum deflection. An aluminum pulley with engagement blocks deflected the spring during ankle dorsiflexion in early stance to store energy (Fig. 39B). The engagement blocks could be adjusted along the pulley radius in 5-degree increments to alter the angle and timing of spring engagement. The leaf spring released energy during toe-off in parallel to the cable transmission system actuating the pulley to provide plantar-flexor assistance. The exoskeleton also featured custom torque and angle sensors in-line with the ankle joint [114] (Fig. 39B). The spring assembly and engagement blocks had a total mass of 36 grams per leg; the remaining ankle assembly including the footplate had a mass of 415 grams per leg.

The exoskeleton included a waist-mounted assembly that housed motors (Maxon EC-4pole), electronics (PCB, drivers, signal processing chips), and battery, the design of which has been reported in [114] (Fig. 39A). A pressure sensor (FSR, TekScan A502) under the ball of the foot detected gait transitions and informed the high-level state machine of user intent. The exoskeleton had a total mass between 2.4 and 2.6 kg depending on the size of footplates and cuffs, was untethered, and had most of the mass placed on the pelvis to minimize metabolic detriment [63]. The device provided adaptive plantar-flexor assistance during stance based on a proportional joint moment controller (PJMC, [64,98]). The peak plantar-flexor torque that could be generated by the device was 30 Nm [114].

Parallel Elastic Element Modeling and Validation

In order to estimate the leaf spring's torque contribution during walking when the motors were active, we sought to model the spring behavior during use. With the cable transmission system disconnected, a series of walking experiments on a treadmill were conducted. We assessed a range of relevant walking speeds because ankle kinematics, including peak stance phase dorsiflexion, typically change with speed [124]. The walking speeds, 0.75, 1.00, and 1.25 m/s, were selected to ensure that our design would be suitable for the typical range of speeds for our target populations (unimpaired individuals and individuals with CP and stroke[10,26,114,125]). For each walking speed, the spring deflection and torque were measured using previously-validated onboard angle and torque sensors [114] and transmitted to our custom MATLAB interface over Bluetooth at 100 Hz.

We developed an empirical model of the spring's torque response as a function of the measured deflection. The spring had a linear loading region, a nonlinear unloading region, and was disengaged during plantarflexion (Fig. 39C, Fig. 40). The loading and unloading regions were separated at the maximum measured angle of the step. The piecewise model is summarized in Eq. 1:

$$T_{spring} = \begin{cases} T_{load}, & Loading \\ T_{unload}, & Unloading \\ 0, & \theta < \theta_{engage} \end{cases} \quad (1)$$

where θ is the measured pulley angle and θ_{engage} is the engagement angle; the engagement angle was at zero degrees when the footplate was perpendicular to the upright as shown in Fig. 39A. We used simple linear regression to determine the overall leaf spring torsional stiffness K_{spring} and

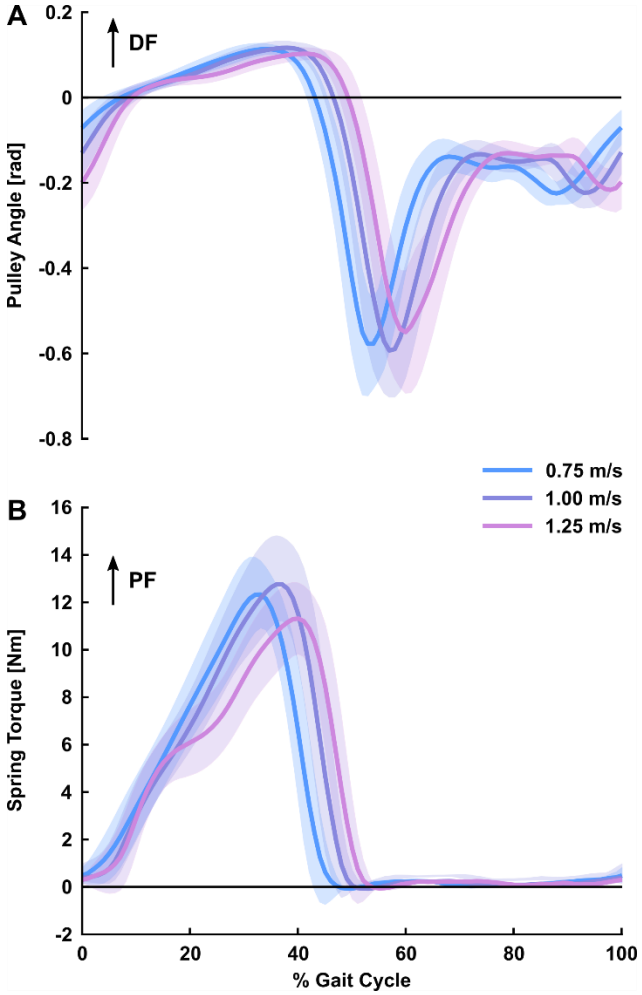

Fig. 40. Measured exoskeleton joint angle (A) and resulting spring torque (B) at different walking speeds. The spring was engaged at a neutral angle of zero degrees and built torque during ankle dorsiflexion. The leaf spring was stiff enough to produce at least 10 Nm of plantarflexion-directed torque on average at all speeds and produced the most torque at slow-to-moderate speeds (up to 15 Nm for some steps at 1.0 m/s).

actual engagement angle θ_{engage} by modeling the loading response as defined in Eq. 2. Some small offset torque T_{offset} was present due to early spring engagement.

$$T_{load} = T_{offset} + K_{spring}\theta_{load} \qquad (2)$$

The spring's unloading behavior was modeled by normalizing the spring deflection θ_{unload} by the maximum measured deflection of each step θ_{max} and normalizing the torque T_{unload} by the corresponding measurement at maximum spring deflection from the loading region $T_{load}(\theta_{max})$ as in Eq. 3.

$$\frac{T_{unload}}{T_{load}(\theta_{max})} = f\left(\frac{\theta_{unload}}{\theta_{max}}\right) \qquad (3)$$

The normalized spring deflection during unloading was transformed using a base-10 exponential function (i.e., $10^{\frac{\theta_{unload}}{\theta_{max}}}$) and used as an input to a simple linear regression predicting normalized spring torque as in Eq. 4.

$$T^*_{unload} = g\left(10^{\frac{\theta_{unload}}{\theta_{max}}}\right) = g(\theta^*_{unload}) \qquad (4)$$

Several exponential functions were evaluated; a base-10 exponential transformation yielded the lowest error between measured and predicted spring torque during unloading. Finally, re-arranging Eq. 3 and 4 yields Eq. 5, the model for estimating the spring torque during the nonlinear unloading regions as a function of the normalized and transformed angle scaled by the torque corresponding to the maximum deflection from the loading phase:

$$T_{unload} = T_{load}(\theta_{max})T^*_{unload} = T_{load}(\theta_{max})g(\theta^*_{unload}) \qquad (5)$$

To validate the spring loading and unloading models, we pooled torque-displacement data for all speeds and randomly selected ¾ of the data for model training and used the rest for testing. Model fit was assessed using the coefficient of determination and accuracy was quantified using the root-mean-squared error (RMSE) between the predicted and measured spring torque.

Variable Engagement Angle Experiment

The ankle angle at which a parallel spring engages affects the timing and amount of spring torque delivered to the system. Engaging the spring too early, and the motors must waste energy by fighting the spring contribution during swing phase; engaging too late, and the spring does not reduce actuator energy requirements during stance. To assess the effect of engagement angle on the potential of parallel elasticity to improve exoskeleton performance, we conducted a series of walking experiments. One adult participant walked with 22 Nm plantar-flexor assistance on a treadmill at 1.0 m/s with the spring engagement angle set to 0 degrees, 5 degrees, and 10 degrees. Exoskeleton data including measured joint torque, pulley angle, and motor current were collected at 500 Hz, averaged with 5-sample moving average filters, and transmitted via Bluetooth to a custom MATLAB interface (R2019b, Mathworks) at 100 Hz for 30 strides at each engagement angle.

Since the peak torque can vary between steps due to human compliance, we selected and analyzed only gait cycles that had an average peak plantar-flexor torque that were statistically similar between conditions. After selecting gait cycles and removing outliers, the data for each trial comprised 10 steps. The mean motor currents for each step were obtained, normalized by the corresponding mean torque, and compared between each engagement angle trial. To assess whether engagement angle had an effect on performance metrics, we ran one-way analysis of

variance (ANOVA) at 95% confidence. For metrics with significantly different means, we ran *post-hoc* Tukey tests with multiple comparisons corrections to detect the effects of engagement angle at 95% confidence. All analyses were conducted in MATLAB.

Spring Effectiveness Experiment Using a Previously-Validated High-Level Controller

We assessed the spring's effectiveness in decreasing actuator energy consumption during motorized exoskeleton walking at speeds of 0.75, 1.00, and 1.25 m/s with a cohort of six unimpaired adults (Table 14). The Institutional Review Board of Northern Arizona University approved this protocol (#986744). For this experiment, we used an unmodified instance of a previously-validated control scheme that has demonstrated an ability to produce a metabolic benefit in unimpaired and impaired individuals and across different terrains and walking conditions [64,98]. The control scheme included a high-level controller that prescribed a torque profile in real time using the footplate FSR as in Eq. 6:

$$T = \begin{cases} t_{set}\dfrac{f_{inst}}{f_{cal}} & , \quad C_{limit} = [-8A\ 8A] \quad (stance) \\ 0 & , \quad C_{limit} = [-8A\ 8A] \quad (swing) \end{cases} \tag{6}$$

Table 14. Participant characteristics.

Participant	Sex	Age [years]	Mass [kg]	Peak Stance Torque [Nm]
P1	F	25	50.0	15.0
P2	M	21	68.2	20.5
P3	M	33	68.0	20.0
P4	M	23	66.0	20.0
P5[1]	M	27	90.9	22.0
P6	M	29	72.7	22.0

[1]P5 received 0.25 Nm/kg peak plantar-flexor assistance

where T was the instantaneous desired torque setpoint, t_{set} was the desired peak exoskeleton torque during stance phase (e.g., 15 Nm), f_{inst} was the instantaneous FSR signal, f_{cal} was the average peak FSR signal established across three strides for each user and walking speed, and C_{limit} was the motor current that was allowed to be sourced during each phase [98]. A low-level PD closed-loop controller was used to carefully track the desired torque signal. The exoskeleton provided peak plantar-flexor assistance of 0.25-0.30 Nm/kg (Table 14). The spring engaged at a neutral angle of 0 degrees. The protocol at each speed was repeated with the engagement blocks removed so that the spring was not engaged. We ensured that the same plantar-flexor torque setpoint was reached at all speeds with and without the spring. As before, exoskeleton data including measured joint torque, pulley angle, and motor current were streamed to MATLAB at 100 Hz. We used the empirical spring model to estimate the spring's torque contribution.

To quantify spring effects on actuator energy consumption, the normalized peak and mean motor current for each step were obtained for each participant at each walking speed. The current was also integrated with respect to time to calculate the overall current consumption per step and normalized by the mean torque of the corresponding step. We selected specific gait cycles such

that the average peak plantar-flexor torque was statistically similar between spring and no spring trials for each participant. We also obtained the normalized mean motor currents for stance phase only as that region of gait has the most potential for benefit from parallel elasticity due to high motor torque demand and represents the ceiling of potential power savings due to parallel elasticity. We also calculated the number of possible steps on a single battery charge for spring and no spring trials at each walking speed by dividing the battery capacity (1800 mAh) by the non-normalized integrated current consumption per step (mAh/step). After removing outliers, the data for each of the spring and no spring trials comprised 10 steps at each walking speed for each participant.

The percent change in current metrics between spring and no spring trials was calculated for each participant at each walking speed, treated as a single observation, and pooled across participants. Metrics at each walking speed were assessed for normality using Shapiro-Wilks tests. All data were normally distributed. To determine whether the parallel element significantly reduced motor current metrics and significantly increased the number of possible steps on a battery charge, one tailed t-tests at 95% confidence compared spring and no spring trials at each walking speed.

Design and Testing of a Custom High-Level Controller to Maximize Spring Benefit

We developed a custom high-level exoskeleton control strategy to maximize the energy saving benefits of the spring. In the experiment detailed above, we used a validated high-level control strategy that would sometimes waste energy by tracking a torque setpoint below the torque generated by the spring. Therefore, we modified the high-level controller by limiting the motor current C during stance and swing as in Eq. 7:

$$T = \begin{cases} t_{set}\dfrac{f_{inst}}{f_{cal}} & , \quad C_{limit} = [0A\ 8A] \quad (stance) \\ 0 & , \quad C_{limit} = [-1A\ 1A] \quad (swing) \end{cases} \tag{7}$$

where each variable was defined as above following Eq. 6. During stance, the motor could only source current in the PF direction and during swing the motor had a limited current range in both PF and DF directions. As a result of these motor current limits that affected the operation of the low-level PD closed-loop controller, this spring-specific controller resulted in slightly greater stance phase torque output than the non-spring specific controller because it prevented the motors from fighting the spring during stance phase.

To assess whether the custom spring-specific controller resulted in greater energy savings than the previously-validated (i.e., non-spring-specific) controller, we conducted a single-subject experiment similar to the variable walking speed experiment. P3 walked on a treadmill at speeds 0.75-1.25 m/s with the spring engaged as before (Table 14). A separate trial for each controller was conducted at each walking speed. A trial using the typical controller with the spring disengaged was also conducted at each walking speed. As before, exoskeleton data including measured joint torque, pulley angle, and motor current were streamed to MATLAB at 100 Hz. The percent change in the number of possible steps compared to the no spring trial was calculated for both the spring controller and the typical controller.

Results

Parallel Elastic Element Modeling and Validation

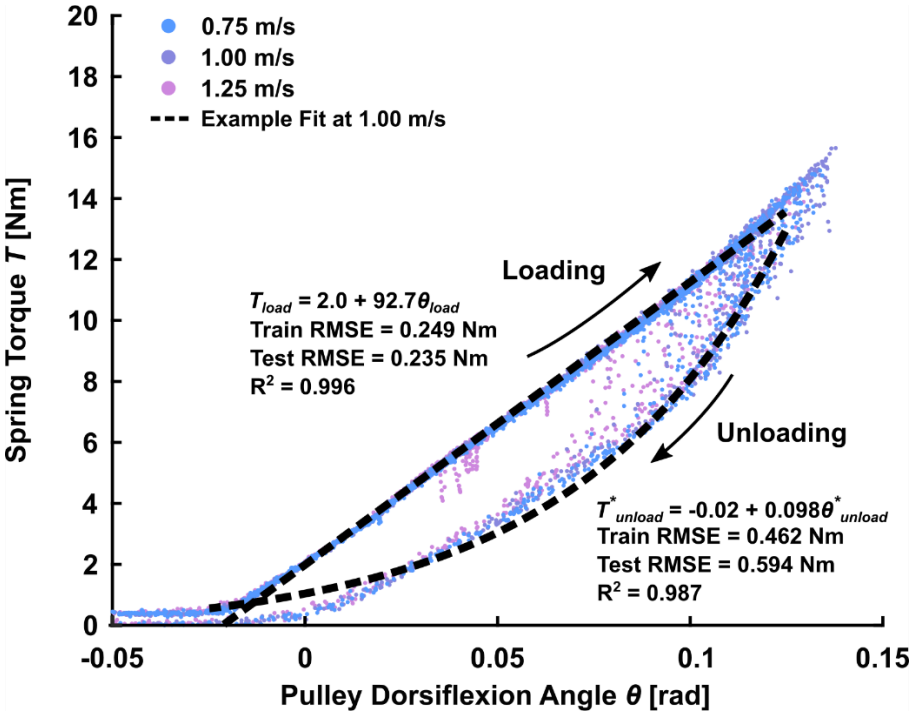

Fig. 41. Parallel spring torque-displacement curve and models. The data from three speeds (Fig. 40) were pooled together and randomly split into ¾ training data and ¼ testing data for loading and unloading regions. The split for loading and unloading regions was made at the maximum measured displacement of each step. Both models had low train and test error. The unloading equation is nonlinear with respect to pulley angle but a transformation linearizes the curve. Refer to Eq. 1-5 for details.

The spring torque loading and unloading models had good fits (R2=0.996 and 0.987, respectively) and low test RMSEs (0.235 Nm and 0.594 Nm, respectively), indicating that the spring behavior was appropriately modeled (Fig. 41). The same piecewise model was used to model spring torque at all walking speeds. The loading region model provides important information concerning the spring assembly stiffness and actual engagement angle (Eq. 8). The overall spring assembly stiffness was 92.7 Nm/rad.

$$T_{load} = 2.0 + 92.7\theta_{load} \qquad (8)$$

Much of the unloading model error was at low torques near the engagement angle which was caused by the base-10 exponential transformation (Fig. 41). Since the most relevant contribution of the unloading region was at high torques near the peak DF angle, we found this error to be acceptable. The unloading model predicting normalized spring torque as a function of normalized, transformed angle is summarized in Eq. 9.

$$T^*_{unload} = -0.02 + 0.098\theta^*_{unload} \qquad (9)$$

Variable Engagement Angle Experiment

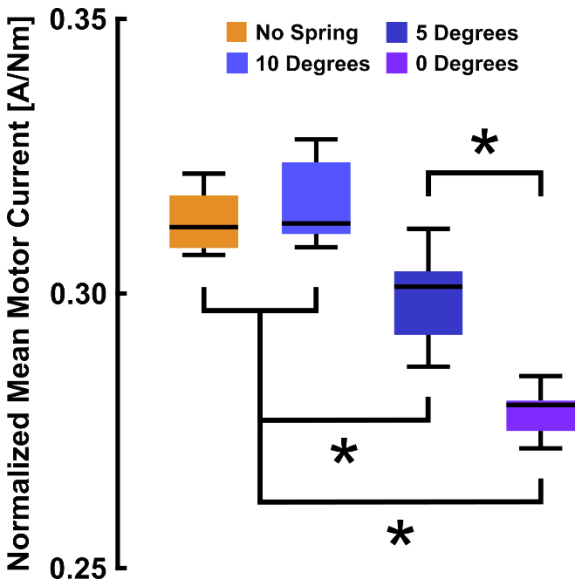

Fig. 42. Engagement angle effects on motor current. * = significant reduction at 95% confidence. Bars represent standard error of the mean. No spring and 10-degree engagement trials had similar normalized mean motor current. 0-degree engagement resulted in the lowest overall mean motor current across all conditions.

Normalized mean motor current varied with engagement angle ($p<0.001$, Fig. 42). More specifically, no spring and 10-degree engagement trials had similar normalized mean motor current ($p=0.82$, Fig. 42). 5-degree and 0-degree engagement angles had significantly lower mean motor

current compared to no spring and 10-degree engagement trials (5.1 ± 3.7%, $p<0.001$ and 11.8 ± 2.3%, $p<0.001$, respectively). 0-degree engagement resulted in 7.6 ± 2.2% lower mean motor current compared to 5-degree engagement ($p<0.001$).

Spring Effectiveness (Previously-Validated Controller)

Normalized peak, gait cycle mean, stance phase mean, and integrated motor currents for trials with spring engagement were all significantly lower compared to no spring for all walking speeds (Fig. 43AB). Specifically, peak current was 20.2 ± 2.0% (mean ± standard error) lower at 0.75 m/s ($p=0.005$), 19.3 ± 1.5% lower at 1.0 m/s ($p<0.001$), and 13.8 ± 2.0% lower at 1.25 m/s ($p=0.017$) with the spring compared to without. Mean gait cycle current was 15.2 ± 1.0% lower at 0.75 m/s, 16.1 ± 0.9% lower at 1.0 m/s, and 16.5 ± 0.8% lower at 1.25 m/s with the spring compared to without ($p<0.001$ for all). Integrated motor current was 19.1% ± 1.5% lower at 0.75 m/s ($p=0.002$), 18.1 ± 0.6% lower at 1.0 m/s ($p<0.001$), and 15.6 ± 0.8% lower at 1.25 m/s ($p<0.001$) with the spring compared to without. Mean stance phase current was 24.9 ± 1.0% lower at 0.75 m/s, 25.5 ± 1.0% lower at 1.0 m/s, and 23.7 ± 0.8% lower at 1.25 m/s with the spring compared to without ($p<0.001$ for all).

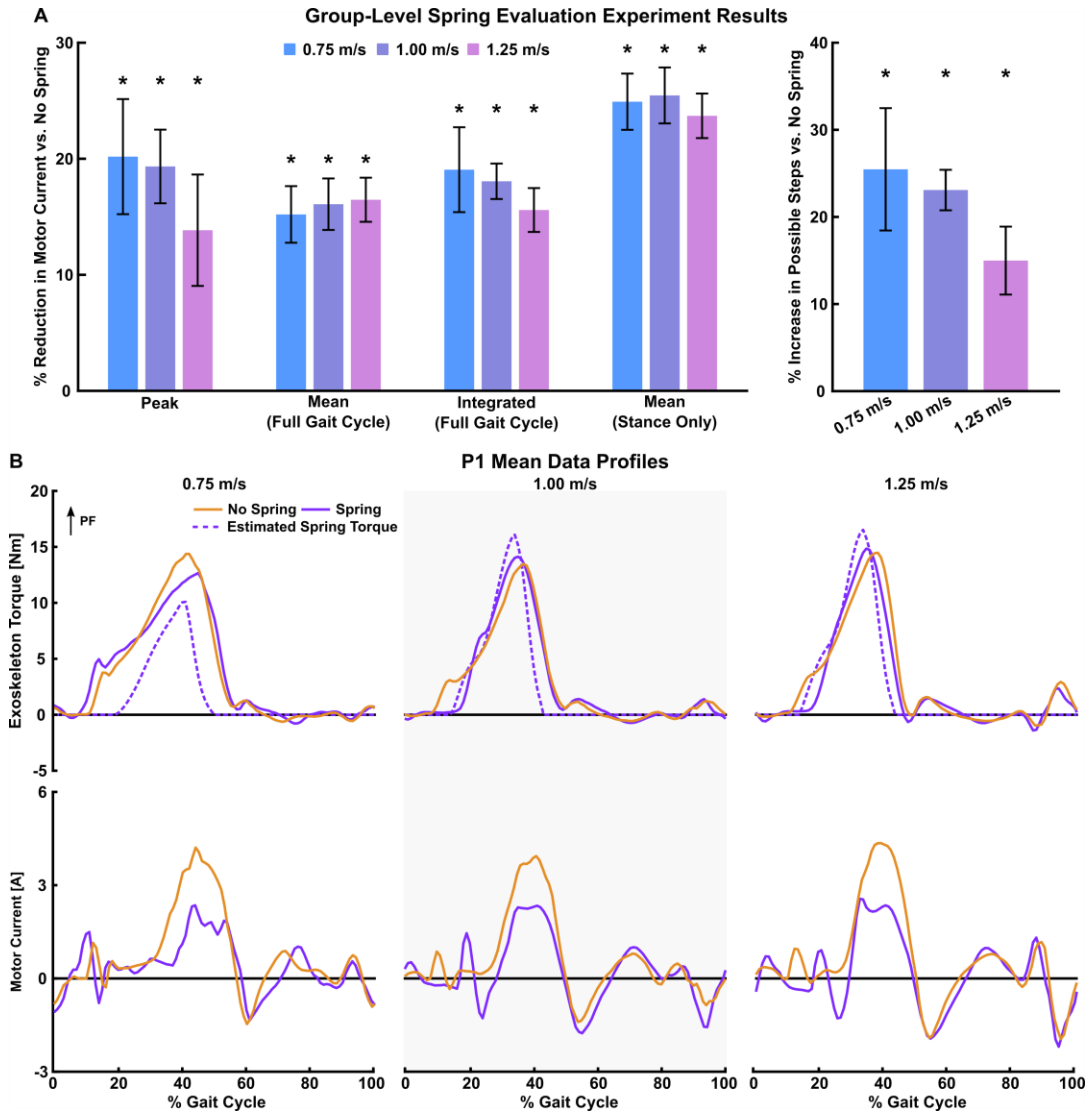

Fig. 43. Spring effectiveness results. A. Group-level reductions in metrics such as peak, mean, and integrated current were significant at all walking speeds. Using the spring significantly lowers the amount of current sourced by the motors during assisted walking with our previously-validated controller. Similarly, there were significant increases in the number of possible assisted steps for the same battery capacity at all walking speeds. This translated to increased battery life and electromechanical efficiency. * = significance at 95% confidence. Error bars represent the standard error of the mean. B. Representative mean measured exoskeleton joint torque and motor current profiles for one participant. Parallel elasticity has a strong favorable effect on motor current for all walking speeds. The spring's torque contribution was estimated using the loading and unloading models in Fig. 4. The profiles presented here are the average of 20 total steps across both legs for spring and no spring trials. It is likely that the spring contribution was slightly overestimated because of device compliance. The corresponding motor current for spring trials should be near or below zero amps during regions when the spring torque exceeded the prescribed exoskeleton joint torque.

The number of possible steps for the same battery capacity with the spring was significantly higher than without the spring for all speeds (Fig. 43A). The number of possible steps was 25.5 ± 2.9% higher at 0.75 m/s ($p=0.008$), 23.1 ± 0.9% higher at 1.0 m/s ($p<0.001$), and 15.0 ± 1.6% higher at 1.25 m/s ($p=0.006$) with the spring compared to without.

Spring Effectiveness (Spring-Specific Controller)

The spring-specific controller increased the energy benefit of the parallel elastic leaf spring at all walking speeds compared to the non-spring-specific controller; improvements were between 20-50% (Fig. 44). The spring with the spring-specific controller configuration resulted in a 46-76% increase in the number of possible steps on the same battery capacity compared to no spring configuration (depending on walking speed).

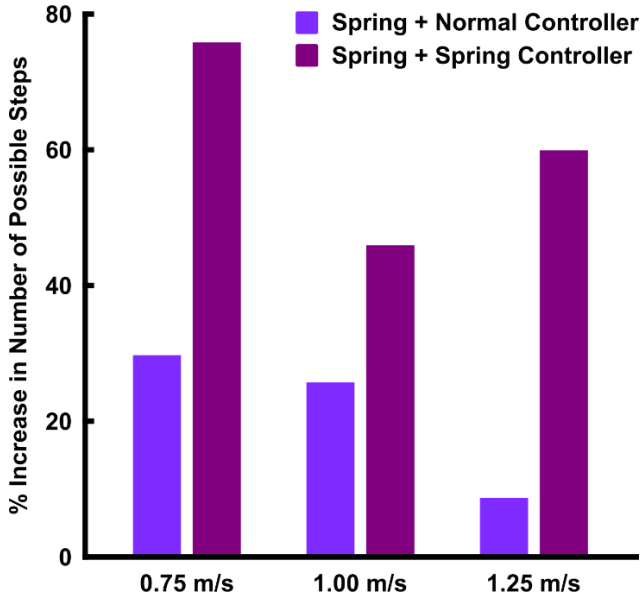

Fig. 44. Single-subject controller experiment results. Using the spring with the spring-specific controller yielded reduced motor current requirements than the spring with the normal controller for the same torque setpoint. The spring controller resulted in a 20-50% increase, depending on walking speed, in the number of possible steps compared to the typical controller. Compared to no spring, the spring and spring controller configuration resulted in a 46-76% increase in the number of possible steps.

Discussion

We accept our primary hypothesis that appropriately-designed parallel elasticity can reduce ankle exoskeleton motor current requirements at different walking speeds. To recap, we designed and modeled a leaf spring element that stored energy during dorsiflexion in early stance and released energy during toe-off to offload motor current requirements. At all walking speeds, significant reductions in peak, mean, and integrated motor current were observed. The reductions in peak and mean motor current during stance phase would likely increase motor lifetime operation as high currents lead to increased winding temperature and resistance and decreased power efficiency [126]. The reduction in integrated motor current across the gait cycle directly transfers to increased battery life and electromechanical efficiency.

It is difficult to compare our results to other studies as we were unable to find any other physical implementation of parallel elastic elements in a lower-extremity exoskeleton. One study, however, performed simulations to determine optimal spring types and stiffnesses for the joints of the lower-body and identified a unidirectional, linear spring with an approximate stiffness of 800 Nm/rad in parallel with the ankle joint to be ideal for reducing motor torque requirements [121]. In the simulations, the peak motor torque decreased by 48% with the addition of the spring, though additional torque was needed during swing to overcome the spring in dorsiflexion. Our spring was about $1/8^{th}$ the stiffness of the simulated spring in Wang et. al. and reductions in peak motor current were more modest at 14-20% depending on walking speed or whether we were using a spring-specific high-level motor controller. In the simulations, the motor had to produce over 100 Nm to overcome the spring during swing phase. Researchers interested in designing their own parallel elastic elements must consider the benefits of spring actuation during stance versus potential detriments during swing. Collins et. al developed an unpowered exoskeleton that featured a

clutched spring mechanism in parallel with the biological ankle joint [41]. The most effective spring had a stiffness of 180 Nm/rad and produced up to about 25 Nm plantar-flexor torque during stance. The clutch mechanism disengaged the spring during swing, permitting free rotation of the exoskeleton joint. Specially designed controllers and clutched springs are both good options for addressing detrimental spring engagement.

Our spring plus spring-specific controller yielded significant improvements in battery life leading to 20-50% more possible assisted steps for the same battery capacity compared to using the spring with a controller not specifically designed to take advantage of the spring. This was mainly because, in an attempt to closely match the desired torque signal, the standard controller would source motor current in early stance phase to fight the torque produced by the spring. There are many benefits to longer exoskeleton battery life; more assisted steps on a single charge means fewer batteries are needed in clinical and at-home environments which could lead to accelerated adoption of exoskeletons for gait rehabilitation and daily mobility augmentation. Lightweight parallel elastic elements have the potential to extend the duration of assisted exercise by reducing motor energy consumption.

There were some limitations to this study. The spring loading and unloading models likely slightly overestimated the spring torque contribution as evidenced in Fig. 43B – accurate models for spring torque are necessary to expand this work to other engagement angles, terrains, and controllers. Another limitation was the lack of variable terrain - though level walking makes up the majority of daily activity, inclined terrains and stairs pose a major obstacle to individuals with neuromuscular disorders that could be addressed using exoskeleton assistance. Another limitation was that our custom spring controller was only tested on one participant. Further testing and refinement are likely needed.

To the best of our knowledge, this is the first study to develop and experimentally evaluate an untethered robotic ankle exoskeleton with parallel elasticity in the form of a carbon fiber leaf spring. Proper design integration of parallel elastic elements appears to be an effective and practical approach to reducing actuator torque and energy consumption for ankle exoskeletons, increasing battery life and motor longevity. Custom controllers can further improve upon the benefits of parallel elastic elements. Future work should investigate the effectiveness of parallel elasticity across variable terrains, for individuals with pathological gait patterns, and validate the spring-specific controller in a larger cohort.

Supplemental Material

Energy Contribution Modeling

Mooney et. al developed a measure of the potential metabolic benefit a user may experience when using an untethered ankle exoskeleton called the Augmentation Factor (AF, [49]) The AF balances the metabolic detriment of wearing extra mass on the body with the positive power contribution to the ankle joint from the exoskeleton. The equation to calculate the AF (in units of Watts) is summarized in Eq. 10 below:

$$AF = \frac{p^{+} + p^{dis}}{\eta} - \sum_{i=1}^{4} \beta_i m_i \qquad (10)$$

where $p^{+}$was the mean positive power across the gait cycle, p^{dis} was zero if the positive power exceeded the negative power or otherwise was the absolute value of the difference between positive and negative power, η was the muscle-tendon efficiency equal to 0.41, and β_i was the

metabolic impact of wearing added mass m_i on body location i. We calculated the AF for several unimpaired participants in our previous study [114].

A limitation of the AF equation is that it does not evaluate the amount of time that an exoskeleton provides assistance. That is, an exoskeleton device may provide significant positive power leading to a high AF but might only be able to provide such power for a short amount of time. Battery life is a significant challenge for untethered exoskeleton devices due to the weight and bulk of batteries. Having a large, heavy battery may counter-act the effects of exoskeleton assistance and result in a net zero or negative AF. We propose a modification to the AF equation that considers the battery life of an exoskeleton. By assuming that p^{dis} is zero (as was the case in Mooney et. al. and our previous work [49,109,114]) and integrating Eq. 10 with respect to time, the energy AF per step of an exoskeleton, AF_E can be calculated via Eq. 11:

$$AF_E = \int \frac{p(t)^+}{\eta} dt - \Delta t \sum_{i=1}^{4} \beta_i m_i \qquad (11)$$

where $p(t)^+$ is the instantaneous positive power of a stride, time is measured from heel strike to heel strike of a single stride, and other terms are defined as before. AF_E has units of Joules per stride. The formulation of AF_E is similar to portions of models estimating the metabolic cost of human walking [127]. A value of AF_E greater than zero means that the user is likely to experience a reduction in total energy expenditure during assisted walking. The overall mechanical energy contribution (EC) that an exoskeleton can provide can thus be calculated when the current consumption per step of the exoskeleton is known as in Eq. 10. Here, the number of assisted strides

$N_{strides}$ was defined as the total battery capacity $C_{battery}$ divided by the mean energy consumption per stride $\bar{I}_{stride}$, both in mAh.

$$EC = AF_E * N_{strides} = AF_E \frac{C_{battery}}{\bar{I}_{stride}} \qquad (10)$$

The benefit of this modification to the AF equation is that improvements to exoskeleton electro-mechanical power efficiency can be evaluated. For example, our exoskeleton had an average 15.6% lower current consumption per step when walking with the parallel elastic element engaged at 1.25 m/s (Fig. 44A). The overall energy contribution (EC) from the exoskeleton would be significantly greater with the spring compared to without for the same AF since the user can take more exoskeleton-assisted strides. The effect of walking speed and cadence can also be seen in Eq. 9; since the amount of metabolic energy lost due to exoskeleton mass depends on the duration of the stride Δt, the positive power demand on the exoskeleton per step increases as walking speed decreases and stride duration increases. It's difficult for an ankle exoskeleton to produce significant positive power at slow walking speeds because the ankle velocity at toe-off tends to be low [124], so the exoskeleton must produce more torque in order to overcome the energy demands of wearing the device.

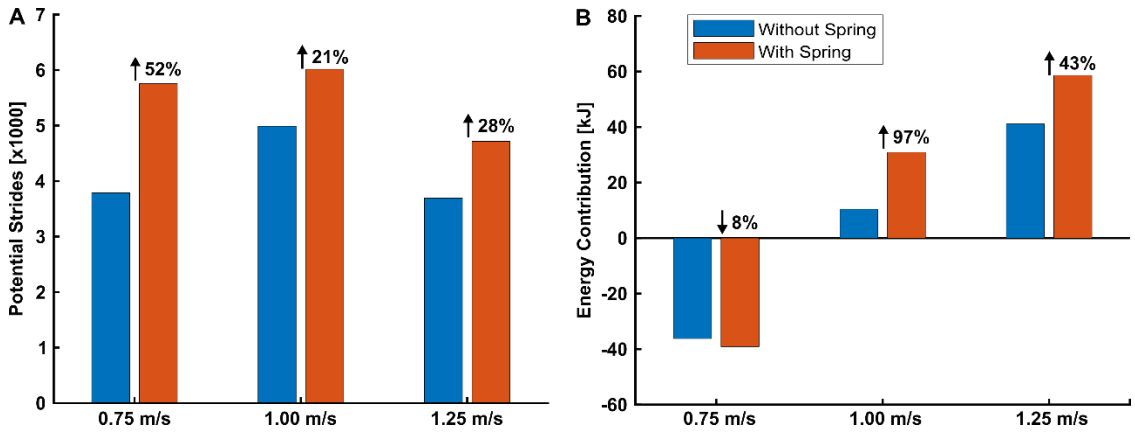

Fig. 45. Battery life with parallel elasticity (A) and its effect on device energy contribution (B). Data presented here are for P1. Parallel elasticity had the greatest impact on battery life at 0.75 m/s. Despite the significant increase in assisted strides due to reduced current consumption at 0.75 m/s, the predicted energy contribution is negative due to low positive power produced at that speed. At the fastest speed, parallel elasticity increased the number of potential strides on a battery charge by 28% and increased the total mechanical energy delivered to the user by 43%.

The EC and AF_E are simple, theoretical models for evaluating exoskeleton designs that have not been related to actual metabolic benefit observed during exoskeleton-assisted experiments with multiple participants. Though Mooney et. al showed good agreement between metabolic benefit predicted by AF and actual experimental results, this relationship did not hold for our unimpaired cohort [114]. A limitation of both AF and EC models is that neither model account for acute physiological changes in response to external joint assistance in the forms of torque and power. Faraji et. al developed a comprehensive model for metabolic cost during walking that comprises energy cost of movement dynamics, center of mass velocity redirection, foot lift, and weight support, all of which depend on other factors such as walking speeds, cadence, and body mass [127]. Each of these individual energy cost pieces need to be considered when developing a model to predict the overall benefit an exoskeleton user may experience from a particular device or control strategy – the AF offers a coarse estimate of at most half the picture (dynamics and weight support). EC is better due to its ability to account for walking speed and cadence, but in the

situation that an individual has difficulty supporting their own weight, both the AF and EC of a device that lessens the energy burden of remaining upright would be strongly negative due to the lack of power transfer. Indeed, there is more to the metabolic benefit puzzle than just positive power input from an external source – our works show that even low-powered devices used at slow walking speeds can meaningfully impact energy consumption for certain users [26,114,123].

The EC model provides a simple metric for comparing exoskeleton devices. In this case, parallel elasticity increases the EC of our device by reducing motor current consumption per step. Other ways to improve EC could be weight or controller optimization to increase AF_E by mitigating energy detriment due to added mass or increasing positive power production, respectively, or reducing friction losses between the motor and end effector to increase the number of assisted strides. A larger battery would also increase the number of assisted strides but would also increase energy detriment due to extra mass – the EC equation accounts for both effects.

Future work should develop better models of the effects of exoskeleton assistance on the human body beyond simple mechanical power and energy transfer. A unified model of metabolic cost of walking that comprehensively accounts for physiological changes throughout the body due to exoskeleton assistance could be the next tool for evaluating exoskeleton devices. Whereas the AF and EC models estimate potential improvements in metabolic power and energy consumption, respectively, neither account for the reduction in plantarflexor muscle activity that occurs when torque assistance is provided during stance [26,27], nor for the changes in muscle activity further up the kinematic chain such as at the vasti or other large muscle groups that account for a significant portion of the metabolic cost of walking [127].

CONCLUSION

The overarching objective of this work was to advance the field of rehabilitation robotics by improving the design and control of a battery-powered ankle exoskeletons making it suitable for a wide range of individuals and walking conditions, with the ultimate, long-term goal of solidifying robotic ankle assistance as a method for maximizing the duration and effectiveness of gait-oriented rehabilitation and training. We identified and addressed the short-comings of our prototype controllers and exoskeletons and developed safer, more efficient systems including a torque sensor-less control scheme and a new exoskeleton hardware platform that was effective for a wider range of impaired and unimpaired users. The ankle exoskeleton reported in this dissertation was effective at improving walking performance for children and young adults with cerebral palsy, and was also just the second untethered device to successfully demonstrate metabolic improvements in unimpaired adults. Our device featured custom joint-level sensing that may open avenues for future research to develop new models, controllers, and mechanical systems to maximize the safety, efficiency, and efficacy of exoskeleton systems. We also developed a novel parallel elastic element that improved the electro-mechanical efficiency of the ankle exoskeleton device. This work is relevant beyond untethered ankle exoskeletons and lifts the standard for the design, validation, and application of robotic devices for targeting neuromuscular impairment and augmenting human performance. Ultimately, we hope this work contributes to the development of new technologies and strategies for improving the quality of life for the millions of people with neuromuscular impairments around the world.

REFERENCES

1. Boyle CA, Boulet S, Schieve LA, Cohen RA, Blumberg SJ, Yeargin-Allsopp M, et al. Trends in the prevalence of developmental disabilities in US children, 1997-2008. Pediatrics. 2011; 127(6): 1034–42.

2. Maddox S. Paralysis Resource Guide. Fourth. New Jersey: Christopher and Dana Reeve Foundation; 2017.

3. Graham HK, Rosenbaum P, Paneth N, Dan B, Lin JP, Damiano DiL, et al. Cerebral palsy. Vol. 2, Nature Reviews Disease Primers. 2016.

4. Armand S, Decoulon G, Bonnefoy-Mazure A. Gait analysis in children with cerebral palsy. EFORT Open Rev. 2016; 1(12): 448–60.

5. Bjornson KF, Belza B, Kartin D, Logsdon R, McLaughlin JF. Ambulatory Physical Activity Performance in Youth With Cerebral Palsy and Youth Who Are Developing Typically. Phys Ther. 2007; 87(3): 248–57.

6. NCHS. Technical Notes for Summary Health Statistics Tables: National Health Interview Survey [Internet]. 2019. Available from: https://www.cdc.gov/nchs/nhis/shs/tables.htm

7. Mayo NE, Wood-Dauphinee S, Ahmed S, Gordon C, Higgins J, McEwen S, et al. Disablement following stroke. Disabil Rehabil. 1999; 21(5–6): 258–68.

8. Farris DJ, Hampton A, Lewek MD, Sawicki GS. Revisiting the mechanics and energetics of walking in individuals with chronic hemiparesis following stroke: From individual limbs to lower limb joints. J Neuroeng Rehabil. 2015; 12(1).

9. Schrack JA, Simonsick EM, Chaves PHM, Ferrucci L. The role of energetic cost in the age-related slowing of gait speed. J Am Geriatr Soc. 2012; 60(10): 1811–6.

10. Abel MF, Damiano DL. Strategies for increasing walking speed in diplegic cerebral palsy. J Pediatr Orthop. 1996; 16(6): 753–8.

11. Moriello C, Finch L, Mayo NE. Relationship between muscle strength and functional walking capacity among people with stroke. J Rehabil Res Dev. 2011; 48(3): 267–75.

12. Damiano DL, Abel MF. Functional outcomes of strength training in spastic cerebral palsy. Arch Phys Med Rehabil. 1998; 79(2): 119–25.

13. Kluding PM, Dunning K, O'Dell MW, Wu SS, Ginosian J, Feld J, et al. Foot drop stimulation versus ankle foot orthosis after stroke: 30-week outcomes. Stroke. 2013; 44(6): 1660–9.

14. Prosser LA, Curatalo LA, Alter KE, Damiano DL. Acceptability and potential effectiveness of a foot drop stimulator in children and adolescents with cerebral palsy.

Dev Med Child Neurol. 2012; 54(11): 1044–9.

15. Ries AJ, Novacheck TF, Schwartz MH. The Efficacy of Ankle-Foot Orthoses on Improving the Gait of Children With Diplegic Cerebral Palsy: A Multiple Outcome Analysis. PM R. 2015; 7(9): 922–9.

16. Awad LN, Bae J, O'Donnell K, De Rossi SMM, Hendron K, Sloot LH, et al. A soft robotic exosuit improves walking in patients after stroke. Sci Transl Med. 2017; 9(400): 1–12.

17. Kerkum YL, Buizer AI, Van Den Noort JC, Becher JG, Harlaar J, Brehm MA. The effects of varying ankle foot orthosis stiffness on gait in children with spastic cerebral palsy who walk with excessive knee flexion. PLoS One. 2015; 10(11).

18. Koh S, Choi W, Lee S. The Effects of Stair Climbing Training with Functional Electrical Stimulation on Muscle Strength, Balance, and Gait in Patients with Chronic Stroke. Phys Ther Rehabil Sci. 2021; 10(1): 32–9.

19. Damiano DL. Activity, Activity, Activity: Rethinking Our Physical Therapy Approach to Cerebral Palsy. Phys Ther. 2006; 86(11): 1534–40.

20. Moreau NG, Bodkin AW, Bjornson K, Hobbs A, Soileau M, Lahasky K. Effectiveness of rehabilitation interventions to improve gait speed in children with cerebral palsy: Systematic review and Meta-Analysis. Vol. 96, Physical Therapy. 2016. p. 1938–54.

21. Jayaraman A, O'brien MK, Madhavan S, Mummidisetty CK, Roth HR, Hohl K, et al. Stride management assist exoskeleton vs functional gait training in stroke: A randomized trial. Neurology. 2019; 92(3): E263–73.

22. Awad LN, Esquenazi A, Francisco GE, Nolan KJ, Jayaraman A. The ReWalk ReStore™ soft robotic exosuit: A multi-site clinical trial of the safety, reliability, and feasibility of exosuit-augmented post-stroke gait rehabilitation. J Neuroeng Rehabil. 2020; 17(1).

23. Sawicki GS, Ferris DP. Mechanics and energetics of level walking with powered ankle exoskeletons. J Exp Biol. 2008; 211(9): 1402–13.

24. McCain EM, Dick TJM, Giest TN, Nuckols RW, Lewek MD, Saul KR, et al. Mechanics and energetics of post-stroke walking aided by a powered ankle exoskeleton with speed-adaptive myoelectric control. J Neuroeng Rehabil. 2019; 16(1).

25. Lerner ZF, Harvey TA, Lawson JL. A Battery-Powered Ankle Exoskeleton Improves Gait Mechanics in a Feasibility Study of Individuals with Cerebral Palsy. Ann Biomed Eng. 2019; 47(6): 1345–56.

26. Orekhov G, Fang Y, Luque J, Lerner ZF. Ankle Exoskeleton Assistance Can Improve Over-Ground Walking Economy in Individuals with Cerebral Palsy. IEEE Trans Neural Syst Rehabil Eng. 2020; 28(2): 461–7.

27. Fang Y, Orekhov G, Lerner ZF. Adaptive ankle exoskeleton gait training demonstrates acute neuromuscular and spatiotemporal benefits for individuals with cerebral palsy: A pilot study. Gait Posture. 2020;

28. Zhang J, Fiers P, Witte KA, Jackson RW, Poggensee KL, Atkeson CG, et al. Human-in-the-loop optimization of exoskeleton assistance during walking. Science (80-). 2017; 356(6344): 1280–3.

29. Mooney LM, Rouse EJ, Herr HM. Autonomous exoskeleton reduces metabolic cost of human walking during load carriage. J Neuroeng Rehabil. 2014; 11(80).

30. Galle S, Derave W, Bossuyt F, Calders P, Malcolm P, De Clercq D. Exoskeleton plantarflexion assistance for elderly. Gait Posture. 2017; 52: 183–8.

31. Mooney LM, Herr HM. Biomechanical walking mechanisms underlying the metabolic reduction caused by an autonomous exoskeleton. J Neuroeng Rehabil. 2016; 13(1).

32. Witte KA, Fiers P, Sheets-Singer AL, Collins SH. Improving the energy economy of human running with powered and unpowered ankle exoskeleton assistance. Sci Robot. 2020; 5(40).

33. Neptune RR, Sasaki K, Kautz SA. The effect of walking speed on muscle function and mechanical energetics. Gait Posture. 2008; 28(1): 135–43.

34. Farris DJ, Sawicki GS. The mechanics and energetics of human walking and running: A joint level perspective. J R Soc Interface. 2012; 9(66): 110–8.

35. Franks PW, Bryan GM, Martin RM, Reyes R, Collins SH. Comparing optimized exoskeleton assistance of the hip , knee , and ankle in single and multi-joint configurations. BioRxiv [Internet]. 2021; Available from: https://doi.org/10.1101/2021.02.19.431882

36. Lin PY, Yang YR, Cheng SJ, Wang RY. The relation between ankle impairments and gait velocity and symmetry in people with stroke. Arch Phys Med Rehabil. 2006; 87(4): 562–8.

37. Davids JR. The foot and ankle in cerebral palsy. Vol. 41, Orthopedic Clinics of North America. 2010. p. 579–93.

38. Barber L, Barrett R, Lichtwark G. Medial gastrocnemius muscle fascicle active torque-length and Achilles tendon properties in young adults with spastic cerebral palsy. J Biomech. 2012; 45(15): 2526–30.

39. Dallmeijer AJ, Rameckers EA, Houdijk H, de Groot S, Scholtes VA, Becher JG. Isometric muscle strength and mobility capacity in children with cerebral palsy. Disabil Rehabil. 2017; 39(2): 135–42.

40. Yılmaz Topçuoğlu MS, Krautwurst BK, Klotz M, Dreher T, Wolf SI. How do children

with bilateral spastic cerebral palsy manage walking on inclines? Gait Posture. 2018; 66: 172–80.

41. Collins SH, Bruce Wiggin M, Sawicki GS. Reducing the energy cost of human walking using an unpowered exoskeleton. Nature. 2015; 522(7555): 212–5.

42. Conner BC, Luque J, Lerner ZF. Adaptive Ankle Resistance from a Wearable Robotic Device to Improve Muscle Recruitment in Cerebral Palsy. Ann Biomed Eng. 2020; 48(4): 1309–21.

43. Conner BC, Schwartz MH, Lerner ZF. Wearable Robotic ankle resistance training improves neuromuscular control and walking efficiency in cerebral Palsy. medRxiv. 2020.

44. Malcolm P, Derave W, Galle S, De Clercq D. A Simple Exoskeleton That Assists Plantarflexion Can Reduce the Metabolic Cost of Human Walking. PLoS One. 2013; 8(2).

45. Galle S, Malcolm P, Collins SH, De Clercq D. Reducing the metabolic cost of walking with an ankle exoskeleton: interaction between actuation timing and power. J Neuroeng Rehabil. 2017; 14(1).

46. Bair MO. The Design and Testing of a Powered Exoskeleton to Reduce the Metabolic Cost of Walking in Individuals with Cerebral Palsy. ProQuest Diss Theses [Internet]. 2018;(May): 65. Available from: https://www.proquest.com/docview/2050214667?accountid=28839%0Ahttp://www.yidu.edu.cn/educhina/educhina.do?artifact=&svalue=The+Design+and+Testing+of+a+Powered+Exoskeleton+to+Reduce+the+Metabolic+Cost+of+Walking+in+Individuals+with+Cerebral+Palsy&stype=2&s

47. Lerner ZF, Gasparri GM, Bair MO, Lawson JL, Luque J, Harvey TA, et al. An untethered ankle exoskeleton improves walking economy in a pilot study of individuals with cerebral palsy. IEEE Trans Neural Syst Rehabil Eng. 2018; 26(10): 1985–93.

48. Babers J. Optimizing the Mechanical Design of an Untethered Ankle Exoskeleton. Northern Arizona University; 2020.

49. Mooney LM, Rouse EJ, Herr HM. Autonomous exoskeleton reduces metabolic cost of human walking during load carriage. J Neuroeng Rehabil. 2014; 11(1).

50. De Mattos C, Patrick Do K, Pierce R, Feng J, Aiona M, Sussman M. Comparison of hamstring transfer with hamstring lengthening in ambulatory children with cerebral palsy: further follow-up. J Child Orthop. 2014; 8(6): 513–20.

51. DahlbÄck GO, Norlin R. The effect of corrective surgery on energy expenditure during ambulation in children with cerebral palsy. Eur J Appl Physiol Occup Physiol. 1985;

52. Romkes J, Brunner R. Comparison of a dynamic and a hinged ankle-foot orthosis by gait analysis in patients with hemiplegic cerebral palsy. Gait Posture. 2002; 15(1): 18–24.

53. McNee AE, Shortland AP, Eve LC, Robinson RO, Gough M. Lower limb extensor moments in children with spastic diplegic cerebral palsy. Gait Posture. 2004; 20(2): 171–6.

54. Waters RL, Mulroy S. The energy expenditure of normal and pathologic gait. Vol. 9, Gait and Posture. 1999. p. 207–31.

55. Kerr C, Parkes J, Stevenson M, Cosgrove AP, Mcdowell BC. Energy efficiency in gait, activity, participation, and health status in children with cerebral palsy. Dev Med Child Neurol. 2008; 50(3): 204–10.

56. Mooney LM, Rouse EJ, Herr HM. Autonomous exoskeleton reduces metabolic cost of walking. In: 2014 36th Annual International Conference of the IEEE Engineering in Medicine and Biology Society, EMBC 2014. 2014. p. 3065–8.

57. Panizzolo FA, Galiana I, Asbeck AT, Siviy C, Schmidt K, Holt KG, et al. A biologically-inspired multi-joint soft exosuit that can reduce the energy cost of loaded walking. J Neuroeng Rehabil. 2016; 13(1).

58. Kim J, Heimgartner R, Lee G, Karavas N, Perry D, Ryan DL, et al. Autonomous and portable soft exosuit for hip extension assistance with online walking and running detection algorithm. In: Proceedings - IEEE International Conference on Robotics and Automation. 2018. p. 5473–80.

59. Lee S, Karavas N, Quinlivan BT, Louiseryan D, Perry D, Eckert-Erdheim A, et al. Autonomous multi-joint soft exosuit for assistance with walking overground. In: Proceedings - IEEE International Conference on Robotics and Automation. 2018. p. 2812–9.

60. Lerner ZF, Damiano DL, Bulea TC. A lower-extremity exoskeleton improves knee extension in children with crouch gait from cerebral palsy. Sci Transl Med. 2017; 9(404).

61. Gasparri GM, Bair MO, Libby RP, Lerner ZF. Verification of a Robotic Ankle Exoskeleton Control Scheme for Gait Assistance in Individuals with Cerebral Palsy. In: IEEE International Conference on Intelligent Robots and Systems. 2018. p. 4673–8.

62. Soule RG, Goldman RF. Energy cost of loads carried on the head, hands, or feet. J Appl Physiol. 1969; 27(5): 687–90.

63. Browning RC, Modica JR, Kram R, Goswami A. The effects of adding mass to the legs on the energetics and biomechanics of walking. Med Sci Sports Exerc. 2007; 39(3): 515–25.

64. Gasparri GM, Luque J, Lerner ZF. Proportional Joint-Moment Control for Instantaneously Adaptive Ankle Exoskeleton Assistance. IEEE Trans Neural Syst Rehabil Eng. 2019; 27(4): 751–9.

65. Brockway JM. Derivation of formulae used to calculate energy expenditure in man. Hum Nutr Clin Nutr. 1987; 41(6): 463–71.

66. Lerner ZF, Damiano DL, Bulea TC. A robotic exoskeleton to treat crouch gait from cerebral palsy: Initial kinematic and neuromuscular evaluation. In: Proceedings of the Annual International Conference of the IEEE Engineering in Medicine and Biology Society, EMBS. 2016.

67. DeJaeger D, Willems PA, Heglund NC. The energy cost of walking in children. Pflugers Arch Eur J Physiol. 2001; 441(4): 538–43.

68. Reinkensmeyer DJ, Akoner OM, Ferris DP, Gordon KE. Slacking by the human motor system: Computational models and implic implications for robotic orthoses. In: Proceedings of the 31st Annual International Conference of the IEEE Engineering in Medicine and Biology Society: Engineering the Future of Biomedicine, EMBC 2009. 2009. p. 2129–32.

69. Ketelaar M, Vermeer A, 'T Hart H, Van Petegem-van Beek E, Helders PJM. Effects of a functional therapy program on motor abilities of children with cerebral palsy. Phys Ther. 2001; 81(9): 1534–45.

70. Salem Y, Godwin EM. Effects of task-oriented training on mobility function in children with cerebral palsy. NeuroRehabilitation. 2009; 24(4): 307–13.

71. Salbach NM, Mayo NE, Wood-Dauphinee S, Hanley JA, Richards CL, Côté R. A task-orientated intervention enhances walking distance and speed in the first year post stroke: A randomized controlled trial. Clin Rehabil. 2004; 18(5): 509–19.

72. Ma HI, Trombly CA, Robinson-Podolski C. The effect of context on skill acquisition and transfer. Am J Occup Ther. 1999; 53(2): 138–44.

73. Felt W, Selinger JC, Donelan JM, Remy CD. "Body-in-the-loop": Optimizing device parameters using measures of instantaneous energetic cost. PLoS One. 2015; 10(8): 1–21.

74. Jayaraman C, Mummidisetty CK, Loesch A, Kaur S, Hoppe-Ludwig S, Staat M, et al. Postural and Metabolic Benefits of Using a Forearm Support Walker in Older Adults With Impairments. Arch Phys Med Rehabil. 2019; 100(4): 638–47.

75. Ralston HJ. Energy-speed relation and optimal speed during level walking. Int Zeitschrift für Angew Physiol Einschl Arbeitsphysiologie. 1958; 17(4): 277–83.

76. Johnston TE, Moore SE, Quinn LT, Smith BT. Energy cost of walking in children with cerebral palsy: Relation to the Gross Motor Function Classification System. Dev Med Child Neurol. 2004; 47(1): 34–8.

77. Rose J, Gamble JG, Burgos A, Medeiros J, Haskell WL. Energy Expenditure Index of Walking for Normal Children and for Children With Cerebral Palsy. Dev Med Child Neurol. 1990; 32(4): 333–40.

78. Young AJ, Ferris DP. State of the art and future directions for lower limb robotic exoskeletons. IEEE Trans Neural Syst Rehabil Eng. 2017; 25(2): 171–82.

79. Kang I, Hsu H, Young A. The Effect of Hip Assistance Levels on Human Energetic Cost Using Robotic Hip Exoskeletons. IEEE Robot Autom Lett. 2019; 4(2): 430–7.

80. Murakam T, Yu F, Ohnishi K. Torque Sensorless Control in Multidegree-of-Freedom Manipulator. IEEE Trans Ind Electron. 1993; 40(2): 259–65.

81. Vitiello N, Lenzi T, De Rossi SMM, Roccella S, Carrozza MC. A sensorless torque control for Antagonistic Driven Compliant Joints. Mechatronics. 2010; 20(3): 355–67.

82. Ugurlu B, Nishimura M, Hyodo K, Kawanishi M, Narikiyo T. A framework for sensorless torque estimation and control in wearable exoskeletons. In: International Workshop on Advanced Motion Control, AMC. 2012.

83. Jeong U, Cho KJ. Feedforward friction compensation of Bowden-cable transmission via loop routing. In: IEEE International Conference on Intelligent Robots and Systems. 2015. p. 5948–53.

84. Wiggin MB, Sawicki GS, Collins SH. An exoskeleton using controlled energy storage and release to aid ankle propulsion. In: IEEE International Conference on Rehabilitation Robotics. 2011.

85. Bishop RH. The Mechatronics Handbook. The Mechatronics Handbook. 2002. 1–1251 p.

86. Campbell MJ, Dobson AJ. An Introduction to Generalized Linear Models. Biometrics. 1991; 47(1): 347.

87. Chung MJ, Wang MJJ. The change of gait parameters during walking at different percentage of preferred walking speed for healthy adults aged 20-60 years. Gait Posture. 2010; 31(1): 131–5.

88. Kang HG, Dingwell JB. Separating the effects of age and walking speed on gait variability. Gait Posture. 2008; 27(4): 572–7.

89. Hreljac A. Determinants of the gait transition speed during human locomotion: Kinematic factors. J Biomech. 1995; 28(6): 669–77.

90. Granata KP, Abel MF, Damiano DL. Joint angular velocity in spastic gait and the influence of muscle- tendon lengthening. J Bone Jt Surg - Ser A. 2000; 82(2): 174–86.

91. Ahn J, Hogan N. Walking is not like reaching: Evidence from periodic mechanical perturbations. PLoS One. 2012; 7(3).

92. Hogan N, Sternad D. Dynamic primitives in the control of locomotion. Front Comput Neurosci. 2013; 7(71).

93. Begnoche DM, Pitetti KH. Effects of traditional treatment and partial body weight treadmill training on the motor skills of children with spastic cerebral palsy: A pilot study. Pediatr Phys Ther. 2007; 19(1): 11–9.

94. Kuys SS, Ada L, Paratz J, Brauer SG. Steps, duration and intensity of usual walking practice during subacute rehabilitation after stroke: an observational study. Brazilian J Phys Ther. 2019; 23(1): 56–61.

95. Hemmerich A, Brown H, Smith S, Marthandam SSK, Wyss UP. Hip, knee, and ankle kinematics of high range of motion activities of daily living. J Orthop Res. 2006; 24(4): 770–81.

96. Hoffmann K. Applying the wheatstone bridge circuit. HBM S1569-11 en, HBM, Darmstadt, Ger. 2001;

97. Honeywell. Hall Effect Sensing and Application [Internet]. Available from: https://www.google.com/url?sa=t&rct=j&q=&esrc=s&source=web&cd=&cad=rja&uact=8&ved=2ahUKEwiS9LSSj6LxAhWM4J4KHb7qBi0QFjABegQIBRAF&url=https%3A%2F%2Fsensing.honeywell.com%2Fhoneywell-sensing-sensors-magnetoresistive-hall-effect-applications-005715-2-en2.pdf&

98. Bishe SSPA, Nguyen T, Fang Y, Lerner ZF. Adaptive Ankle Exoskeleton Control: Validation Across Diverse Walking Conditions. IEEE Trans Med Robot Bionics. 2021; 3(3): 801–12.

99. Section 405.2. In: 2010 ADA Standards for Accessible Design [Internet]. Available from: https://www.access-board.gov/ada/guides/chapter-4-ramps-and-curb-ramps/

100. Sawicki GS, Ferris DP. Mechanics and energetics of incline walking with robotic ankle exoskeletons. J Exp Biol. 2009; 212(1): 32–41.

101. MacLean MK, Ferris DP. Energetics of walking with a robotic knee exoskeleton. J Appl Biomech. 2019;

102. Sienko Thomas S, Buckon CE, Jakobson-Huston S, Sussman MD, Aiona MD. Stair locomotion in children with spastic hemiplegia: The impact of three different ankle foot orthosis (AFOs) configurations. Gait Posture. 2002; 16(2): 180–7.

103. Eken MM, Brændvik SM, Bardal EM, Houdijk H, Dallmeijer AJ, Roeleveld K. Lower limb muscle fatigue during walking in children with cerebral palsy. Dev Med Child Neurol. 2019; 61(2): 212–8.

104. Shinya Yamauchi SM. Rating of Perceived Exertion for Quantification of the Intensity of Resistance Exercise. Int J Phys Med Rehabil. 2013; 01(09).

105. Brooke J. SUS -A quick and dirty usability scale Usability and context. Usability Eval Ind. 1996; 189(194): 4–7.

106. Bangor A, Kortum P, Miller J. Determining what individual SUS scores mean: adding an adjective rating scale. J usability Stud. 2009; 4(3): 114–23.

107. Ghasemi A, Zahediasl S. Normality tests for statistical analysis: A guide for non-

statisticians. Int J Endocrinol Metab. 2012; 10(2): 486–9.

108. Hillside NJ. Statistical power analysis for the behavioural sciences.[Google Scholar]. In: Statistical Power Anaylsis for the Behavioral Sciences. 1988.

109. Mooney LM, Rouse EJ, Herr HM. Autonomous exoskeleton reduces metabolic cost of human walking. J Neuroeng Rehabil. 2014; 11(151).

110. Unnithan VB, Clifford C, Bar-Or O. Evaluation by exercise testing of the child with cerebral palsy. Sport Med. 1998; 26(4): 239–51.

111. Meyer JT, Schrade SO, Lambercy O, Gassert R. User-centered design and evaluation of physical interfaces for an exoskeleton for paraplegic users. In: IEEE International Conference on Rehabilitation Robotics. 2019. p. 1159–66.

112. Sawicki GS, Ferris DP. Powered ankle exoskeletons reveal the metabolic cost of plantar flexor mechanical work during walking with longer steps at constant step frequency. J Exp Biol. 2009; 212(1): 21–31.

113. Bae J, Siviy C, Rouleau M, Menard N, Odonnell K, Geliana I, et al. A lightweight and efficient portable soft exosuit for paretic ankle assistance in walking after stroke. In: Proceedings - IEEE International Conference on Robotics and Automation. 2018. p. 2820–7.

114. Orekhov G, Fang Y, Cuddeback CF, Lerner ZF. Usability and performance validation of an ultra-lightweight and versatile untethered robotic ankle exoskeleton. J Neuroeng Rehabil [Internet]. 2021; 18(1): 163. Available from: https://doi.org/10.1186/s12984-021-00954-9

115. Au SK, Herr H, Weber J, Martinez-Villalpando EC. Powered ankle-foot prosthesis for the improvement of amputee ambulation. In: Annual International Conference of the IEEE Engineering in Medicine and Biology - Proceedings. 2007. p. 3020–6.

116. Au SK, Weber J, Herr H. Powered ankle-foot prosthesis improves walking metabolic economy. IEEE Trans Robot. 2009; 25(1): 51–66.

117. Jimenez-Fabian R, Geeroms J, Flynn L, Vanderborght B, Lefeber D. Reduction of the torque requirements of an active ankle prosthesis using a parallel spring. Rob Auton Syst. 2017; 92: 187–96.

118. Mazumdar A, Spencer SJ, Hobart C, Salton J, Quigley M, Wu T, et al. Parallel Elastic Elements Improve Energy Efficiency on the STEPPR Bipedal Walking Robot. IEEE/ASME Trans Mechatronics. 2017; 22(2): 898–908.

119. Pratt GA, Williamson MM. Series elastic actuators. In: IEEE International Conference on Intelligent Robots and Systems. 1995. p. 399–406.

120. Hurst J, Rizzi a, Hobbelen D. Series elastic actuation: Potential and pitfalls. Int Conf …

[Internet]. 2004; Available from: http://mime.oregonstate.edu/research/drl/publications/_documents/hurst_2004a.pdf

121. Wang S, Van Dijk W, Van Der Kooij H. Spring uses in exoskeleton actuation design. In: IEEE International Conference on Rehabilitation Robotics. 2011.

122. Au SK, Herr HM. Powered ankle-foot prosthesis. IEEE Robot Autom Mag. 2008; 15(3): 52–9.

123. Fang Y, Orekhov G, Lerner ZF. Improving the Energy Cost of Incline Walking and Stair Ascent with Ankle Exoskeleton Assistance in Cerebral Palsy. 2021; Available from: In Review

124. Schwartz MH, Rozumalski A, Trost JP. The effect of walking speed on the gait of typically developing children. J Biomech. 2008; 41(8): 1639–50.

125. Jonkers I, Delp S, Patten C. Capacity to increase walking speed is limited by impaired hip and ankle power generation in lower functioning persons post-stroke. Gait Posture. 2009; 29(1): 129–37.

126. Fussell BK. Thermal effects on the torque-speed performance of a brushless DC motor. In: Proceedings of the 21st Electrical Electronics Insulation Conference and Electrical Manufacturing and Coil Winding. 1993. p. 403–11.

127. Faraji S, Wu AR, Ijspeert AJ. A simple model of mechanical effects to estimate metabolic cost of human walking. Sci Rep. 2018; 8(1).